THE

ASTROPHYSICAL JOURNAL

An International Review of Spectroscopy and Astronomical Physics

FOUNDED IN 1895 BY GEORGE E. HALE AND JAMES E. KEELER

EDITORS

HENRY G. GALE
Ryerson Physical Laboratory of the University of Chicago

FREDERICK H. SEARES
Mount Wilson Observatory of the Carnegie Institution of Washington

OTTO STRUVE
Yerkes Observatory of the University of Chicago

COLLABORATORS

WALTER S. ADAMS, *Mount Wilson Observatory;* JOSEPH S. AMES, *Johns Hopkins University;* HENRY CREW, *Northwestern University;* CHARLES FABRY, *Université de Paris;* EDWIN HUBBLE, *Mount Wilson Observatory;* HEINRICH KAYSER, *Universität Bonn;* PAUL W. MERRILL, *Mount Wilson Observatory;* ROBERT A. MILLIKAN, *Institute of Technology, Pasadena;* HUGH F. NEWALL, *Cambridge University;* FRIEDRICH PASCHEN, *Reichsanstalt, Charlottenburg;* HENRY N. RUSSELL, *Princeton University;* FRANK SCHLESINGER, *Yale Observatory;* HARLOW SHAPLEY, *Harvard College Observatory;* F. J. M. STRATTON, *Cambridge University*

VOLUME 92

JULY–NOVEMBER, 1940

THE UNIVERSITY OF CHICAGO PRESS
CHICAGO, ILLINOIS

THE CAMBRIDGE UNIVERSITY PRESS, LONDON
THE MARUZEN COMPANY LIMITED, TOKYO
THE COMMERCIAL PRESS LIMITED, SHANGHAI

PUBLISHED JULY, SEPTEMBER, NOVEMBER, 1940

COMPOSED AND PRINTED BY THE UNIVERSITY OF CHICAGO PRESS
CHICAGO, ILLINOIS, U.S.A.

Astron Obs.
Wahr.

CONTENTS

NUMBER 1

PAGE

ON THE INTERPRETATION OF SPIRAL STRUCTURE IN THE NEBULAE. Bertil Lindblad 1

THE OPACITY OF GAS MIXTURES IN STELLAR INTERIORS. Philip M. Morse 27

A STUDY OF *He* I LINES IN THE BALMER CONTINUUM. F. E. Roach and Leon Blitzer 50

HETEROCHROMATIC SURVEYS OF INFRARED VARIABLE STARS. Charles Hetzler 59

CONTRIBUTIONS TOWARD A PHYSICAL MODEL OF γ CASSIOPEIAE. Ralph B. Baldwin 82

THE KINETIC TEMPERATURE OF THE SOLAR REVERSING LAYER. Pearl J. Rubenstein 114

RECENT EVIDENCE ON THE NUCLEAR REACTIONS IN THE CARBON CYCLE. H. A. Bethe 118

SPECTROPHOTOMETRIC OBSERVATIONS OF THE MINIMUM OF ζ AURIGAE. C. A. Wirtanen 122

NOTES

NOTES ON PROPER-MOTION STARS. G. P. Kuiper 126

NUMBER 2

TRANSITION PROBABILITIES OF FORBIDDEN LINES. Simon Pasternack . 129

ACCIDENTAL AND SYSTEMATIC ERRORS IN SPECTROSCOPIC ABSOLUTE MAGNITUDES FOR DWARF Go–K2 STARS. Gustaf Strömberg . . . 156

GALACTIC ROTATION AND ABSORPTION. Ralph E. Wilson 170

THE MEAN COEFFICIENT OF SELECTIVE ABSORPTION IN THE GALAXY. Joel Stebbins, C. M. Huffer, and A. E. Whitford 193

ON THE CLUSTERING TENDENCIES AMONG THE NEBULAE. Erik Holmberg 200

A NOTE ON THE EVOLUTION OF EXTRAGALACTIC NEBULAE. Gunnar Randers 235

ON THE POSSIBLE EXISTENCE OF FORMALDEHYDE IN THE ATMOSPHERE OF VENUS. Rupert Wildt 247

PAGE

On the Classification of the A Stars. I. The Spectral Types of the Brighter Members of the Hyades Cluster. John Titus and W. W. Morgan 256

A Spectrophotometric Study of Nova Lacertae, 1936. Daniel M. Popper 262

DO Aquilae 1925—an Unusual Nova of the Nova Pictoris 1925 Type. B. Vorontsov-Velyaminov 283

The Spectrum of NGC 6543 and Its Nucleus. P. Swings 289

The Nebular Spectra of Two Slow Novae, DQ Herculis and RT Serpentis. P. Swings and O. Struve 295

The Galactic Clusters NGC 6649 and NGC 6694. James Cuffey . 303

Notes

Six New Be Stars. Orren Mohler 315

The Spectrum of the Companion of α Scorpii. O. Struve and P. Swings 316

Erratum 318

Reviews 319

NUMBER 3

The Internal Temperature of White Dwarf Stars. R. E. Marshak 321

The Systematic and Accidental Errors of Spectroscopic Parallaxes. Henry Norris Russell and Charlotte E. Moore 354

The Light-Curve of ζ Aurigae. William H. Christie 392

Spectroscopic Observations of Barnard's Variable in Messier 3. Alfred H. Joy 396

The 48-Inch Schmidt Telescope for the Astrophysical Observatory of the California Institute of Technology. Frank E. Ross . . 400

Physical Processes in Gaseous Nebulae. X. Collisional Excitation of Nebulium. Malcolm H. Hebb and Donald H. Menzel . . 408

Relative Frequencies of Meteors. J. D. Williams 424

Proper Motions in the Galactic Cluster Messier 39. E. G. Ebbighausen 434

Notes

Note on Algol. John S. Hall 440

Errata 440

The Dynamics of Stellar Systems. IX–XIV. S. Chandrasekhar . . 441

Index 643

NOTICE TO SUBSCRIBERS

* * *

FROM NOW ON the *Astrophysical Journal* will appear six times a year, making two volumes of three issues. In 1939 the *Journal* printed 1458 pages, the largest number in its history. It is the desire of the editors to maintain the present amount of material in each volume, or to increase it, if there should be a demand for such an increase. However, the war in Europe has resulted in a serious decline in income from foreign subscriptions and the proposed change is required in order to reduce expenses.

OTTO STRUVE, *Managing Editor*

THE ASTROPHYSICAL JOURNAL

AN INTERNATIONAL REVIEW OF SPECTROSCOPY AND ASTRONOMICAL PHYSICS

VOLUME 92 JULY 1940 NUMBER 1

ON THE INTERPRETATION OF SPIRAL STRUCTURE IN THE NEBULAE*

BERTIL LINDBLAD

ABSTRACT

The development of spiral structure in the nebulae is discussed in adherence to principles expressed in earlier papers but with a strenghthening of some of the arguments and renewed comparison with observed conditions.

The series of types of increasing flattening among the extragalactic nebulae is interpreted as a series of increasing angular momentum when this quantity is considered in relation to the mass and mean density of the system. An internal condensation leading to an increase of flattening may be the formation of small solid particles in gaseous material and the formation of the stars themselves in an original extended medium.

The instability of matter at the edge of a rotating stellar system of great flattening is discussed, and the mechanism by which a spiral arm may be formed in a steady process of disturbed motion is described, with reference to the properties of the characteristic diagram of the system. The reasons for the natural selection of a type of disturbance giving two spiral arms, extending from two opposite points which are fixed in space, are explained, and the possible analogy with the sectorial harmonic wave which makes the Maclaurin ellipsoid unstable at a certain flattening is mentioned.

Previous work had indicated that the full development of spiral structure is likely to give an approximately *logarithmic shape of the arms, in which the particles of the arm describe roughly circular orbits of uniform angular velocity around the center.* It is concluded here that such a formation is possible. Still, the process of segregation leading to such a formation is perhaps of a more complicated nature than indicated by the schematic theoretical picture.

The characteristics of the "amorphous" central system of a nebula, its successive formation, the physical character of the individual stars—which appear to be dwarf stars of late type, in contrast to the more massive white stars in the spiral arms—and the angular velocity of rotation are discussed. The normal case is probably the one where the nuclear regions rotate with a higher angular speed than the spiral structure. An exception is perhaps found in the barred spirals, where the "bar" is possibly to be considered as a remnant of a kind of interior spiral structure and has, presumably, a low angular speed of rotation.

* This paper was presented at the symposium on galactic and extragalactic structure, held in connection with the dedication of the McDonald Observatory on May 5–8, 1939.

The verification of the theoretical results by observational data is discussed in some detail. H. W. Babcock's results concerning the rotation of the Andromeda nebula are in good agreement with the main theoretical result concerning the possibility of a uniform rotation of the spiral structure.

The question of orientation of the nebular plane is discussed for the Andromeda nebula, for M 81, and for twelve typical nebulae which show different degrees of development of the central mass. The formation of characteristic lanes on the near and the farther sides of the nebular disk is discussed. The relative arrangement of bright and dark matter in nebulae of small central mass, the polarization of light in the dark clouds as observed by Öhman, and the different illumination of dark clouds on the near and farther side, respectively, are factors of great importance in this connection. The evidence seems to be in favor of the theoretical result that the rotation is in the direction in which the spiral arms wind when followed outward from the center. In the case of "spindle" nebulae, where the apparent direction in which the spiral arms wind cannot be determined directly, the intensity distribution along the major axis may indicate the side of concave and convex arms, respectively, as seen by the observer.

A method of deriving the direction of rotation independently of the dark lanes in a tilted nebula is afforded by the phenomenon of a spiral arm breaking up into a fan-shaped structure of secondary branches. In the absence of detailed observations of the velocities of rotation for the individual branches, the assumption of a uniform value of the area constant has been made. The arms of the nebula M 101 then give a direction of rotation in agreement with the theory.

The main principles of the theory of the development of spiral structure in the nebulae which will be discussed below have been presented in previous papers.[1] A review of the general line of thought of the theory will be given here, with references to previous papers for some of the details, but in a development which to a considerable extent brings new points of view into the discussion. The important question of the observational test of some of the fundamental conclusions will be approached as far as appears to be possible at present.

A fundamental fact which is of the greatest importance for an interpretation of the phenomenon of spiral structure is the appearance of the spiral type of nebula as a natural continuation of a series of elliptical types of increasing degree of flattening. This feature has been recognized very fully by Jeans[2] in his theory of the development of spiral structure. It lies very near at hand, from a general theoretical point of view, to assume that this series of types corresponds

[1] "Cosmogonic Consequences of a Theory of the Stellar System," *Ark. mat., astr. och fys.*, 19A, No. 35, *Upsala Medd.*, No. 13, 1926; "On the Spiral Orbits in the Equatorial Plane of a Spheroidal Disk," *K. Sv. Vetenskapsakademiens Handlingar*, **4**, No. 7, *Upsala Medd.*, No. 31, 1927; "Contributions to the Theory of Stellar Systems," *Stockholm Ann.*, **12**, No. 4, 1936; "On the Theory of Spiral Structure in the Nebulae," *Zs. f. Ap.*, **15**, 124, *Stockholm Medd.*, No. 40, 1938.

[2] *Problems of Cosmogony and Stellar Dynamics*, Cambridge University Press, 1917; *Astronomy and Cosmogony*, Cambridge University Press, 1928.

to an increase of the angular momentum, considered in a certain relation to the mass and the mean density of the system. In the case of the series of homogeneous Maclaurin ellipsoids, if H is the angular momentum, M the mass, and ρ the density, the quantity

$$HM^{-5/3}\rho^{1/6} \tag{1}$$

is a function only of the flattening of the system. We may assume that the increase of flattening in the case of stellar systems corresponds to an increase of an analogous quantity, where ρ is a representative mean density. It is possible that one and the same mass, with a given value of the angular momentum H, may go through successive forms of equilibrium on account of an internal process of condensation. We may have in mind here a condensation of interstellar gas into small, solid particles and even the formation of the stars themselves in an original, extended medium. We must consider in the first place, however, that in all probability the systems were "born" with a wide range in angular momentum and that the variation of type is thus to a great extent dependent on original conditions.

When treating the dynamics of the nebulae, we may consider the mass motions of matter in a way which is in several respects analogous to the developments of hydrodynamics and the dynamics of gases. A fundamental difference, however, lies in the circumstance that in stellar systems the motions of the individual particles must be considered as free motions under the gravitational forces of the system. The assumption made in hydrodynamics that a small closed surface, supposed to move with the fluid, will always inclose the same matter cannot be true here, even approximately, for any great length of time.

The special clue to an understanding of the development of spiral structure which forms the foundation of the present theory starts from the properties of individual motions close to the edge of a flattened system. Moreover, this theory has immediate connection with the theory of galactic rotation. We know that in our own galactic system there is, according to this theory, a concentration of matter toward the circular motions. When examining the circular mo-

tion at the edge of a system of great flattening toward the plane of rotation, which we assume to be an equatorial plane of symmetry, we find that at a certain degree of flattening the circular motion at the edge becomes unstable, and by an infinitely slight disturbance the particle will depart in an asymptotic orbit which at first winds in a close spiral around the system but at greater distances departs rapidly from the system. After attaining a certain maximum distance, the orbit returns symmetrically toward the original circular motion. In the case of a spheroidal, homogeneous system the instability begins at the ratio 0.55 between the polar and equatorial axes of the spheroid, corresponding to an eccentricity of the meridian section amounting to 0.834. With increasing flattening, the maximum distance of the orbit increases; for an infinite degree of flattening, the maximum distance extends to infinity. If the system has symmetry of rotation, as well as an equatorial plane of symmetry, the component of force at right angles to the equatorial plane close to this plane may be written

$$\frac{\partial V}{\partial z} = -4\pi G\bar{\rho}z\,, \tag{2}$$

where G is the constant of gravitation, and z is the elevation above the equatorial plane. The condition for the appearance of the instability then is

$$\frac{\omega_c^2}{2\pi G} \leq \bar{\rho} - \rho\,, \tag{3}$$

where ω_c is the angular velocity of the circular orbit and ρ is the density of matter at the point considered. This relation may be written

$$\frac{\omega_c^2}{2\pi G\bar{\rho}} + \frac{\rho}{\bar{\rho}} \leq 1\,. \tag{4}$$

The first term may be assumed to decrease continuously with increasing degree of flattening of the system, in analogy with a corresponding quantity in the case of the equilibrium figures of liquid spheroids. The second term depends more on local conditions. A low value of this term is likely to occur if there is a rapid increase of

density with distance in the equatorial plane in the neighborhood of the point considered. This may be fulfilled in particular if there is a strong radial density gradient in the equatorial plane close to the point in question.

The instability may be fully described by the so-called "characteristic diagram," which has the energy I_1 and the area velocity I_2 of a particle as axes. If Π, Θ, and Z, are the velocity components in the radial, tangential, and vertical directions, respectively, and if, further, V is the potential and R the distance from the axis of rotation, we have

$$\left.\begin{aligned} I_1 &= \Pi^2 + \Theta^2 + Z^2 - 2V \\ I_2 &= R\Theta\,. \end{aligned}\right\} \tag{5}$$

The region in the diagram which represents possible combinations of I_1 and I_2 at a given point in the system is bounded by a certain parabola, and the region of possible combinations of I_1 and I_2 for the system as a whole is defined by a certain curve, the "characteristic envelope-curve," which ordinarily represents the envelope of the characteristic parabolae for successive values of R in the equatorial plane. The point of contact between a characteristic parabola and the envelope represents the circular motion in this plane for the value of R in question. For homogeneous spheroidal systems the envelope-curves for the interior part of the system are straight lines, as shown in Figure 1. In a more general case, which is illustrated in Figure 2, the angle φ between the tangent of the envelope-curve and the I_2 axis obeys the relation

$$\tan \varphi = 2\omega_c\,, \tag{6}$$

where ω_c is the angular velocity of the circular orbit for the value of I_2 in question. In the case of an instability at the edge, the envelope-curve of the outer regions recedes "backward" from a turning-point P_2 to another turning-point P_1, so that in this interval I_1 and I_2 decrease with increasing R, whereas for the regions of stable circular orbits, I_1 and I_2 increase with R. In this case the I_1, I_2 diagram may be divided into three parts,[3] two situated below the singular part

[3] Cf. *Bergstrand festskrift*, p. 23, 1938.

P_1P_2 of the envelope-curve and one above this part of the curve. Points in the last-mentioned region represent particles which under some circumstances may depart from the central system in wide orbits.

We must now consider that the real significance of the development of the singular course of the envelope-curve will be that a great part of the matter situated close to the edge of the system moves in a state close to instability, though still in stable orbits. It should be expressly remarked that a point in the diagram above P_1P_2 does

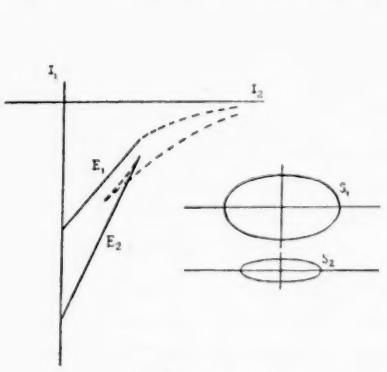

FIG. 1

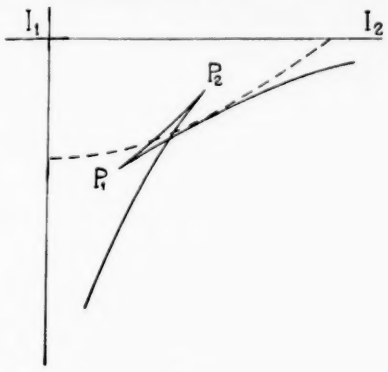

FIG. 2

FIG. 1.—The characteristic diagram for homogeneous spheroids

FIG. 2.—The characteristic diagram for a general system of rotational symmetry and great flattening.

not necessarily, at least for a considerable time, correspond to an orbit of ejection. If the particle has a finite motion in z, it may still remain entirely within a region of stable orbits, passing through the equatorial plane with a finite value of the velocity component Z. The successive development of an instability of the kind in question, however, would lead to an ejection of a certain amount of matter across the circle where the instability begins. In the first instance this would tend to smooth the radial density gradient at this circle and thereby to counteract the development of the instability by making $\rho/\bar{\rho}$ increase in the region of instability. A further increase of the flattening, however, leading to a further increase of $\bar{\rho}$ and thereby to a decrease of the first term in equation (4) and a restoration of the instability, would not mean an immediate ejection of any

considerable amount of new material, as the matter likely to be ejected at the circle of instability has already been supposed to have crossed this circle. A further development of the instability by further increase of the flattening of the system would make all the ejected matter recede to greater distances. For this reason and by the increased density of the central system due to the increase of flattening and the general contraction, we may expect in the first instance the formation of a central lens with a fairly sharp edge and at the same time around the central lens the appearance of a faint ring-shaped structure formed by the ejected matter. According to observations by Hubble,[4] this seems to agree well with what is actually observed in those nebulae which represent the transition from the elliptical to the spiral type.

The ejection of matter will not, in general, be perfectly evenly distributed around the edge, and on account of this fact the assembled mass of the ejected matter will exert a complicated disturbing action on the central system. By the law of areas in the motion of the ejected matter this will have a general tendency to recede along the edge relative to the matter following the circular motion here, in a direction opposite to the direction of the circular motion. According to Hubble, it seems as if the dark matter in the outer parts of the central lens would be most sensitive to the disturbing forces, which might possibly be attributed to an increased radiation pressure on such matter helping to upset the balance by reducing the net central force. In an advancing disintegration we are most interested in a type of ejection which is of a steady character, in which the ejection continues steadily by the tidal action of the previously ejected matter. A possible disturbance of this type is shown in Figure 3. In this case the point of ejection is supposed to be fixed in space. The relative displacement of the ejected matter from its original position at the edge to the positions in the "arm" causes a tangential disturbing force at T. We may now construct the characteristic envelope-curve along the path OTS and compare it with the envelope-curve along the radius under undisturbed conditions (E_0 in Fig. 3). The curve E_{OTS} will be depressed relative to E_0 in about the way indicated. In

[4] Communicated by Dr. Hubble in a lecture at the dedication of the McDonald Observatory in May, 1939.

particular, the increased depression of the "receding" part of the envelope-curve will cause a considerable amount of matter arriving at T with representative points above this part of the curve to follow the arm TS in orbits of ejection. The diagram explains the way in

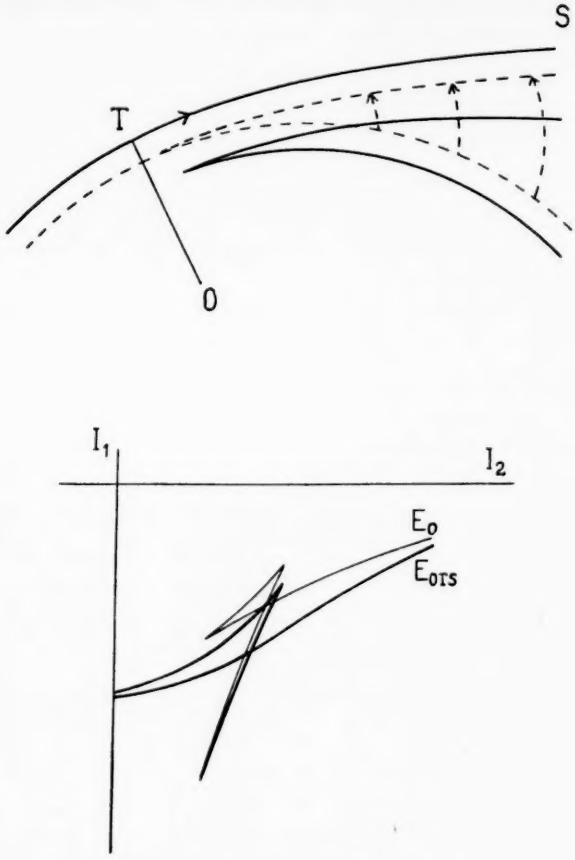

FIG. 3.—The formation of a spiral arm

which the edge of the central system is successively "cut off" to form the arm.

We may ask if other assumptions regarding the speed of the point of ejection T are possible. If we introduce a rotating co-ordinate system moving with the angular speed ω, in order to follow the matter at the edge, we have assumed above that the point of ejection

moves in the rotating co-ordinate system with the relative angular speed ω in the direction against the rotation. It is clear that the speed actually selected will depend not only on the kind of tidal force which is developed as a consequence of this speed but also on the resonance of the disturbing action with the free oscillation of the particles. If the system has approximately uniform angular velocity of rotation ω, the speed of internal density variations in a co-ordinate system following the rotation will be approximately 2ω.[5] If the disturbance is in resonance with this oscillation, its intensity at the edge, which we may measure by the intensity of the tangential force in the direction of rotation, may be developed in a series

$$\sum_n (A_n \cos [2\omega t + n\theta] + B_n \sin [2\omega t + n\theta]) . \qquad (7)$$

For disturbances proceeding against the velocity of rotation, n is positive. The value $n = 1$ gives a disturbance with only one maximum along the circumference, proceeding with the speed 2ω against the velocity of rotation. It does not seem that an arm produced by such a disturbance would, in general, give a sufficient disturbing force.[6] The case $n = 2$, however, corresponds to a disturbance with two opposite maxima, proceeding with the relative speed ω against the velocity of rotation, i.e., fixed in space. The contraction of the matter in the arm due to the law of areas in the motion from the fixed point of ejection will cause a considerable disturbance at this point, as explained above in reference to Figure 3. For higher values of n the disturbance becomes more complicated, as the number of maxima around the circumference increases. It seems, therefore, probable that the tidal force will be most effective in the case $n = 2$, in which case we should expect the appearance of two diametrically opposite spiral arms, in agreement with observation.

If an ejection process of the kind just described is present at a certain moment, it may either decrease or increase with time. In the former case the system is stable for a disturbance of this type; in the latter, unstable. It is evident that the instability will be favored

[5] Cf. *Zs. f. Ap.*, **15**, 132, 1938.

[6] An exception may be a nebula with one main arm like NGC 4725 on Pl. II.

by a great flattening of the system, which gives asymptotic orbits of wide extension. This may be seen also by reference to the sectorial harmonic waves in the case of a rotating homogeneous ellipsoid. The proceeding disturbance $n = 2$ in our case has a certain analogy to the two-dimensional, sectorial harmonic wave of two opposite maxima, which makes the Maclaurin ellipsoid "ordinarily" unstable at the eccentricity $e = 0.9529$ of the meridian section.[7] The spiral arms may perhaps be considered as the advancing front of such a wave of steadily increasing amplitude, proceeding with higher angular speed than the wave as a whole, which in the case of the liquid has the speed $\omega/2$ against the direction of rotation. We may then expect the spiral phenomenon to take place at a flattening corresponding to about the eccentricity $e = 0.95$ of the meridian section. This corresponds to the ratio of the axes in this section equal to 0.3 and seems to agree well with the limiting flattening of the elliptical nebulae where these merge into the spiral type.

In the case of nebulae of fairly thin arms, like M 81, we should expect the arms to follow the asymptotic orbits from the circular motion at the edge. It is actually found that the arms of M 81 correspond very well to the asymptotic orbits for an eccentricity $e = 0.965$ of the meridian. When the disintegration of the central system becomes more complete, however, the spiral arm no longer represents the orbit of an individual particle. On account of the successive decrease of the central system, the particles must instead be expected to describe approximately circular orbits entirely outside of the remaining nucleus. Under these circumstances I have shown[8] that a roughly logarithmic form of the arms may be expected and that the speed of rotation of such a spiral structure may be approximately uniform, if the original system was one of uniform angular speed.

In the asymptotic orbit extending from the edge of a flattened system, the ratio of the centrifugal force at the point of maximum extension to the centrifugal force at the edge of the central system will be f^{-3}, if f is the ratio of the radii vectors for the two positions. The ratio of the central forces will only slightly exceed the value

[7] Bryan, *Phil. Trans. R. Soc. London*, **180**, 187, 1889.

[8] *Zs. f. Ap.*, **15**, 133, 1938.

f^{-3}, which makes the orbit at the maximum distance adhere rather closely to a circular orbit. The slight excess of the ratio over f^{-3} makes the orbit return toward the center. In the case of a development of heavy spiral structure, however, the contraction of the remaining central system and the decrease of its mass due to the departure of matter in the spiral arms will mean a decrease of the central force at the maximum distance of the orbit, and the ejected matter will, therefore, no longer return to the central system. The balance of centrifugal and central force in approximately circular motion may thus be restored in the spiral structure.

The logarithmic shape of the arms,

$$r = Ce^{c\theta}, \qquad (8)$$

follows if we assume the distances from the center in the spiral structure to be proportional to the distances from the center in the original system and the radial thickness of the arm to be proportional to these distances, taking into account also the contraction of the arm in its own direction at larger distances from the center, which follows by the law of areas in the motion. If the original system has roughly uniform angular velocity of rotation, this will evidently be the case also for the spiral structure under these assumptions. That the central force in the spiral structure will be roughly proportional to the distance from the center may be seen in the following way. In the schematic picture of the two spiral arms in Figure 4, we consider the radial component of force at two consecutive intersections P_n and P_{n+1} of an arm with the vertical line through the center. We denote the force at the lower point with F_n, at the upper point with F_{n+1}. We further denote with F'_{n+1} the force at the upper point when we prolong the spiral arms as shown by the dotted curves. Assuming the radial thickness of the arm to be proportional to the distance from the center and the thickness at right angles to the plane of the figure

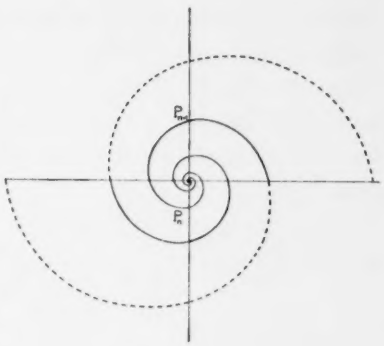

FIG. 4

to be small and one and the same throughout the structure, we should have

$$F'_{n+1} = F_n \,, \tag{9}$$

because the difference between the two cases is one of scale only. The mass of similarly situated parts in the two cases increases as the square of the scale factor and thus balances everywhere the effect of the scale factor on the inverse square of the distances. In order to obtain F_{n+1}, we must subtract from F'_{n+1} the gravitational force due to the dotted parts of the arms. We propose to calculate first this force on a point P situated on the vertical line at the distance a from the center. We take the positive x axis upward in the figure and count the angle θ from this direction. We denote the distance from the center for a point on the spiral arm with r, and the distance from the point P with ρ. The mass dm of a part of the spiral arm corresponding to an interval $d\theta$, when we assume the radial thickness of the arm to be proportional to r, may be expressed

$$dm = \mu r^2 d\theta \,, \tag{10}$$

where μ is a certain constant. If the spiral structure expands, μ will keep its value unchanged on account of the constancy of $r^2 d\theta$ in the motion. The force G_1 in the x direction exerted on P by the upper dotted part of the spiral arm will be

$$G_1 = \int_{-\pi/2}^{+\pi/2} \frac{\mu r^2}{\rho^3} (x - a) d\theta \,, \tag{11}$$

where

$$\rho = (r^2 + a^2 - 2ar \cos\theta)^{1/2} \,, \qquad r = Ce^{c\theta} \,, \qquad x = r \cos\theta \,.$$

We may develop in powers of a/r and assume $a/r < 0.4$, so that

$$1 > \left(\frac{a}{r}\right)^2 - 2\frac{a}{r}\cos\theta > -1 \,.$$

In this case we know that the rest term in the development of ρ^{-3} will be of the order of the first term omitted. In the present case the

terms of even order in a have no influence on the final result, and the third-order terms may be shown to have only small influence. We are, therefore, entitled to consider, as an approximation, a development keeping only the terms of the first order, and we get

$$G_1 = \mu \int_{-\pi/2}^{+\pi/2} \left(\cos\theta - \frac{a}{C} e^{-c\theta} + \frac{3a}{C} e^{-c\theta} \cos^2\theta \right) d\theta .$$

In the third term, which contains $\cos^2\theta$ as a factor, we may with very good approximation take together numerically equal θ of opposite sign and for the factor $e^{-c\theta}$ take the geometrical mean, which is equal to unity. Then by performing the integration, we obtain

$$G_1 = 2\mu + \frac{\mu a}{Cc} \left(e^{-c(\pi/2)} - e^{+c(\pi/2)} + \tfrac{3}{2} c\pi \right) .$$

The force G_2 due to the lower dotted part of the spiral arm is obtained by changing the sign of G_1, after changing the sign of a. Adding together, we get

$$G_1 + G_2 = \frac{2\mu a}{Cc} \left[\tfrac{3}{2} c\pi - \left(e^{+c(\pi/2)} - e^{-c(\pi/2)} \right) \right] = ka . \qquad (12)$$

Thus, in the first approximation the combined gravitational force of the dotted parts of the spiral arms in Figure 4 is directed outward along the radius and is proportional to the distance from the center. We have, then, in particular for the points on the spiral arms considered above

$$F'_{n+1} = F_{n+1} + kr_{n+1}$$

or, by equation (9),

$$F_{n+1} - F_n = -kr_{n+1} = -\kappa(r_{n+1} - r_n) , \qquad (13)$$

where the constants k and κ obey the relation

$$\kappa = \frac{k}{1 - e^{-c\pi}} . \qquad (14)$$

We may now repeat the process for two similarly situated points which we denote by P_{n-1} and P_n and obtain, in an analogous way,

$$F_n - F_{n-1} = -\kappa(r_n - r_{n-1}) .$$

Assuming the two spiral arms to wind indefinitely inward to an infinitely small distance from the center, we may put

$$\left.\begin{aligned} F_{n-i+1} - F_{n-i} &= -\kappa(r_{n-i+1} - r_{n-i}) , \\ F_{n-i+2} - F_{n-i+1} &= -\kappa(r_{n-i+2} - r_{n-i+1}) , \\ &\cdots\cdots\cdots\cdots\cdots , \\ F_{n+1} - F_n &= -\kappa(r_{n+1} - r_n) . \end{aligned}\right\} \tag{15}$$

Thanks to the small but finite thickness at right angles to the spiral plane, we may assume F_{n-i} to vanish with r_{n-i} for very large values of i. Equations (15) are still valid without perceptible changes of κ. Adding together equations (15), we get as the general expression for the radial force

$$F = -\kappa r \tag{16}$$

for points along the arms. That the result will hold approximately also for other sections through the center than the one just considered can easily be verified.

We may now calculate, on the same assumptions, the change of the radial force F_p on one and the same particle of an arm by an expansion of the spiral structure in the ratio f, during a motion obeying the law of areas. The coefficient c will increase in the ratio f^2 to $c_0 f^2$, say, if c_0 is an initial value. The coefficient C, when θ is reckoned as before, will obey the relation

$$C \sim f e^{c_0 f^2(\pi/2)} . \tag{17}$$

The coefficient k will change as follows:

$$k \sim \frac{1}{c_0 f^3 e^{c_0 f^2(\pi/2)}} \left[\tfrac{3}{2} c_0 f^2 \pi - \left(e^{c_0 f^2(\pi/2)} - e^{-c_0 f^2(\pi/2)}\right)\right] . \tag{18}$$

The force $F_p = -\kappa r$, when r increases in the ratio f, is finally found to be

$$F_p \sim -\left(e^{c_0 f^2(\pi/2)} - e^{-c_0 f^2(\pi/2)}\right)^{-1} + \frac{2}{3\pi c_0 f^2}. \qquad (19)$$

For observed spiral arms, which according to Danver correspond in the mean nearly to $c\pi = 1$, the rate of change of the central force according to formula (19) lies between f^{-2} and f^{-3}, but for slightly larger values of c the rate of change becomes much accelerated and more rapid than f^{-3}. According to equation (19), F_p may even pass zero and become positive for very great values of $c_0 f^2$. Though this cannot be true for the outer regions in higher approximations, it seems that we may draw the conclusion that the spiral structure would become unstable for very large values of $c_0 f^2$.

Though we must keep in mind that the numerical results will of course be subject to modifications if the schematic assumptions regarding the mass distribution are changed, the considerations above show the harmony between, on the one hand, a logarithmic shape of the arms and a uniform speed of rotation deduced from the process of disintegration and, on the other hand, the gravitational forces to be expected along the arms in a fully developed spiral structure. The assumption of uniform thickness of the arms in the direction at right angles to the spiral plane may be justified by the circumstance that the mass detached to form the spiral arms probably constitutes a higher percentage of the entire mass in the outer regions of the system than in the inner regions. On the other hand, for this reason we must take into account a remaining central mass not included in the spiral structure. In the case of very well-developed spiral structure, however, we assume this remaining central mass to be small compared with the mass of the arms, which seems to be a reasonable assumption from the actual appearance of such nebulae.

The adjustment assumed above between the centrifugal force and the central force at the maximum distance in the asymptotic orbit is, of course, a somewhat schematic assumption. An adjustment to balance in circular motion may mean considerable shifts in the radius vector. Furthermore, it is not to be excluded that the final motion at various points may differ perceptibly from the circular motions and

may include pulsating motions in the radial direction. The value of the coefficient c in equation (8), when determined from observed spirals, agrees, however, with the assumption of an adjustment into circular orbits at distances from the center which, at least to the order of magnitude, agree with the maximum distances in asymptotic orbits. We have, approximately,

$$c = ab^2 , \tag{20}$$

where πa is the ratio between the radial thickness of the arm and the original distance from the center and b is the ratio between the distance from the center in the spiral structure and the original distance from the center. If v is the angle between the radius vector and the tangent of the arm, we have

$$c = \frac{1}{\tan v} . \tag{21}$$

According to Danver,[9] v is close to 74°, which gives c close to $\frac{1}{3}$.

We may also look upon this problem from the point of view of the virial theorem. If a system with constant energy settles over from one equilibrium form to another, the potential energy must be the same in the two cases. The increase of potential energy due to the expansion in radius vector will be partly compensated by the decrease of potential energy due to the contraction of the arms in their own direction, which is a consequence of the law of areas, but to some extent the compensation will also be due to a contraction of the remaining central mass. Such a contraction must follow when a considerable part of the outer regions departs to greater distances, which must give an increase of the central force on the remaining matter. The angular speed of the central mass will increase by the contraction, which will, in a way, favor the continued development of spiral structure in this mass, but the angular momentum of the central mass will, nevertheless, decrease successively, and at last the central system remains only as an "amorphous" elliptical mass. This mass may have a high angular speed of rotation, but in spite of this, by a high degree of concentration toward the nucleus it will possess

[9] *Vierteljahrschrift*, **72**, 340, 1937.

too low an angular momentum to take on a very much flattened figure of equilibrium. We thus get the typical picture of the nebula as a spiral structure surrounding an apparently "amorphous" central system of low degree of flattening and of strong concentration toward a dense nucleus. The characteristic difference in color between the spiral arms and the nuclear regions can then be explained. The nuclear regions contain stars which have formed outside of the equatorial plane, often with smaller original velocities of rotation than the stars which follow circular orbits in this plane at the same distance from the center. The former stars, which have a tendency to condense toward the center, are mostly dwarf stars of advanced color. The abundance of matter with low internal velocity in the neighborhood of the equatorial plane, on the other hand, favors the development of massive stars of high surface brightness in these regions. These heavy stars thus belong to the rotating "subsystem" which contributes most of the material to the spiral structure.

We have considered heretofore a uniform angular motion of a fully developed spiral structure as a quality which may follow from the geometrical and dynamical properties of a process of dissolution of an original closed central system, when the process takes place from the edge inward. We must consider, however, that the picture thus given of the dissolution into spiral structure is possibly a considerable simplification of the real process as it actually occurs in nature. It is probable that in many cases the dissolution begins at various points in the original rotating mass, at different distances from the center where instabilities of motion originate. The spiral arms may develop to more and more distinct features and catch in their whorls the matter of greatest angular momentum and of low internal velocity dispersion, by a process similar only in its broad lines to the one which we have described. It is possible that in this way an exchange of momentum over different intervals of distance from the center may take place along the spiral arms in such a way that in a regular, fully developed spiral structure the uniformity of angular speed becomes well realized.

This does not mean, however, that one and the same angular speed prevails throughout the entire system. We have seen that the central regions where the spiral structure is not fully developed are

likely to possess a higher angular speed than the spiral structure. This should apply especially to the elliptical mass immediately surrounding the nucleus, which in several nebulae is known to have a high and uniform angular speed. The region of transition between the spiral structure and the central mass may be expected to show complicated conditions. In the Andromeda nebula this region shows traces of spiral structure, especially in the dark markings, which is probably due to direct tidal effects of the surrounding main spiral arms. A complicated variation of the observed angular speed with distance from the center may be expected here, as has actually been observed at the Lick Observatory by H. W. Babcock.[10]

In the case of the "barred" spirals the conditions in the nuclear regions may deviate still more strongly from normal conditions. With "normal conditions" we mean here the case when the nuclear regions show an increased angular speed compared with the spiral structure. It is possible that the "bar" is a remnant of a kind of inner spiral structure, more developed than in the case of the Andromeda nebula, and perhaps caused by, but largely independent of, the outer spiral structure. The degeneration of this inner spiral structure into a straight bar, presumably by a process of extension, would suggest that the angular speed of rotation of the bar structure is low, perhaps equal to or even smaller than the rotation of the outer structure.

We shall at last proceed to consider the verification by observation of some of the vital points in the theory developed above. The conclusion that a uniform angular speed of rotation may prevail in a fully developed spiral structure agrees well with Babcock's observations of the variation of the radial velocity along the large axis of the Andromeda nebula. In particular, the very high velocities observed by him for a couple of gaseous nebulae situated outside of the main spiral structure are of extremely great interest. The fact that these nebulae seem to belong to secondary branches of the main spiral arms is important in this connection. If they have the same area constant in their motion around the center as the neighboring parts of the main arm, we should expect the linear velocities of the extreme parts of the main arm to be still higher, which would actual-

[10] *Pub. A.S.P.*, **50**, 174, 1938.

ly improve the linearity of the variation of the velocity with the distance from the center in Babcock's diagram. The variation in the region of transition between the nuclear regions and the main spiral structure has been found[11] to stand in intimate connection with the distribution of light in the region in question. If we multiply the intensity I with the distance R from the center, this product has a minimum where Babcock finds the minimum velocity. It is possible that this fact may have something to do with the diffuse spiral structure in this region and that the matter left between the nuclear region and the diffuse spiral arm has a low velocity of rotation. It is also possible that we are concerned here with a higher level in the nebula. The minimum of IR may be due partly to interior absorption in the nebula, which prevents us from penetrating here to the more rapidly rotating equatorial layers of matter. In this connection it may be added that the importance of the absorption of light in the interior of stellar systems for the interpretation of spectrographic observations of internal motions has recently been emphasized by E. Holmberg.[12] He shows how a strong internal absorption in a nebula seen edgewise may cause an apparently uniform rotation. In the case of the nuclear regions of the Andromeda nebula it does not seem probable, however, that the linear variation of velocity may be caused to any great extent in this way. The decreasing flattening of the isophotes surrounding the strong nucleus (Fig. 5) suggests that the nucleus is fairly transparent for the angle of incidence under which we see the nebula. On the whole, the measured velocities are, therefore, probably fairly representative for the motion of matter close to the equatorial plane of the nebula.

The present theory favors the opinion that the direction of rotation of the system agrees with the direction in which the spiral arms wind around the center when followed outward from the central mass. In order to test this conclusion, we need, in the first place, observations of spectrographic rotations for typical spiral nebulae for which the true inclination toward the line of sight can be inferred with some degree of probability. An independent method based on the formation of secondary branches of spiral arms will be

[11] *Ark. mat., astr. och fys.*, 27A, No. 2; *Stockholm Medd.*, No. 45, 1939.

[12] *M.N.*, **99**, 650, 1939.

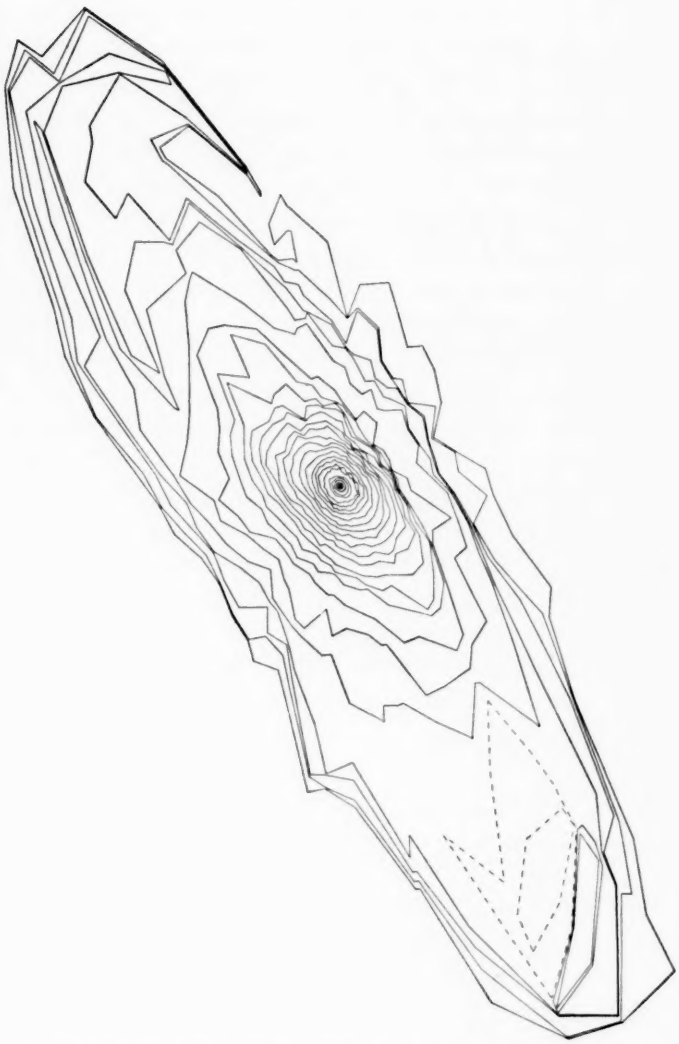

FIG. 5.—The photographic isophotes of the Andromeda nebula according to Lindblad and Ramberg.

mentioned below. When trying to solve the question of orientation of tilted nebulae from the appearance of the absorption lanes due to light absorption in dark matter, it is reasonable to begin with the great Andromeda nebula. A detailed photometric analysis of the nebula is in progress at the Stockholm Observatory, and a preliminary picture of the run of the isophotes, drawn as straight lines between different radii for which the intensity distribution has been measured, is given in Figure 5. The isophotes of individual dark clouds are not indicated in the figure, except in the southern (lower) part, where some isophotes which have been drawn as broken lines surround an intensity minimum due to certain widespread dark clouds. On the north-preceding side, however, when going outward from the center, the influence of the clouds on the general intensity distribution is especially visible in a sudden crowding of the isophotes along certain lanes. From the general appearance of the absorption, which, on the whole, proceeds from intense dark lanes stepwise in the direction away from the nucleus, I have drawn the conclusion that the part of the nebula which shows heavy obscuration is in all probability the one farther from us.[13] The obscuring clouds have probably considerable extension at right angles to the equatorial plane, and they may also be asymmetrically distributed in the angular co-ordinate around the center. An investigation by Öhman[14] on the polarization of light in the Andromeda nebula has strengthened the conclusion as to the orientation. He has found that the dark clouds near the minor axis on the north-preceding side of the nebula are slightly deeper and more marked in the polarized component, where the plane of vibration is perpendicular to the plane passing through the center of the nebula and the observer, than in the other component. This would mean a negative polarization of the light scattered in the clouds, which it would be possible to explain if the angle nucleus-cloud-observer is far from 180°. In this connection, the possibility of a different degree of illumination of the clouds on the near and the far side of the nucleus, respectively, on account of a different intensity of scattered light in the direction of the ob-

[13] *Ark. mat., astr. och fys.*, 24A, No. 21; *Stockholm Medd.*, No. 14, 1934; *Ann. d'ap.*, **1**, 173, 1938.

[14] *M.N.*, **99**, 624, 1939.

server, should be mentioned. As we must have a considerable flux of radiation from the central region outward, the angle center-cloud-observer should be of great importance for the intensity of diffused radiation if the diameters of the particles are of the order of the wave length of light. In general, for such particles the intensity of scattered light is much greater in a direction close to that of the incident beam than in directions forming an angle exceeding 90° with the direction of the incident light. Under such conditions we must expect clouds at angles close to 180°—i.e., clouds on the near side—to be more strongly illuminated, and hence less visible by contrast, than clouds for which the angle is small. If, in accordance with these indications, the north-preceding side of the nebula is the farther one from us, then the direction of rotation found by Slipher and by Pease[15] will be the direction in which the spiral arms wind outward, in accordance with our theoretical rule.

The difficulty of applying a criterion derived directly from the "spindle" nebulae is illustrated by M 81. Plate I gives two reproductions, with the same orientation, of a photograph of this nebula taken at the Lick Observatory, one showing only the nuclear region, which is ordinarily much overexposed in prints of the nebula, the other showing also the surrounding regions. In the first-mentioned picture there is a characteristic lane below and to the left of the nuclear region; in the second picture the lanes are stronger in the upper right-hand part. If the inner lane close to the nucleus is situated on the near side of the nebula, in analogy with the lanes of the spindles, then the orientation of the nebula is such that the rotation and the direction of the arms agree with the present theory, according to a determination of the direction of rotation by Babcock. Certain other details in the distribution of bright and dark matter in the nebula, especially the appearance and position of certain neatly defined dark lanes along the spiral arms, are strongly in favor of this conclusion. In such a case, however, the stronger appearance of the lanes in the right-hand part of Plate I on the farther side of the nebula, if it is not due to an actual dissymmetry of the distribution of dark matter in the angular co-ordinate, might be caused by an actual elevation of the dark matter in these regions of the central

[15] *Proc. Nat. Acad.*, 4, 21; *Mt. W. Comm.*, No. 51, 1918.

PLATE I

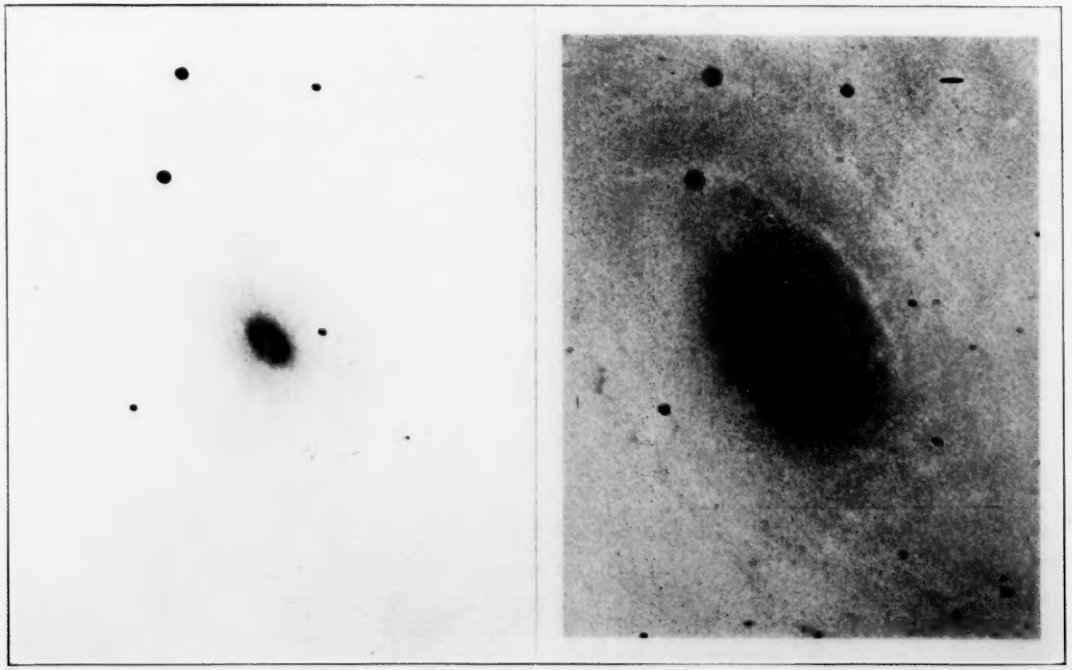

DARK LANES IN THE CENTRAL REGION OF THE NEBULA M 81

The left-hand picture shows lanes close to the nucleus; the right-hand picture shows lanes in the outer regions of the central system.

PLATE II

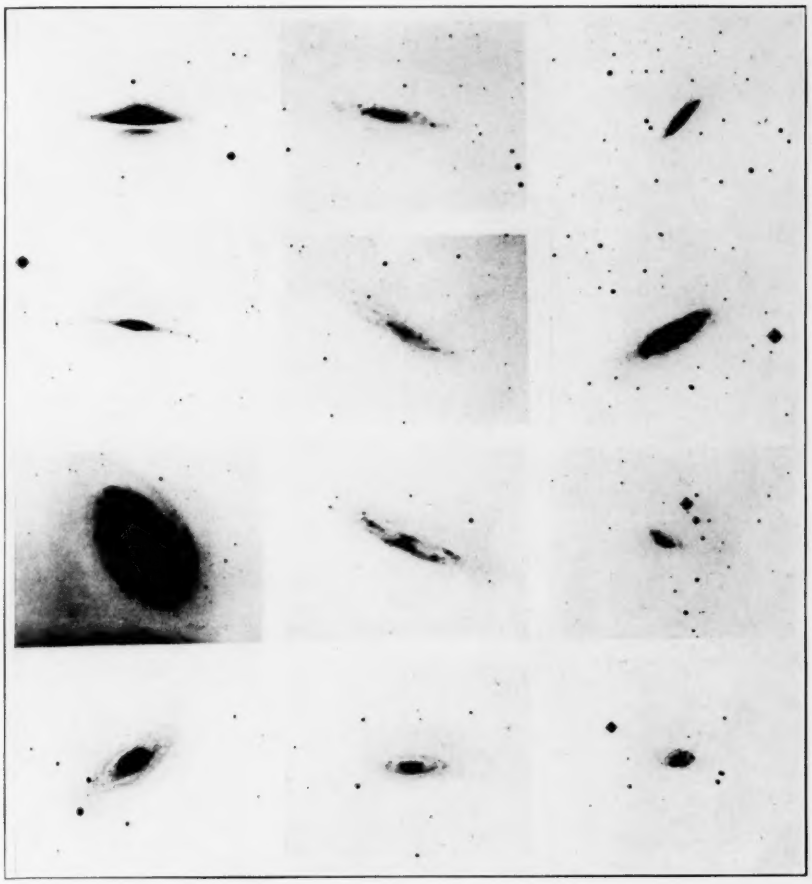

DIFFERENT TYPES OF TILTED NEBULAE

a–c, NGC 4594, 3003, 7817; *d–f*, NGC 5746, 1337, 6503; *g–i*, NGC 4725, 4192, 972; *j–l*, NGC 2841, 3675, 5678. Lick Observatory photographs, except NGC 4725, which is a Mount Wilson photograph.

system over the most intensely radiating layers close to the equatorial plane or may be an effect of a different illumination of the dark matter on the near and the far side of the central system. A combination of all these effects, in analogy with what has been said concerning a corresponding effect in the Andromeda nebula, is perhaps the most likely explanation.

An attempt to form a system of tilted nebulae of varying types is given here in Plate II. The nebulae are all orientated in the picture in such a way that the edge which is supposed to be the near one is turned downward (right or left), the farther edge upward. The three successive columns are intended to show different degrees of the development of central mass. The left-hand column shows early types with large amorphous central parts, the right-hand column shows nebulae of very small central mass, and the column in the middle shows an intermediate type.

The first nebula in the middle column shows unmistakably a lane on the near side analogous to that of the two real spindles in the first column. The central mass is small, and it is evident that the apparent disk has its maximum intensity close to the lane on the near side of the nucleus.

The second and third nebulae in the middle column are obviously related in type to the uppermost one. The third nebula in this column shows a very broad dark lane along the lower edge of the central system, though the faintly luminous lower border of the lane does not show well in the reproduction. A similar very large lane is faintly visible in the third nebula of the first column, in which the central mass is very much larger and where the spiral arm extends from a ring-shaped formation.

The third column contains nebulae of very small central mass. In the nebula at the top of this column the nucleus is, in a characteristic way, displaced toward the lower edge of the apparent ellipse which is formed by the inner spiral arms, and the true orientation of the object is scarcely doubtful. The analogy between this nebula and the one immediately below it is very great, though the inner spiral structure is not so well developed in the last-mentioned object. That the inner structure in this case is not an amorphous central mass analogous to that of the early types in the first column is

shown by its richness of detail, and the real nuclear region is small. The nebula is classed by Hubble as Sc. The true orientation of the two lower nebulae in this column is rather obvious. On the whole, the sequence formed by the nebulae in the last column and the first nebula in the second column, taken together, is rather strong. The fact that in all these nebulae the light-intensity in the apparent ellipse formed by the inner spiral arms is a maximum at a lane similar to that of the spindles and presumably situated on the near side, will be most readily understood if we assume the degree of flattening of the luminous matter in the central region to be so great that a con-

FIG. 6.—Schematic vertical section of luminous and dark matter in a nebula of small central mass. Intersections with density surfaces of luminous matter are full drawn, intersections with dark matter are dotted curves. The oblique lines indicate the line of sight.

siderable amount of dark matter actually may be considered as lying above the luminous matter. By an effect somewhat analogous to the darkening of the limb on the solar disk we then get a darkening toward the farther limb of the nebular disk.

We now proceed to the last nebulae of the two first columns. By analogy with the neighboring nebulae their probable orientation has been derived. The nebula in the middle column shows the darkening toward the farther limb extremely strongly developed. The general explanation is analogous to that just given and is further illustrated by Figure 6, where the luminous matter is schematically represented by full-drawn curves, dark matter by dotted curves. Though the dark matter may have a very strong condensation toward the equatorial plane, it is very probable that widespread and thin clouds extend in an irregular way to a considerable height over this plane, forming, more or less, an envelope around the central regions. The effect of a longer path through this dark matter on the farther side may then produce a very effective darkening of the far half of the nebula. It is further conceivable, however, that the greater intensity

of the near side may be due partly to the diffusion of light emitted from the intense central region in the surrounding dark clouds. If the scattering of light by a particle of the dark matter is greater in the direction of the incident radiation than in the opposite direction, the dark clouds on the near side of the nebula are likely to appear illuminated by scattered radiation to a higher degree than the dark clouds on the farther side. Accurate measurements of the polarization of light may throw light on the extent to which such an effect may contribute to the apparent asymmetry of the light-distribution.

A spectrographic determination of the rotation has been made by N. U. Mayall at the Lick Observatory for the second nebula in the last column of Plate II, NGC 6503. With the orientation in space suggested here the rotation is in the direction of the spiral whorls when proceeding outward, in agreement with the present theory. The nebula M 7331, for which the spectrographic rotation has been measured by H. W. Babcock, resembles, at least in its central regions, the nebula NGC 3675, which is the last nebula of the second column in Plate II. If NGC 7331 conforms to the ideas expressed here concerning the orientation, the observed rotation is in agreement with the present theory for this nebula as well. A photometric study of NGC 6503 and 7331 in various colors based on plates taken with the Crossley reflector of the Lick Observatory is at present in progress, and it is hoped that the results will help to interpret further the distribution of light in nebulae of these types.

In the case of nebulae which are so much inclined that we cannot distinguish the spiral arms sufficiently to determine which way they wind around the nucleus, we can perhaps infer this direction indirectly by the following way of reasoning. If we go in the direction of the major extension of the nebula to both sides from the nucleus, the dark matter may be expected to have the strongest obscuring effect on the concave side of the spiral arms, as seen by us. This follows if we assume that the obscuring matter of some elevation above the equatorial plane and close to the arms is more abundant inside the arms than outside of them. The half of the nebula which is relatively faint is then likely to be the one which turns the concave side of the arms in our direction. This criterion, applied to NGC 4594—for which the spectrographic rotation has been deter-

mined by Slipher[16] and by Pease[17]—appears to give a result in accordance with the present theory.

A phenomenon of a quite different kind, which may contribute to throw light on the dynamics of the nebulae, is the way in which a spiral arm often breaks up into a fan-shaped structure of "secondary" branches. This phenomenon is very well shown, for instance. in M 101 and M 33. Neighboring parts of the secondary arms are likely to possess about the same values of the area constant in the motion around the center. In such a case we should expect the branches extending to the greatest distances from the center to recede relative to the branches of smaller distance from the center in a direction opposite to the direction of rotation. This criterion, applied, for instance, to the fan-shaped spiral arm of M 101, evidently shows the direction of rotation to be the direction of winding of the arms, when we go outward. Measurements of radial velocity for different points of such fan-shaped spiral arms in nebulae of some inclination against the line of sight might contribute to test the assumption just made concerning the value of the area constant.

Stockholm Observatory
Saltsjöbaden, Sweden
October 1939

[16] *Pop. Astr.* **23**, 24, 1915.

[17] *Proc. Nat. Acad.*, **2**, 517; *Mt. W. Comm.*, No. 32, 1916.

THE OPACITY OF GAS MIXTURES IN STELLAR INTERIORS

PHILIP M. MORSE

ABSTRACT

The opacity of mixtures of hydrogen, helium, oxygen, sodium, magnesium, silicon, potassium, calcium, and iron is computed for any proportions of hydrogen and helium, and for four different mixtures of the heavier elements, for temperatures from 4×10^4 to 10^9 degrees centigrade, and for densities from 10^{-2} to 10^4 gm/cm^3. Absorption cross-sections for Coulomb-field wave functions are used; but these are corrected for the screening of filled shells by using effective nuclear charges and quantum numbers, and for the effect of pressure ionization (excluded volume) by the use of the solutions of the Thomas-Fermi equation for electronic distribution in dense materials. A table of correction factors for Kramers' opacity formula (guillotine factors) is given for the four mixtures, for the ranges of temperature and density covered. Instructions for determining the value of the opacity, for a given temperature and density and for intermediate chemical mixtures, are given in the Summary. There are comments on the dependence of the opacity on the chemical constitution of the mixture, and on the effect of these results on the calculation of hydrogen concentrations in stars.

With increasing knowledge about the processes of energy generation in stellar interiors it has become important to have accurate and extensive tables of the opacity of stellar material. B. Strömgren[1] has made calculations for a particular mixture of heavy elements (the Russell mixture) and for a limited range of temperature and density. It is the purpose of this paper to extend and improve Strömgren's results, covering a wider range of temperature and density, using several different mixtures of heavy elements, and utilizing improved quantum mechanical techniques to obtain a more accurate result.

The three processes that are important in opacity are the photoelectric absorption (bound-free transitions), collision absorption (free-free transitions), and scattering. Stobbe, Gaunt, Menzel and Pekeris,[2] and others have computed the probability of the absorption processes for hydrogenic wave functions. Their results can be expressed in terms of effective cross-sections for absorption of light

[1] *Zs. f. Ap.*, **4**, 118, 1932. See also Chandrasekhar, *An Introduction to the Study of Stellar Structure*, chap. vii, University of Chicago Press, 1939. In the present paper the notation of Chandrasekhar is followed as closely as possible.

[2] M. Stobbe, *Ann. d. Phys.*, **7**, 661, 1930; J. A. Gaunt, *Phil. Trans.*, A, **229**, 163, 1930; D. H. Menzel and C. H. Pekeris, *M.N.*, **96**, 77, 1935.

of frequency ω atomic units[3] from a filled shell of total quantum number n or from an energy band $d(k^2)$ of free states (k^2 in atomic energy units), for an atom of nuclear charge Ze,

$$\left.\begin{aligned} Q_n(\omega) &= \frac{2^5e^2}{3\sqrt{3}\,mc}\,\frac{1}{(Ry)}\,\frac{Z^4}{n^3\omega^3}\begin{cases} 0 & (W_n > \omega) \\ g_n(\omega) & (W_n < \omega) \end{cases}\Bigg\}\ \text{cm}^2\,, \\ dQ_k(\omega) &= \frac{2^4e^2}{3\sqrt{3}\,mc}\,\frac{1}{(Ry)}\,\frac{Z^2}{\omega^3}\,g(k)d(k^2)\ cm^2\,. \end{aligned}\right\} \tag{1}$$

The factor $(e^2/mc) = 8.40\times10^{-3}$ cm^2/sec, (Ry) is the Rydberg constant 3.29×10^{15} sec^{-1}; and g is the so-called Gaunt factor, which varies slowly with ω and n or k and has been shown [1,2] to have the order of magnitude of unity. The energy W_n is the absorption limit in atomic units; its value will be given in equations (8) and (12).

To obtain the absorption coefficient per gram of material one must multiply these cross-sections by the probability of an electron's being in the nth shell or in the range $d(k^2)$ (only the Fermi factor needs to be used, since the statistical weight of the state is already included in the Q's), by the probability that the final state is unoccupied, and by the number of atoms Z per gram of material; and, finally, one must sum the products over all initial states and over all values of Z.

At high temperatures this absorption opacity becomes negligible, compared with the opacity due to scattering. In these cases the Klein-Nishina modification of the Thomson scattering formula can be used, and the scattering cross-section per electron can be written

$$Q_s(\omega) = 6.57\times10^{-25}N(\omega)\ \text{cm}^2\,, \tag{2}$$

[3] Many of the intermediate formulae in the calculations are expressed in simpler form in atomic units:

Symbol	Quantity	One Atomic Unit Equals:
r_a, x_a	Length	$(\hbar^2/4\pi^2me^2) = 0.528\times10^{-8}$
W, E	Energy	$(2\pi^2me^4/\hbar^2) = 13.53\ ev = 2.152\times10^{-11}$ ergs
ω	Frequency	$(2\pi^2me^4/\hbar^3) = 3.29\times10^{15}$ sec^{-1} = Rydberg constant (wave length of light of frequency ω atomic units equals $909/\omega$ angstrom units)
ρ_a	Density	11.2 gm/cm^3 (one hydrogen atom per unit atomic volume corresponds to unit density in atomic units)
T_a	Temperature	$(2\pi^2me^4/k\hbar^2) = 157{,}000°$ C (i.e., the corresponding Boltzmann factor is unity)

where values of the function N are given in Table 1. The function has the following limiting behavior:

$$N(\omega) \cong \left\{ \begin{array}{ll} 1 - \dfrac{\omega}{18{,}750} & (1000 > \omega) \\ \dfrac{14{,}060}{\omega} \cdot \ln \dfrac{\omega}{11{,}400} & (10^5 < \omega) \end{array} \right\}. \qquad (3)$$

The scattering coefficient is the product of Q_s and the total number of electrons per gram. The total opacity is the sum of the absorption and scattering coefficients and is a function of the light frequency ω, of the chemical composition, and of the temperature.

THE EXCLUDED VOLUME

Equations (1) have been derived for hydrogenic wave functions and for exceedingly small gas densities. In stellar interiors each electronic orbit is distorted by the presence of other electrons in orbits about the same nucleus, and also by the presence of other atoms near by. Equations (1) should be corrected for both of these effects. The correction due to the presence of other electrons about the same nucleus can be made by using the effective charge and the effective quantum number, instead of actual Z and n, in the equations. This will be discussed later.

The effect of the presence of neighboring atoms can be computed by the help of the quantum theory of metals. According to this theory, the atomic energy states are modified as the atoms are squeezed closer and closer together to form a dense material. The bound states have sharp, discrete levels in an isolated atom; but, as the density is increased, the levels spread out into bands. The band width is greater the higher the level, so that, above a certain band, all the bands will overlap, and the upper states will be more like free states than bound ones. In other words, for any given density there will be a lower limit of energy, above which the states, originally bound, are now virtually free states and below which the states are still tightly bound with very little spreading-out of the energy bands. This depression of the lower limit of the free electron states increases with increasing density, and for high-enough densities the bound states will all be absorbed by the free states. The effect has been

TABLE 1*

VALUES OF THE SCATTERING FUNCTION, THE NORMALIZING CONSTANT FOR FERMI STATISTICS, AND THE STRÖMGREN FUNCTION S

$\log \omega$	$N(\omega)$ (Eq. [18])	$\log \eta$	$\log A$ (Eq. [6])	F_0 (Eq. [16])	u	$S(u)$ (Eq. [15])	u	$S(u)$
2.0	0.995	$\bar{2}.0$	$\bar{2}.0015$	0.9981	0.0	0.00000	7.5	94.6856
2.2	.991	.2	$\bar{2}.2024$	.9969	0.5	0.00029	7.6	97.5219
2.4	.985	.4	$\bar{2}.4038$	.9952	1.0	0.01071	7.7	100.3346
2.6	.976	.6	$\bar{2}.6060$	.9931	1.5	0.08954	7.8	103.1223
2.8	.963	.8	$\bar{2}.8096$	.9902	2.0	0.39955	7.9	105.8825
					2.5	1.2434		
3.0	.945	$\bar{1}.0$	$\bar{1}.0152$	.9857			8.0	108.6119
3.1	.936	.1	$\bar{1}.1191$	.9825	3.0	3.0480	8.1	111.3053
3.2	.922	.2	$\bar{1}.2241$	.9785	3.2	4.1483	8.2	113.9608
3.3	.904	.3	$\bar{1}.3303$	.9733	3.4	5.5041	8.3	116.5797
3.4	.882	.4	$\bar{1}.4382$	.9670	3.6	7.1469	8.4	119.1587
3.5	.856	.5	$\bar{1}.5480$	.9592	3.8	9.0957	8.5	121.6939
3.6	.826	.6	$\bar{1}.6605$	.9499	4.0	11.3676	8.6	124.1825
3.7	.792	.7	$\bar{1}.7760$	.9385	4.2	13.9808	8.7	126.6251
3.8	.755	.8	$\bar{1}.8956$	.9245	4.4	16.9409	8.8	129.0210
3.9	.715	.9	0.0201	.9082	4.6	20.2476	8.9	131.3691
					4.8	23.8940		
4.0	.672	0.0	0.1511	.8880			9.0	133.6682
4.1	.627	.1	0.2898	.8640	5.0	27.8664	9.2	138.1127
4.2	.583	.2	0.4380	.8370	5.1	29.9725	9.4	142.3489
4.3	.540	.3	0.5982	.8061	5.2	32.1510	9.6	146.3742
4.4	.498	.4	0.7730	.7726	5.3	34.4014	9.8	150.1856
4.5	.457	.5	0.9654	.7367	5.4	36.7225	10.0	153.7856
4.6	.417	.6	1.1804	.6993	5.5	39.1128	10.2	157.1759
4.7	.378	.7	1.4215	.6601	5.6	41.5698	10.4	160.3624
4.8	.340	.8	1.6959	.6187	5.7	44.0895	10.6	163.3490
4.9	.303	.9	2.0090	.5751	5.8	46.6656	10.8	166.1404
					5.9	49.2917	11.0	168.7424
5.0	.268	1.0	2.3699	.5281				
5.1	.235	.1	2.7816	.4746	6.0	51.9633	11.5	174.4525
5.2	.205	.2	3.2672	.4123	6.1	54.6755	12.0	179.1535
5.3	.178	.3	3.8191	.3431	6.2	57.4249	12.5	182.9749
5.4	.154	.4	4.4628	.2772	6.3	60.2082	13.0	186.0382
5.5	.133	.5	5.2193	.2213	6.4	63.0213	13.5	188.4766
5.6	.115	.6	6.0944	.1758	6.5	65.8637	14.0	190.3846
5.7	.099	.7	7.1137	.1397	6.6	68.7225	15.0	193.0267
5.8	.085	.8	8.3010	.1109	6.7	71.5978	16.0	194.5800
5.9	.073	.9	9.6872	.0881	6.8	74.4853	18.0	195.9583
					6.9	77.3810	20.0	196.3685
6.0	.063	2.0	11.299	.0700				
6.2	.046	.1	13.176	.0556	7.0	80.2800	22.0	196.4813
6.4	.033	.2	15.364	.0442	7.1	83.1773	24.0	196.5103
6.6	.023	.3	17.915	.0351	7.2	86.0698	26.0	196.5174
6.8	.015	.4	20.892	.0279	7.3	88.9546	30.0	196.5194
7.0	0.009	.5	24.364	0.0222	7.4	91.8283	∞	196.5194

* The symbol "log" characterizes the logarithm to the base 10, whereas "ln" in text characterizes the logarithm to the base e.

called "pressure ionization." The amount of the depression can be computed approximately by means of the Thomas-Fermi equation.[4]

The usual Thomas-Fermi solution gives the effective potential energy of an electron in an isolated atom when the atomic electrons are considered to form a degenerate gas. If the uppermost filled levels are placed at zero energy, then the potential is approximately equal to $-(Ze^2/r)$ for small values of r (the distance from the nucleus) and approaches zero asymptotically for large r. This potential is valid for an isolated atom. Slater and Krutter[5] have computed the Thomas-Fermi potential when the atomic electrons are confined inside a sphere of radius a, corresponding to the case of an atom in a compressed gas. In this case the potential is again equal to $-(Ze^2/r)$ for small r; but it rises to a maximum value, less than zero, at $r = a$. The upper limit of the filled levels is above zero, since the squeezing has increased the average kinetic energy of the electrons. It turns out[6] that the position of this potential maximum coincides fairly closely with the position of the lower limit of the free states mentioned above. To a fairly good approximation the atomic states with levels below the maximum can be considered to be bound states, unchanged by the presence of the near-by atoms, whereas the levels that were above this limit in the isolated atom are effectively merged in the continuous states for free electrons. Figure 1 shows the potential energy-curves for a given density for three elements and shows the lower limit of the continuum and the bound levels below this limit.

The problem of joining the effective potential-curves about each nucleus to the curves for the next nuclei becomes somewhat complicated when the gas is a mixture of different kinds of atoms. One must choose a radius for each nucleus such that the energy difference between the potential maxima at the edge of each atomic sphere and the top of the filled levels is the same for every nucleus. When this is true, the top of the filled levels is the same throughout the gas, and the potential energy in the interspaces between atoms is nearly constant. Slater and Krutter's tables[6] enable one to compute the ratio

[4] L. H. Thomas, *Proc. Camb. Phil. Soc.*, **23**, 542, 1927; E. Fermi, *Zs. f. Phys.*, **48**, 73, 1928.

[5] *Phys. Rev.*, **47**, 559, 1935. [6] *Rev. Mod. Phys.*, **6**, 210, 1934.

of the atomic radius a_z for atom Z in terms of the radius a_1 for hydrogen. These ratios are approximately proportional to the cube root of the nuclear charge; $(a_z/a_{z'}) \cong (Z/Z')^{1/3}$, for most of the values of a_1 that are important in the present problem. It is possible, therefore, to find an approximate value for a_1 as a function of density for any mixture of elements.

Let U_z be[7] the proportion by weight of the element of nuclear charge Ze and atomic weight M_z. Then the number of such nuclei

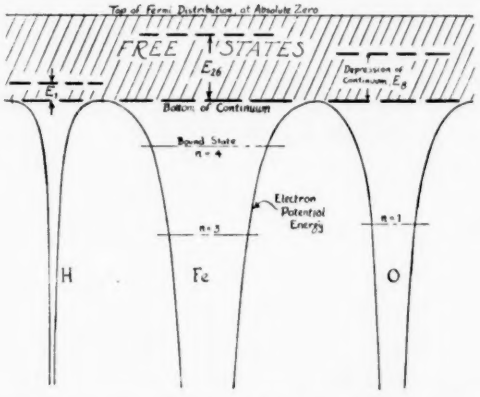

FIG. 1.—Effective electronic potential as a function of distance from three nuclei, as computed by the Thomas-Fermi equation, for $\rho = 100$ gm/cm^3 and for $X = 0.16$. The dashed lines above the bottom of the continuum show the asymptotic value of the potential of the corresponding isolated atom. The dashed lines below the bottom of the continuum show the positions of bound states not merged in the continuum.

per unit atomic volume is $(U_z\rho_a/M_z)$, where ρ_a is the density of the gas in atomic units.[3] The volume occupied by such an atom is $(4\pi a_z^3/3)$; and, since a_z^3 is approximately equal to $a_1^3 Z$, the total volume occupied by all the atoms in the unit volume must be

$$\frac{4\pi a_1^3 \rho_a}{3} \sum_z \frac{U_z Z}{M_z},$$

[7] In later discussions in this paper we shall find it more useful to let the proportions by weight of hydrogen and helium in the total mixture be $U_1 = X$ and $U_2 = Y$, respectively, and the proportions of the heavier elements be $U_z = (1 - X - Y)c_z$, so that c_z is the proportion by weight of atom Z in the heavy mixture before it is diluted with hydrogen and helium. The use of X and Y follows the notation of Chandrasekhar (n. 1, above).

which must equal unity. For hydrogen the ratio $(Z/M_z) = 1$, and for all other elements $(Z/M_z) \cong \frac{1}{2}$. Therefore, the summation reduces[7] to $\frac{1}{2}(1+X)$, since $\sum U_z = 1$. The approximate value of a_1 is thus

$$a_1 \cong \left[\frac{3}{2\pi\rho_a(1+X)}\right]^{1/3}, \tag{4}$$

where $(\rho_a/2)\,(1+X)$ is the number of electrons per unit atomic volume.

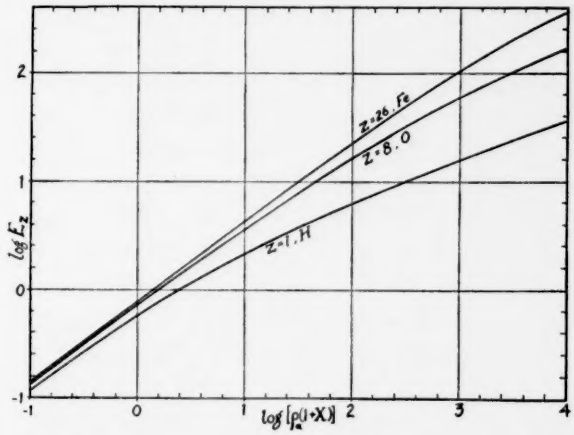

FIG. 2.—Depression of continuum E_z in atomic units as a function of the number of electrons per unit atomic volume, $\rho_a(1+X)$, for three elements.

Once a_1 is known for a given ρ_a and X, it is possible to go back to the tables of Slater and Krutter to obtain more accurate values for a_z for the various nuclei in the mixture, and also to calculate E_z, the energy difference (in atomic units) between the potential maximum for the computed a_z and the asymptotic value of the potential for the same atom when isolated. The energy E_z is, therefore, the amount by which the lower limit of the continuous free states has been depressed for this nucleus by the squeezing-together of the atoms. The values of E_z in atomic units for three different elements are given as functions of $\rho_a(1+X)$ in Figure 2.

These calculations have been made for zero temperature, for a completely degenerate gas; and a correction should be made for the fact that the gas under consideration is hot. It turns out, however,

that whenever absorption by the bound states is important this correction has a negligible effect on the computed opacity, so that the correction has been neglected.

THE FERMI DISTRIBUTION

Since the electrons follow Fermi-Dirac statistics, the probability of an electron's being in a given state of energy W is

$$P(W) = \left[1 + \frac{1}{A} e^{W/T_a}\right]^{-1}, \tag{5}$$

where W and T_a are both in atomic units and where the constant A is determined by the requirement that the sum of the P's over all states per unit volume equals the number of electrons per unit volume $(\rho_a/2)\ (1+X)$. The zero of energy is taken to be the lower limit of the free states. At the temperatures and densities occurring in stellar interiors the great majority of the electrons are in free states, either because the temperature has forced them out of the bound states or because pressure ionization has squeezed them out. Therefore, A is determined primarily by the distribution of free states.

The number of free states per unit volume having momentum in atomic units between k and $k + dk$ is $(k^2/\pi^2)dk$. The energy of these states is k^2. Therefore, an approximate equation for A is

$$\frac{2}{\sqrt{\pi}} \int_0^\infty \frac{\sqrt{x}\, dx}{1 + \frac{e^x}{A}} \cong \eta = 2\rho_a(1 + X) \left(\frac{\pi}{T_a}\right)^{3/2} \quad \left(x = \frac{k^2}{T_a}\right). \tag{6}$$

A table of values of $\log A$ as a function of $\log \eta$ is given[8] in Table 1. The solutions for A for limiting ranges of η are

$$A \cong \begin{cases} \eta + 0.35\eta^2 & (\eta < 0.1) \\ \exp[(1.21\eta)^{2/3}(1 - 0.56\eta^{-4/3})] & (\eta > 10) \end{cases}. \tag{7}$$

[8] The quantity η corresponds to $N_e/G(T)$ in the notation of Chandrasekhar (n. 1, above).

The values of A for intermediate values of η must be obtained from Table 1.

Once values of A are obtained, it is possible to correct formulae (1) for the effect of other electrons inside the atom. For a given density and temperature one computes for each atom the number of shells which are filled (i.e., those for which P is close to unity) and applies the screening constants given by Slater[9] to obtain an effective charge Z_e to use instead of Z in equations (1). Sometimes these corrections alter the number of shells shown to be filled, and the calculations must be remade until a self-consistent result is obtained. The values for W_n in equations (1) are then given by

$$W_{zn} = \left(\frac{Z_e}{n}\right)^2 - E_z \quad \text{(see also eq. [12])}, \tag{8}$$

where E_z is the depression of the lower limit of the free states given in Figure 2. Bethe[10] has shown that formulae (1) still hold when screening and pressure ionization occur, as long as one considers states with $W_{zn} > 0$ to be the only bound states.

After all these corrections have been made, one can form a general picture of the relevant phenomena that occur in the gas as the pressure and temperature are varied. Figure 3 shows a general sketch of these occurrences in the ρ, T plane (cgs units). To the right, for high temperatures, the scattering opacity predominates; and to the left, the absorption does. As we reduce the temperature, the various shells fill up, first the K shell of iron (the heaviest atom considered), and so on, until at about 500,000° C so many shells are filled that equations (1) begin to be inadequate even with the corrections made for screening given above. Consequently, no results are given in this paper for temperatures below 400,000°.

As the density is increased, one shell after another is merged in the continuum of free states, until finally even the K shell of iron disappears. By this time the free states have become degenerate and electronic conductivity begins to short-circuit the opacity, as is

[9] *Phys. Rev.*, **36**, 57, 1930.

[10] *Handbuch der Physik* (2d ed.), **24**, Part I, 478, Berlin: Springer, 1933.

shown by Marshak.[11] Consequently, no results are given in this paper for densities larger than 10^4 gm/cc.

THE ABSORPTION AND SCATTERING OPACITIES

We are now in a position to calculate the opacity as a function of frequency. The opacity due to scattering may be obtained from

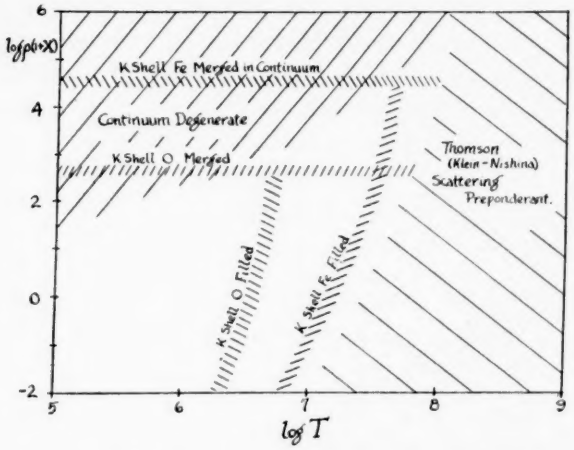

FIG. 3.—Sketch of ρ, T plane, showing phenomena important in opacity

equation (2), by multiplying by the number of electrons per unit mass of material, 3.03×10^{23} $(1+X)$ per gram, giving

$$\kappa_s(\omega) = 0.20(1 + X)N(\omega) \text{ cm}^2/\text{gm} . \tag{9}$$

The opacity due to free-free transitions is somewhat more complicated. We multiply dQ_k by the number of Z atoms per gram and sum over Z. Since there is a strong dependence of Q on Z, we may neglect the effect for hydrogen and helium and sum over only the heavier elements. There results a factor $\Gamma = \sum c_z(Z^2/M_z)$, where c_z is the proportion by weight[7] of atom Z in the mixture of heavy elements, and Γ is the average value of (Z^2/M_z) over this mixture. Γ may be called the "composition factor" of the mixture.

It is also necessary to multiply by $P(k^2)$ to give the probability of

[11] *Ap. J.*, in press. The writer is indebted to Dr. Marshak for the opportunity to read his paper in advance of publication.

the electron's being in initial state k^2, and by $[1 - P(k^2+\omega)]$ to give the probability of the final state being vacant. Integration over k gives the absorption for free-free transitions,

$$\left.\begin{aligned}\kappa_f &= 4.76 \times 10^6(1 - X - Y)\Gamma\bar{g}\,\frac{T_a}{\omega^3}\int_0^\infty e^{x-x_0+y} \\ &\qquad\qquad [(1 + e^{x-x_0})(1 + e^{x-x_0+y})]^{-1}dx \\ &= 4.76 \times 10^6(1 - X - Y)\Gamma\bar{g}\,\frac{T_a}{\omega^3}(1 - e^{-\omega/T_a})^{-1} \\ &\qquad\qquad \times \ln\left[\frac{1 + A}{1 + Ae^{-\omega/T_a}}\right] \text{cm}^2/\text{gm}\,,\end{aligned}\right\} \quad (10)$$

where $x = k^2/T_a$, $y = \omega/T_a$, $x_0 = \ln A$, and $\bar{g}$ is the average value of the Gaunt factor. Values of A can be obtained from Table 1.

To obtain the total absorption opacity we must add to this the absorption due to bound-free transitions. From equations (1), by the same method used for κ_f, we obtain the total absorption opacity,

$$\left.\begin{aligned}\kappa_a &= 4.76 \times 10^6\omega^{-3}g(1 - X - Y)\left\{\Gamma T_a(1 - e^{-\omega/T_a})^{-1}\right. \\ &\times \ln\left[\frac{1 + A}{1 + Ae^{-\omega/T_a}}\right] + 2\sum\frac{Z_e^4 c_Z}{M_z n^3}P(W_{zn})[1 - P(\omega - W_{zn})]\left.\right\}\,,\end{aligned}\right\} \quad (11)$$

where the summation is for all states with values of W_{zn} (see eq. [12]) smaller than ω. The most important term in κ_a is usually the term with largest W_{zn}, and no large error is made in making g equal to the Gaunt factor for this term. Values can be obtained from the work of Menzel and Pekeris.[2] In addition, a correction must be made at high densities for the fact that the integration for the transition probabilities is made over a sphere of radius a_z instead of over all space. This does not make so large a correction as might be expected, since the bound-free transitions involved are always those with wave functions that have small values beyond a_z.

Both these corrections can be combined into an effective Gaunt factor $g_e = g(\omega)g_d$, where $g(\omega)$ is the Gaunt factor for the largest term in the summation of equation (11), and g_d is the term involving the density correction. Table 2 gives approximate values of these g

factors. Instead of $g(\omega)$, there is given the factor g_t, the average of $g(\omega)$ over the Planck distribution, as discussed in the next section.

The factor $[1 - P(\omega - W_{zn})] = [1 + A exp(1/T_a)\ (W_{zn} - \omega)]^{-1}$ is nearly equal to unity whenever A is smaller than unity. For large densities and low temperatures, however, A is much larger than unity, and the expression above is very small for small values of ω,

TABLE 2*

CORRECTION FACTORS FOR GAUNT FACTOR, $\bar{g} = g_d g_t$; INTERPOLATION FACTORS TO OBTAIN MEAN OPACITY FROM ABSORPTION AND SCATTERING OPACITIES

$\log \rho$	$-\log\ (g_d)$ (Eq. [16])	$\log T$	$-\log\ (g_t)$ (Eq. [16])	$\log (\bar{\kappa}_s/\bar{\kappa}_a)$	$\log (\bar{\kappa}/\bar{\kappa}_a)$	$\log (\bar{\kappa}_s/\bar{\kappa}_a)$	$\log (\bar{\kappa}/\bar{\kappa}_a)$
1.0	0.00	5.6	0.00	$\bar{3}.0$	0.00	0.0	0.41
1.2	.00	5.8	.01	.2	.00	.2	0.50
1.4	.01			.4	.00	.4	0.64
1.6	.01	6.0	.02	.6	.01	.6	0.79
1.8	.02	6.2	.04	.8	.01	.8	0.95
		6.4	.06				
2.0	.03	6.6	.08	$\bar{2}.0$	.02	1.0	1.11
2.2	.04	6.8	.09	.2	.03	.2	1.28
2.4	.06			.4	.04	.4	1.46
2.6	.08	7.0	.10	.6	.05	.6	1.64
2.8	.10	7.2	.11	.8	.07	.8	1.83
		7.4	.12				
3.0	.13	7.6	.12	$\bar{1}.0$	.09	2.0	2.02
3.2	.16	7.8	.13	.2	.11	.2	2.21
3.4	.19			.4	.15	.4	2.40
3.6	.23	8.0	.12	.6	.20	.6	2.60
3.8	.27	8.2	.12	.8	.27	.8	2.80
		8.4	.11				
4.0	0.30	8.6	0.10	0.0	0.41	3.0	3.00

* Logarithms are to base 10.

rising rapidly to unity when ω becomes larger than $W_{zn} + T_a \ln A$. Therefore, one further approximation has been made in equation (11). The factor $[1 - P(\omega - W_{zn})]$ was omitted, and a new absorption limit was used, whenever degeneracy is present (i.e., whenever $\ln A$ is positive). The effective limit used is

$$W_{zn} = \left(\frac{Z_e}{n}\right)^2 - E_z + \left\{\begin{array}{ll} 0 & (\log A < 0) \\ 2.3 T_a \log A & (\log A > 0) \end{array}\right\}, \qquad (12)$$

where E_z is given in Figure 2, and $\log A$ in Table 1.

To obtain the opacity in a form for easy comparison with Kramers' formula, we multiply and divide by $\eta = 11.14\rho_a(1+X)T_a^{-3/2}$; and, to make calculation easier, we arrange the terms in the summation in equation (11) in order of increasing *value* of W_{zn}, rather than in order of increasing n or Z. The smallest value of W_{zn} will be relabeled W_1, and so on, so that the sth term in size is W_s, where $W_{s-1} < W_s < W_{s+1}$. Then the total absorption opacity becomes

$$\left.\begin{aligned} \kappa_a(\omega) &= 5.30 \times 10^7(1+X)(1-X-Y)\left(\frac{\rho_a\Gamma}{T_a^{1/2}}\omega^3\right) \\ &\qquad \times [F_s + F_0(\omega)]\,, \quad W_s < \omega < W_{s+1}\,, \\ F_0(\omega) &= \frac{\frac{1}{\eta}}{1-e^{-\omega/T_a}} \ln\left[\frac{1+A}{1+Ae^{-\omega/T_a}}\right], \\ F_s &= \frac{1}{T_a\Gamma}\sum_{\sigma=1}^{s}\frac{Z_\sigma^4 c_\sigma}{M_\sigma n_\sigma^3 \eta}\,P(W_\sigma)\,. \end{aligned}\right\} \quad (13)$$

The quantities Z_σ, n_σ, etc., are the values of Z, n, etc., corresponding to the σth absorption limit in the ordered sequence of W_{zn}. The quantity F_s is, therefore, a step function, changing value only when ω passes through an absorption limit W_s.

THE AVERAGE OPACITY

The important quantity in stellar calculations is the Rosseland mean of the opacity

$$\bar{\kappa} = \frac{15}{4\pi^4}\left[\int_0^\infty \frac{1}{\kappa}\,u^4e^{2u}(e^u-1)^{-3}du\right]^{-1} \quad \left(u = \frac{\omega}{T_a}\right). \quad (14)$$

Since the reciprocal of the opacity is averaged, it is not possible to obtain the average total opacity by adding the average absorption opacity and the average scattering opacity. For those temperatures where both opacities have the same magnitude, formulae must be devised to combine the two opacities, but for other temperature ranges the problem is fairly simple.

In the low-temperature regions the scattering opacity κ_s is negligible compared with κ_a, so that equation (13) is the expression to be

averaged. The method of calculation is that of Strömgren[1] and uses Strömgren's function

$$S(u) = \frac{4\pi^4}{15}\int_0^u x^7 e^{2x}(e^x - 1)^{-3}dx\,, \tag{15}$$

which is given in Table 1 for convenience. The function has been recalculated to obtain a somewhat greater accuracy than that of Strömgren's original table. Intermediate values can be obtained by four-point interpolation.

When κ_a predominates, the integrand of equation (14) has a fairly sharp maximum at $u \cong 7$, so that[12] for slowly varying quantities we may replace ω by $7T_a$ and place the quantities outside the integral. After the integration is performed, it is convenient to return to units of grams per cubic centimeter for density and degrees centigrade for temperature. The result is

$$\bar{\kappa}_a \cong 7.23 \times 10^{24}\Gamma\rho(1 + X)(1 - X - Y)T^{-7/2}\frac{\bar{g}}{t}\ \mathrm{cm}^2/\mathrm{gm}\,, \tag{16}$$

where

$$\bar{g} = g_a g_t \text{ (see Table 2)}\,, \qquad \Gamma = \sum_z \frac{c_z Z^2}{M_z}\,,$$

$$t = \sum_s \frac{S(W_{s+1}) - S(W_s)}{F_s + \bar{F}_0}\,, \quad \bar{F}_0 = \frac{1}{\eta}\ln\left[\frac{1 + A}{1 + Ae^{-7}}\right] \cong \begin{cases} 1 (\eta < 0.01) \\ \dfrac{7}{\eta}\ (\eta > 100) \end{cases},$$

and where F_s is given in equation (13). The function $\bar{F}_0$ is given in Table 1 as a function of η.

The formula for $\bar{\kappa}_a$ without the factor $(\bar{g}/t)$ is just Kramers' formula, the correction factor t being called the "guillotine" factor. The results below show that, in most cases, t is larger than unity, indicating that the actual opacity is smaller than that predicted by the simple Kramers' formula. Tables of $(t/\bar{g})$ are given for four different mixtures of heavy elements in Table 3. Case 1 is for the Russell mixture. No values are given for high temperatures when $\bar{\kappa}_a$ becomes negligible with respect to $\bar{\kappa}_s$.

[12] If the quantity F_s in eq. (13) were independent of ω, the maximum of the integrand would come at $\omega = 7T_a$. However, the dependence of F_s on ω makes this maximum come nearer to $6T_a$. Therefore, for those parts of the opacity dependent on the free-free transitions we set $\omega_{\max} = 7T_a$, and for those parts corresponding to bound-free transitions we set $\omega_{\max} = 6T_a$.

TABLE 3

VALUES OF THE LOGARITHM OF THE GUILLOTINE FACTOR $\log_{10}(t/\tilde{g})$
(See Eq. [16])

CASE 1: $c_{Fe}=0.125$, $c_{K,Ca}=c_{Si}=0.0625$, $c_{Na,Mg}=0.25$, $c_O=0.5$

LOG T	LOG $\rho(1+X)$												
	−2.0	−1.5	−1.0	−0.5	0.0	0.5	1.0	1.5	2.0	2.5	3.0	3.5	4.0
5.6	0.10	0.28	0.56	0.88	1.23	1.62	2.02	2.46	2.92	3.43	3.98	4.55	5.14
5.7	0.09	0.17	0.44	0.76	1.09	1.48	1.90	2.34	2.80	3.30	3.83	4.41	5.00
5.8	0.13	0.17	0.36	0.67	1.01	1.38	1.78	2.21	2.66	3.16	3.69	4.27	4.86
5.9	0.23	0.27	0.38	0.65	0.98	1.30	1.68	2.09	2.54	3.03	3.56	4.13	4.72
6.0	0.32	0.35	0.42	0.63	0.92	1.22	1.58	1.98	2.41	2.90	3.42	4.00	4.58
6.1	0.27	0.30	0.35	0.55	0.81	1.12	1.47	1.85	2.27	2.76	3.28	3.86	4.44
6.2	0.21	0.23	0.28	0.45	0.69	0.98	1.32	1.71	2.13	2.61	3.14	3.72	4.30
6.3	0.20	0.22	0.26	0.37	0.56	0.84	1.18	1.57	2.00	2.47	3.00	3.58	4.16
6.4	0.17	0.19	0.22	0.28	0.42	0.70	1.04	1.43	1.85	2.33	2.86	3.44	4.02
6.5	0.11	0.13	0.15	0.20	0.32	0.58	0.92	1.28	1.71	2.19	2.72	3.30	3.88
6.6	0.10	0.12	0.14	0.19	0.28	0.50	0.81	1.17	1.58	2.05	2.58	3.16	3.74
6.7	0.13	0.15	0.17	0.21	0.28	0.45	0.72	1.07	1.47	1.92	2.44	3.02	3.60
6.8	0.22	0.23	0.25	0.27	0.33	0.47	0.70	1.01	1.38	1.82	2.32	2.88	3.46
6.9	0.31	0.32	0.34	0.37	0.43	0.53	0.72	0.99	1.32	1.73	2.21	2.75	3.32
7.0	0.41	0.42	0.45	0.49	0.54	0.62	0.77	1.00	1.30	1.67	2.11	2.63	3.19
7.1	0.49	0.50	0.52	0.54	0.58	0.65	0.77	0.98	1.25	1.61	2.02	2.52	3.07
7.2	0.56	0.56	0.57	0.58	0.60	0.64	0.73	0.92	1.18	1.52	1.93	2.42	2.95
7.3	0.63	0.63	0.64	0.65	0.67	0.69	0.74	0.87	1.06	1.41	1.83	2.32	2.84
7.4	0.75	0.75	0.75	0.76	0.77	0.79	0.83	0.91	1.05	1.36	1.76	2.25	2.74
7.5	0.90	0.90	0.90	0.91	0.93	0.95	0.98	1.04	1.16	1.40	1.75	2.19	2.66
7.6	1.10	1.10	1.10	1.10	1.11	1.13	1.16	1.21	1.31	1.53	1.82	2.19	2.61
7.7	1.33	1.33	1.33	1.33	1.34	1.36	1.38	1.42	1.52	1.69	1.93	2.23	2.58
7.8	1.59	1.59	1.59	1.59	1.59	1.60	1.62	1.66	1.73	1.86	2.04	2.29	2.58
7.9	1.81	1.81	1.81	1.81	1.81	1.82	1.83	1.85	1.90	2.00	2.14	2.35	2.69
8.0	2.00	2.00	2.00	2.00	2.00	2.00	2.01	2.03	2.06	2.12	2.24	2.41	2.62
8.1	2.14	2.14	2.14	2.14	2.14	2.14	2.14	2.16	2.18	2.23	2.33	2.46	2.65
8.2	2.27	2.27	2.27	2.27	2.27	2.27	2.27	2.28	2.29	2.34	2.41	2.52	2.68
8.3	2.36	2.36	2.36	2.36	2.36	2.36	2.36	2.36	2.37	2.41	2.47	2.56	2.71
8.4	2.44	2.44	2.44	2.44	2.44	2.44	2.44	2.44	2.45	2.47	2.52	2.60	2.74

CASE 2: $c_{Fe}=0.3$, $c_{K,Ca}=c_{Si}=0.05$, $c_{Na,Mg}=0.2$, $c_O=0.4$

LOG T	LOG $\rho(1+X)$												
	−2.0	−1.5	−1.0	−0.5	0.0	0.5	1.0	1.5	2.0	2.5	3.0	3.5	4.0
5.6	+0.13	0.31	0.59	0.91	1.25	2.64	2.03	2.46	2.92	3.43	3.97	4.55	5.14
5.7	+0.09	0.18	0.45	0.77	1.11	1.50	1.91	2.33	2.79	3.29	3.83	4.41	5.00
5.8	+0.09	0.13	0.36	0.68	1.03	1.40	1.79	2.21	2.66	3.16	3.69	4.27	4.86
5.9	+0.20	0.24	0.41	0.67	0.99	1.32	1.69	2.10	2.53	3.03	3.55	4.13	4.72
6.0	+0.36	0.40	0.48	0.69	0.97	1.26	1.61	1.99	2.41	2.90	3.42	4.00	4.58
6.1	+0.35	0.38	0.45	0.66	0.93	1.19	1.52	1.87	2.28	2.76	3.28	3.86	4.44
6.2	+0.26	0.29	0.36	0.55	0.81	1.09	1.41	1.76	2.15	2.62	3.14	3.72	4.30
6.3	+0.16	0.19	0.25	0.40	0.63	0.94	1.28	1.64	2.03	2.48	3.00	3.58	4.16
6.4	+0.07	0.10	0.15	0.25	0.45	0.77	1.12	1.50	1.90	2.35	2.87	3.44	4.02
6.5	−0.01	0.02	0.05	0.14	0.30	0.61	0.96	1.36	1.76	2.22	2.74	3.30	3.88
6.6	+0.02	0.02	0.04	0.10	0.23	0.48	0.82	1.21	1.63	2.08	2.59	3.16	3.74
6.7	+0.12	0.12	0.13	0.15	0.24	0.41	0.72	1.09	1.51	1.95	2.46	3.02	3.60
6.8	+0.24	0.24	0.24	0.25	0.30	0.44	0.69	1.03	1.41	1.84	2.32	2.88	3.46
6.9	+0.35	0.36	0.38	0.40	0.43	0.52	0.71	1.01	1.33	1.74	2.21	2.76	3.33
7.0	+0.44	0.45	0.48	0.51	0.55	0.62	0.77	1.00	1.29	1.66	2.10	2.63	3.19
7.1	+0.50	0.52	0.55	0.58	0.62	0.69	0.80	0.99	1.24	1.56	1.97	2.49	3.06
7.2	+0.54	0.56	0.59	0.63	0.66	0.70	0.77	0.93	1.15	1.44	1.84	2.36	2.93
7.3	+0.61	0.62	0.64	0.66	0.68	0.69	0.71	0.82	1.00	1.30	1.72	2.23	2.79
7.4	+0.74	0.73	0.72	0.71	0.70	0.69	0.67	0.72	0.85	1.17	1.60	2.12	2.67
7.5	+0.90	0.86	0.82	0.78	0.75	0.71	0.71	0.75	0.89	1.16	1.56	2.04	2.57
7.6	+1.07	1.03	0.98	0.92	0.88	0.86	0.88	0.93	1.05	1.30	1.62	2.03	2.50
7.7	+1.30	1.27	1.24	1.20	1.16	1.14	1.14	1.18	1.29	1.50	1.74	2.07	2.46
7.8	+1.52	1.51	1.49	1.46	1.43	1.41	1.40	1.44	1.51	1.66	1.86	2.13	2.46
7.9	+1.73	1.71	1.71	1.70	1.69	1.67	1.67	1.69	1.73	1.82	1.98	2.20	2.48
8.0	+1.90	1.90	1.90	1.90	1.89	1.87	1.87	1.88	1.90	1.96	2.09	2.28	2.51
8.1	+2.04	2.04	2.04	2.04	2.03	2.03	2.02	2.03	2.05	2.10	2.20	2.35	2.55
8.2	+2.15	2.15	2.15	2.15	2.15	2.14	2.13	2.14	2.16	2.21	2.29	2.41	2.59
8.3	+2.24	2.24	2.24	2.24	2.24	2.23	2.23	2.24	2.25	2.28	2.36	2.47	2.63
8.4	+2.32	2.32	2.32	2.32	2.32	2.32	2.32	2.34	2.35	2.36	2.42	2.51	2.66

TABLE 3—*Continued*

CASE 3: $c_{Fe}=0.2$, $c_{K,Ca}=c_{Si}=0.133$, $c_{Na,Mg}=0.2$, $c_O=0.333$

LOG T	LOG $\rho(1+X)$												
	−2.0	−1.5	−1.0	−0.5	0.0	0.5	1.0	1.5	2.0	2.5	3.0	3.5	4.0
5.6	0.13	0.31	0.60	0.93	1.29	1.66	2.04	2.47	2.92	3.43	3.97	4.55	5.14
5.7	0.10	0.21	0.46	0.79	1.15	1.52	1.92	2.34	2.79	3.29	3.83	4.41	5.00
5.8	0.13	0.17	0.37	0.69	1.04	1.41	1.81	2.22	2.67	3.16	3.69	4.27	4.86
5.9	0.22	0.27	0.39	0.66	0.98	1.32	1.70	2.11	2.54	3.03	3.55	4.13	4.72
6.0	0.26	0.30	0.39	0.62	0.93	1.24	1.60	2.00	2.42	2.90	3.42	4.00	4.58
6.1	0.23	0.25	0.32	0.53	0.83	1.13	1.49	1.87	2.28	2.75	3.28	3.83	4.44
6.2	0.19	0.20	0.25	0.42	0.68	0.99	1.35	1.73	2.13	2.60	3.14	3.72	4.30
6.3	0.16	0.17	0.19	0.31	0.52	0.85	1.21	1.58	1.99	2.45	2.99	3.58	4.16
6.4	0.14	0.15	0.17	0.24	0.39	0.70	1.05	1.42	1.82	2.30	2.85	3.44	4.02
6.5	0.12	0.13	0.15	0.20	0.31	0.56	0.91	1.28	1.67	2.15	2.72	3.30	3.88
6.6	0.06	0.07	0.09	0.14	0.24	0.47	0.79	1.15	1.54	2.01	2.56	3.15	3.74
6.7	0.06	0.07	0.09	0.12	0.22	0.42	0.69	1.04	1.41	1.88	2.41	3.01	3.60
6.8	0.17	0.17	0.18	0.20	0.26	0.41	0.64	0.96	1.32	1.75	2.27	2.86	3.45
6.9	0.26	0.26	0.28	0.32	0.36	0.43	0.64	0.91	1.24	1.64	2.14	2.62	3.32
7.0	0.34	0.33	0.35	0.37	0.41	0.48	0.64	0.88	1.18	1.54	2.02	2.59	3.18
7.1	0.42	0.41	0.40	0.40	0.42	0.47	0.62	0.83	1.11	1.46	1.90	2.46	3.05
7.2	0.51	0.47	0.43	0.41	0.41	0.46	0.57	0.77	1.03	1.37	1.80	2.34	2.93
7.3	0.61	0.55	0.48	0.45	0.42	0.48	0.58	0.72	0.94	1.28	1.70	2.22	2.81
7.4	0.73	0.67	0.60	0.56	0.54	0.58	0.67	0.77	0.92	1.22	1.62	2.12	2.69
7.5	0.85	0.81	0.76	0.72	0.69	0.72	0.78	0.90	1.01	1.26	1.62	2.06	2.60
7.6	1.00	0.98	0.95	0.89	0.87	0.90	0.97	1.06	1.18	1.41	1.70	2.07	2.53
7.7	1.25	1.24	1.21	1.17	1.15	1.18	1.23	1.29	1.41	1.59	1.82	2.12	2.50
7.8	1.48	1.47	1.45	1.43	1.41	1.43	1.47	1.54	1.62	1.76	1.94	2.19	2.50
7.9	1.70	1.70	1.70	1.69	1.67	1.69	1.72	1.76	1.80	1.89	2.05	2.26	2.51
8.0	1.89	1.89	1.89	1.89	1.88	1.89	1.91	1.93	1.96	2.02	2.15	2.33	2.55
8.1	2.05	2.05	2.05	2.05	2.04	2.04	2.05	2.07	2.10	2.14	2.25	2.40	2.59
8.2	2.18	2.18	2.18	2.18	2.18	2.17	2.18	2.19	2.21	2.26	2.33	2.45	2.63
8.3	2.26	2.26	2.26	2.26	2.26	2.26	2.26	2.28	2.30	2.34	2.40	2.50	2.67
8.4	2.38	2.38	2.38	2.38	2.38	2.38	2.38	2.39	2.39	2.42	2.46	2.55	2.70

CASE 4: $c_{Fe}=0.125$, $c_{K,Ca}=c_{Si}=0.125$, $c_{Na,Mg}=0.125$, $c_O=0.5$

LOG T	LOG $\rho(1+X)$												
	−2.0	−1.5	−1.0	−0.5	0.0	0.5	1.0	1.5	2.0	2.5	3.0	3.5	4.0
5.6	0.13	0.31	0.59	0.92	1.27	1.64	2.02	2.46	2.92	3.43	3.98	4.55	5.14
5.7	0.11	0.20	0.45	0.78	1.11	1.49	1.90	2.34	2.80	3.30	3.83	4.41	5.00
5.8	0.14	0.18	0.36	0.67	1.01	1.38	1.78	2.21	2.66	3.16	3.69	4.27	4.86
5.9	0.28	0.31	0.38	0.63	0.94	1.29	1.68	2.09	2.54	3.03	3.56	4.13	4.72
6.0	0.32	0.34	0.40	0.60	0.90	1.21	1.58	1.98	2.41	2.90	3.42	4.00	4.58
6.1	0.24	0.27	0.34	0.51	0.81	1.11	1.46	1.85	2.27	2.76	3.28	3.86	4.44
6.2	0.16	0.19	0.24	0.40	0.65	0.96	1.31	1.71	2.13	2.61	3.14	3.72	4.30
6.3	0.11	0.14	0.19	0.31	0.52	0.85	1.20	1.58	2.01	2.48	3.00	3.58	4.16
6.4	0.08	0.11	0.15	0.24	0.41	0.72	1.07	1.47	1.88	2.35	2.87	3.44	4.02
6.5	0.04	0.08	0.12	0.20	0.34	0.62	0.96	1.35	1.75	2.21	2.73	3.30	3.88
6.6	0.03	0.07	0.11	0.18	0.29	0.53	0.84	1.21	1.61	2.08	2.59	3.16	3.74
6.7	0.09	0.11	0.14	0.19	0.26	0.46	0.74	1.08	1.49	1.94	2.44	3.02	3.60
6.8	0.20	0.21	0.22	0.23	0.28	0.42	0.65	0.97	1.35	1.80	2.31	2.87	3.46
6.9	0.29	0.30	0.31	0.33	0.36	0.45	0.64	0.92	1.26	1.69	2.19	2.74	3.32
7.0	0.35	0.36	0.38	0.41	0.45	0.52	0.67	0.90	1.22	1.59	2.08	2.61	3.19
7.1	0.41	0.42	0.43	0.45	0.47	0.52	0.65	0.84	1.17	1.51	1.97	2.49	3.07
7.2	0.50	0.50	0.49	0.48	0.49	0.51	0.60	0.80	1.08	1.44	1.87	2.39	2.94
7.3	0.61	0.58	0.56	0.56	0.57	0.59	0.65	0.82	1.01	1.38	1.81	2.31	2.83
7.4	0.73	0.73	0.72	0.72	0.73	0.74	0.78	0.87	1.02	1.34	1.75	2.23	2.73
7.5	0.90	0.90	0.89	0.89	0.90	0.92	0.95	1.01	1.11	1.38	1.74	2.18	2.65
7.6	1.07	1.07	1.07	1.07	1.09	1.11	1.14	1.19	1.29	1.51	1.80	2.18	2.60
7.7	1.31	1.31	1.31	1.31	1.32	1.34	1.36	1.40	1.50	1.68	1.91	2.22	2.57
7.8	1.57	1.57	1.57	1.57	1.58	1.59	1.61	1.65	1.72	1.85	2.02	2.28	2.57
7.9	1.81	1.81	1.81	1.81	1.81	1.81	1.82	1.84	1.89	1.99	2.13	2.34	2.58
8.0	2.00	2.00	2.00	2.00	2.00	2.00	2.00	2.02	2.05	2.11	2.23	2.40	2.61
8.1	2.14	2.14	2.14	2.14	2.14	2.14	2.14	2.16	2.18	2.23	2.33	2.46	2.65
8.2	2.27	2.27	2.27	2.27	2.27	2.27	2.27	2.28	2.29	2.34	2.41	2.52	2.68
8.3	2.36	2.36	2.36	2.36	2.36	2.36	2.36	2.36	2.37	2.41	2.47	2.56	2.71
8.4	2.44	2.44	2.44	2.44	2.44	2.44	2.44	2.44	2.45	2.47	2.52	2.60	2.74

Values of $(t/\bar{g})$ for any temperature in the range $5 \times 10^5 < T < 10^7$ and for any density in the range $10^{-2} < \rho < 10^4$ can be obtained by graphical or four-point interpolation. Values for intermediate chemical mixtures can be obtained by making use of two properties of equation (16). In the first place, because of the maximum[12] in the integrand at $\omega \cong 6T_a$, the most important term in t is the one corresponding to the absorption limit W_s, which is nearest in value to $6T_a$. In the second place, other things being equal, the heaviest elements have the greatest effect on the value of F_s. These properties, plus a study of the computed results, enable one to set up an approximate scheme for interpolation for any mixture of *O*, *Na*, *Mg*, *Si*, *K*, *Ca*, and *Fe*, diluted with *H* and *He*, subject to the following limitations:

$$0.125 < c_{Na+Mg} < 0.25\,, \qquad 0.0625 < c_{Si} = c_{K+Ca} < 0.133\,,$$
$$0.125 < c_{Fe} < 0.3\,,$$

where c is the proportion by weight of the element in the undiluted mixture.

The results given in Table 3 for the four mixtures can be labeled t_1, t_2, t_3, and t_4, respectively. The value of t for an intermediate mixture is then a linear combination of the four tabulated t's:

$$\left.\begin{aligned} t = \alpha(T) \cdot (a_1t_1 + a_2t_2 + a_3t_3 + a_4t_4) \\ + \beta(T) \cdot (b_1t_1 + b_2t_2 + b_3t_3 + b_4t_4)\,. \end{aligned}\right\} \quad (17)$$

Table 4 gives values of the coefficients a and b in terms of the concentrations of the heavier elements, and of α and β in terms of the temperature. By this procedure it is possible to obtain the absorption opacity for any specified case.

In the high-temperature regions the absorption opacity is negligible, compared with the scattering opacity. From equation (2) we can find that the integrand in equation (14) has its maximum at $\omega = 4T_a$. Since the function N changes slowly, we obtain a formula for the scattering opacity.

$$\bar{\kappa}_s \cong 0.19(1 + X) \cdot N(4T_a)\ \text{cm}^2/\text{gm}\,, \quad (18)$$

which is fairly accurate. The function N is given in Table 1, and T_a is the temperature in atomic units.[3]

In the temperature regions where $\bar{\kappa}_a$ and $\bar{\kappa}_s$ are the same order of magnitude, the two opacities should be added before averaging. To do this accurately would require graphical integration for each separate case. However, by simplifying the form of $\kappa_a(\omega)$ somewhat, it is possible to perform the joining integration in a manner that can be used in any case. We replace the step function F_s by a straight line, and thus make $\kappa_a(\omega)$ proportional to ω^{-3}. It is then possible to obtain the Rosseland average of $(a/\omega)^3 + b$ in terms of the average values of $(a/\omega)^3$ and b. The results in Table 2 give approximate values of the ratio $(\bar{\kappa}/\bar{\kappa}_a)$ as a function of the ratio $(\bar{\kappa}_a/\bar{\kappa}_s)$. Once the values of $\bar{\kappa}_a$ and $\bar{\kappa}_s$ are determined from equations (16) and (18), the total average opacity $\bar{\kappa}$ can be obtained from Table 2.

TABLE 4

INTERPOLATION COEFFICIENTS FOR INTERMEDIATE CHEMICAL MIXTURES
(See Eq. [17])

c_{Fe}	0.125				0.200				0.250				0.300			
c_{Si}	0.04	0.07	0.10	0.13	0.04	0.07	0.10	0.13	0.04	0.07	0.10	0.13	0.04	0.07	0.10	0.13
a_1	1.0	0.9	0.4	0	0	0	0	0	0.0	0.0	0.0	0.0	0	0	0	0
a_2	0.0	0.0	0.0	0	0	0	0	0	0.6	0.5	0.5	0.5	1	1	1	1
a_3	0.0	0.0	0.0	0	1	1	1	1	0.4	0.5	0.5	0.5	0	0	0	0
a_4	0.0	0.1	0.6	1	0	0	0	0	0.0	0.0	0.0	0.0	0	0	0	0
b_1	0	0.9	0.4	0	0	0.9	0.4	0.0	0	0.0	0.0	0.0	0	0.0	0.0	0.0
b_2	1	0.0	0.0	0	1	0.0	0.0	0.0	1	0.8	0.4	0.1	1	0.8	0.4	0.1
b_3	0	0.0	0.0	0	0	0.1	0.5	0.5	0	0.2	0.6	0.9	0	0.2	0.6	0.9
b_4	0	0.1	0.6	1	0	0.0	0.0	0.5	0	0.0	0.0	0.0	0	0.0	0.0	0.0

$\log T$	5.5	5.6	5.7	5.8	5.9	6.0	6.1	6.2	6.3	6.4	6.5	6.6	6.7
α	0.5	0.5	0.3	0.6	0.8	0.5	0.2	0.0	0.0	0.3	0.7	1.0	0.7
β	0.5	0.5	0.7	0.4	0.2	0.5	0.8	1.0	1.0	0.7	0.3	0.0	0.3

$\log T$	6.8	6.9	7.0	7.1	7.2	7.3	7.4	7.5	7.6	7.7	7.8	7.9	8.0
α	0.3	0.0	0.0	0.0	0.2	0.5	0.8	1.0	1.0	0.9	0.7	0.6	0.5
β	0.7	1.0	1.0	1.0	0.8	0.5	0.2	0.0	0.0	0.1	0.3	0.4	0.5

Figure 4 gives the curves for average opacity for the Russell mixture (case 1) as functions of T, for different densities and hydrogen

concentrations. The vertical scale includes the factor $(1 - X - Y)$ in order that the curves for low temperature be independent of X and Y, the proportions of the light elements. Since the plots are on a

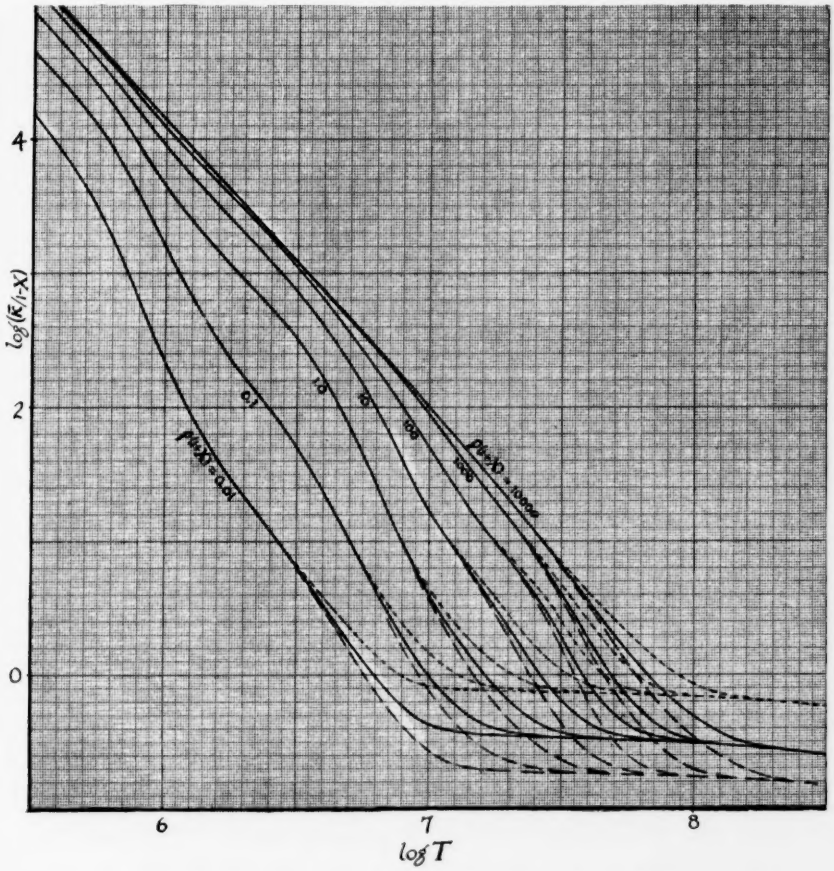

FIG. 4.—Average opacity $\bar{\kappa}$ for the Russell mixture diluted with hydrogen, as a function of temperature for different densities. The dotted lines are for the mixture diluted with 60 per cent hydrogen; the solid line, for $X = 0.30$; the dashed line, for no hydrogen.

log-log scale, the slope of the curves gives directly the exponent of the dependence on T. We note that at high densities the opacity is proportional to T^{-2} over most of the range, and that it is nearly independent of the density. At low densities the average dependence on

T is as $T^{-7/2}$, but the exponent changes considerably with temperature, being as large as $-9/2$ near a million degrees. At high temperatures the scattering predominates, and the dependence on temperature and density is less marked.

DISCUSSION

In the integral in equation (14) giving the mean absorption opacity, the integrand has a maximum for ω somewhere between $6T_a$

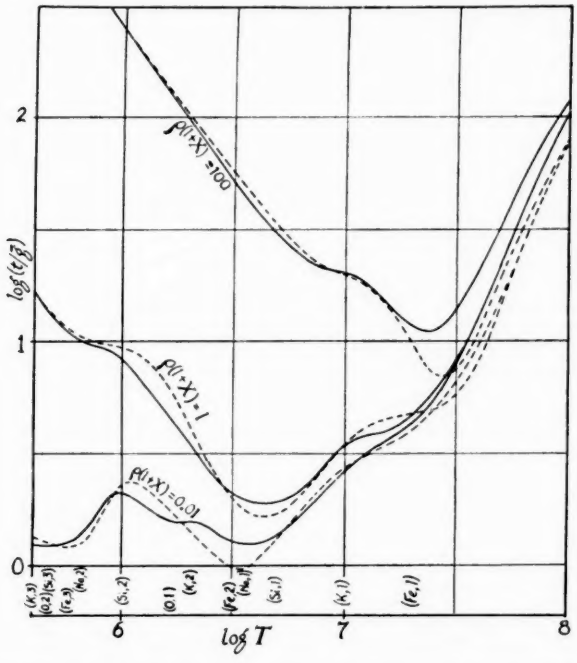

FIG. 5.—Values of the guillotine factor $(t/\bar{g})$ as function of T for three different values of ρ and for two different mixtures of heavy elements. The solid line is for the Russell mixture, case 1 of Table 3; and the dotted line is for case 2. Below the curves the different bound states are noted at the temperatures where the absorption due to this state is the most important part of the opacity.

and $7T_a$.[12] Therefore, the part of the opacity $\kappa_a(\omega)$ that has the greatest weight in the Rosseland mean is for $\omega \approx 6T_a \approx (T/26{,}000)$. This behavior has been used earlier in the derivation of equation (17) for interpolation. It is illustrated by the behavior of the curves in Figure 5.

In Figure 5 are given curves of log $(t/\bar{g})$ against log (T) for three chemical mixtures and three densities. When log $(t/\bar{g}) = 0$, the opacity follows Kramers' law; when it is larger than zero, the opacity is smaller than Kramers' value. A negative slope of the curve means that the opacity depends on T according to a negative power less than $7/2$; a positive slope means that the opacity-curve goes down more steeply than a $(T^{-7/2})$-curve. When the curves for different density overlie each other, the opacity is proportional to the density; when the curves for different ρ are spaced widely apart, the opacity is nearly independent of ρ.

Below the curves are placed notations of bound states at points on the temperature scale corresponding to the absorption limit for the state $(T \cong 26{,}000 W_{zn})$. According to the discussion above, the state noted should have a predominant effect on the opacity in the temperature range near the notation. That this is correct is shown in several places in the curves. For instance, for temperatures near 25,000,000° (and also near 3,000,000°) the mixture having the most iron has the lowest value of $(t/\bar{g})$ and, therefore, the largest value of $\bar{\kappa}_a$. In addition to the increase due to change in $(t/\bar{g})$, the opacity is also increased because the value of Γ for a mixture rich in iron is large. For certain temperatures an increase in the amount of iron by a factor of 2.5 at the expense of the other heavy elements will increase the opacity by a factor of 2. This increase does not involve an appreciable change in the mean molecular weight, and it would therefore produce an appreciable change in the predicted hydrogen abundances from those given by Strömgren[1] for the Russell mixture. The change in hydrogen abundance from Strömgren's values would probably not be by a factor greater than 1.4, however.

The results show that the hydrogen abundance computed for a star will depend on the particular mixture of heavy elements chosen. Therefore, the contours for constant hydrogen content on the Russell diagram, computed by Strömgren,[1] would be changed somewhat if a mixture of heavy elements differing from the Russell mixture were chosen for the stars. The change would be most marked if the assumed iron abundance were increased, and would perhaps be still more marked if the presence of appreciable amounts of still heavier atoms were assumed.

The general trend of the curves for $(l/\bar{g})$ indicates the various physical phenomena which are important. At the high-temperature end all bound states are poorly populated, and the opacity is small and proportional to the density, so that $(l/\bar{g})$ is large and independent of density. As the temperature is reduced, the states become more populated, and $(l/\bar{g})$ decreases. Below $T = 20{,}000{,}000°$ the K-shell absorption for iron loses its importance, and below $T = 4{,}000{,}000°$ the L-shell absorption preponderates. At about this point the K shells of the heavy elements begin to be filled, the effective nuclear charge for the L shells is thereby reduced, and $(l/\bar{g})$ increases again (the opacity falls again below Kramers' value). As the temperature is further reduced, the opacity becomes less dependent upon density due to the filling of the L shells, so that $(l/\bar{g})$ depends more strongly on the density, the curves for large density rising more steeply than those for small values of ρ. The curve for $\rho = 0.01$ even drops back down, owing to a bunching-together of absorption limits near the lower end of the frequency scale (and is therefore important at low temperatures).

At temperatures below $400{,}000°$ the L shells are nearly filled, and the actual wave functions for the atoms depart so far from the hydrogenic form that the use of an effective nuclear charge is not an adequate correction of equation (1) to give the correct form for the absorption cross-sections. Hartree wave functions, or variational forms, must be used for calculating the cross-sections.

For densities less than 0.01 gm/cm^3, the quantity $(l/\bar{g})$ will not differ very markedly from the curve for $\rho(1+X) = 0.01$ shown, in the range of temperature considered. The minimum value of (l/g) will, in general, be unity; and the smaller the density, the lower must be the temperature before $(l/\bar{g})$ increases again.

SUMMARY

The calculations outlined above make it possible to compute the mean opacity of a mixture of six heavy elements having[7] proportions by weight equal to c_Z, diluted with proportions X and Y of hydrogen and helium, at a temperature $T°$ C and a density ρ gm/cm^3. If the gas is a mixture of hydrogen and helium in any amount, with one of the four mixtures of heavy elements given in Table 3, we can com-

pute the absorption opacity $\bar{\kappa}_a$ by using equation (16) and Table 3. The scattering opacity $\bar{\kappa}_s$ can be computed by using equation (18) and Table 1. The total opacity $\bar{\kappa}$ is then obtained by finding in Table 2 the value of $(\bar{\kappa}/\bar{\kappa}_a)$ corresponding to the ratio $(\bar{\kappa}_a/\bar{\kappa}_s)$, which has been found, and multiplying $(\bar{\kappa}/\bar{\kappa}_a)$ by $\bar{\kappa}_a$.

If the mixture of heavy elements does not correspond to one of those considered in Table 3 but has a composition intermediate between them, a value of $\bar{\kappa}_a$ can be obtained by the interpolation process given in equation (17) and Table 4. The total opacity can be obtained from Table 2, as before. Values of the opacity for densities larger than those considered in this paper can be obtained from the paper of Marshak.[11]

EASTMAN LABORATORY
MASSACHUSETTS INSTITUTE OF TECHNOLOGY
CAMBRIDGE, MASSACHUSETTS

A STUDY OF *He* I LINES IN THE BALMER CONTINUUM

F. E. ROACH AND LEON BLITZER

ABSTRACT

Measurements of the equivalent widths of *He* I lines of the diffuse series have been made for 22 stars of classes Oe5 to B5. In all cases the higher members of the triplet diffuse series, located in the Balmer continuum, are abnormally weak. This weakening has been interpreted in terms of an increase in the continuous absorption coefficient in the Balmer continuum. A comparison of our results with Unsöld's theoretical calculations suggests a high hydrogen content for the stars of this study.

The two diffuse series of neutral helium offer a convenient test of the effect of the depression of the continuous background on the violet side of the head of the Balmer series (λ 3647) upon the intensity of absorption lines. The first five members of the triplet diffuse series have wave lengths greater than λ 3647, while the higher members are in the Balmer continuum. The theoretical absolute intensities of these lines, as well as of the singlet diffuse lines, have been computed by Goldberg,[1] who has shown that it should be possible to combine the two series into a single curve of growth,[2] provided there is thermodynamic equilibrium. This is feasible, in spite of a rather marked difference in the damping constants of the singlet and triplet lines, because in neither case is the damping portion of the curve of growth reached in stellar spectra.

However, when an attempt is made to combine *all* the singlet and triplet lines into a single curve of growth, it is found that the triplet lines in the Balmer continuum are systematically weakened, an effect which makes it necessary to construct two separate curves of growth. This was first observed by Struve and Roach[3] in the spectrum of P Cygni.

The spectrograms of O- and B-type stars for the present study were loaned to us by Dr. Struve from the collection of plates made at the McDonald Observatory with the two-prism quartz spectrograph. Some of the plates have been examined in the near ultraviolet

[1] *Ap. J.*, **90**, 414, 1939. [2] *Ibid.*, **89**, 623, 1939. [3] *Ap. J.*, **90**, 727, 1939.

by Struve, and a number were reproduced in his paper.[4] In all, we were able to measure spectrograms of 22 stars.

The equivalent widths, with respect to the adjacent background, of all the available helium lines were determined in the usual manner. The lines in the portion of the spectrum available to glass spectrographs have been previously measured by Williams[5] and by Rudnick.[6] Our measures are in satisfactory agreement with both, al-

TABLE 1

EQUIVALENT WIDTHS OF HELIUM LINES

(Unit = 0.01 A)

Star (HD)	4471	4026	3819	3634	3587	3554	3530	3512	3498	3487	3479	4922	4388	4144	4009	3926	3872
886	130	120	126	38	30	16	6	....	....	....	....	123	86	76	57	70	35
2905	63	58	60	16	18	11	7	8	12	....	....	....	42	34	26	21	36
3360	138	106	126	32	30	20	....	....	....	....	....	123	89	80	68	68	27
5394	121	143	104	29	23	15	12	10	8	5	4	....	68	81	47	28	....
30512	94	66	48	18	10	7	....	....	....	....	....	....	58	28	17	11	....
30822	109	115	56	26	14	9	6	9	....	....	....	....	70	72	35	9	10
36861	72	84	48	9	7	....	....	....	....	....	....	43	27	16	11	15	....
44743	99	90	69	22	22	14	9	....	....	....	....	116	67	45	41	29	11
52089	78	70	74	29	12	....	....	....	....	....	....	....	53	30	31	....	12
53138	77	65	73	18	15	8	16	....	....	....	....	....	94	42	22	24	14
91316	112	78	65	26	24	16	9	20	14	5	....	84	59	41	32	29	16
149438	112	108	91	38	23	5	11	....	....	....	....	84	62	60	40	29	10
157056	112	113	85	40	28	17	12	9	....	....	....	....	73	62	50	29	9
160762	123	143	116	13	10	....	....	....	....	....	....	106	82	83	62	52	25
164353	102	83	60	20	16	....	....	....	....	....	....	....	42	46	37	34	....
166182	120	111	91	34	29	27	19	11	6	5	....	....	77	73	53	53	18
180163	89	94	83	11	10	6	6	7	....	....	....	....	49	56	50	39	....
193237*	82	75	64	24	....	20	10	16	13	....	....	....	73	44	32	30	34
198478	82	76	62	21	23	....	14	12	12	9	14	85	51	41	33	40	26
205021	158	119	103	27	17	17	6	5	4	....	....	103	74	68	51	45	23
206165	97	82	70	19	22	14	11	8	12	4	....	87	54	40	37	44	32
214680	82	90	59	18	13	5	5	....	....	....	....	62	42	24	17	20	....

* Data for 193237 are from Struve and Roach, *Ap. J.*, **90**, 727, 1939.

though we find that, for the stronger lines, Rudnick's values are slightly lower than ours. In Table 1 we record the values of the equivalent widths, A, adopted in this study. We have averaged our measures with those of Rudnick and Williams whenever there were common values, and have used our measures alone for all other lines. The line λ 3705 is blended with $H\,\lambda$ 3704 and was therefore omitted from Table 1.

For each star the observed values of $\log A/\lambda$ were plotted against the corresponding $\log X_0'$ as defined by Goldberg.[2] The values of $\log X_0'$ in our Table 2 are from his Table 1, except for the higher

[4] *Ap. J.*, **90**, 699, 1939.

[5] *Ap. J.*, **83**, 279, 1936.

[6] *Ap. J.*, **83**, 439, 1936.

members of the triplet series, for which they were determined from Goldberg's asymptotic expression for the oscillator strengths. Figures 1 and 2 show the resultant plots for some of the stars investi-

TABLE 2

LOG X'_0 FOR HELIUM LINES
(From Goldberg)

Transition	λ	log X'_0	Transition	λ	log X'_0
2^3P-4^3D	4472	+1.38	2^1P-4^1D	4922	+0.79
5^3D	4026	+1.05	5^1D	4388	+0.45
6^3D	3820	+0.81	6^1D	4144	+0.15
7^3D	3705	+0.59	7^1D	4009	−0.03
8^3D	3634	+0.43	8^1D	3926	−0.22
9^3D	3587	+0.27	9^1D	3872	−0.40
10^3D	3554	+0.13			
11^3D	3530	+0.02			
12^3D	3512	−0.09			
13^3D	3498	−0.18			
14^3D	3487	−0.28			
15^3D	3479	−0.39			

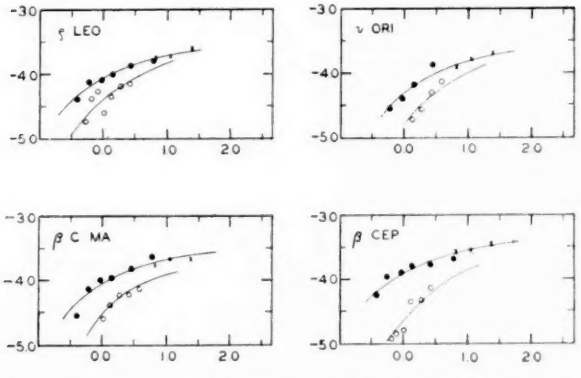

FIG. 1.—Curves of growth. The ordinates are log A/λ; the abscissae, log X'_0. Open circles designate triplet lines in the Balmer continuum; crosses, other triplet lines; closed circles, singlet lines.

gated. It is apparent that the points representing triplet lines on the violet side of λ 3647 fail to lie on the main curve of growth.

Goldberg's theoretical curve of growth for 20,000° K was next fitted to the observed points by moving it vertically and horizontally, these shifts corresponding to the V and Δ, respectively, of his

paper. In the cases for which the data were sufficient, this procedure was followed independently for both sets of points. It was found in this way that for each star the same V will serve for both but that different Δ's are required. In case there were too few points in the continuum to give a completely independent determination of both V and Δ, it was assumed that V has the same value for the points in the continuum as in the unaffected region, and Δ was then determined by a horizontal shift of the theoretical curve. The difference in Δ be-

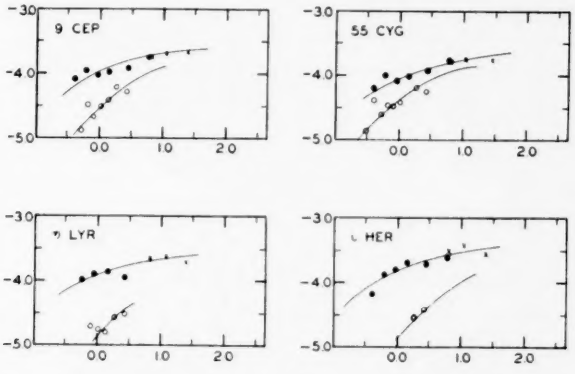

FIG. 2.—Curves of growth. The ordinates are log A/λ; the abscissae, log X'_0. Open circles designate triplet lines in the Balmer continuum; crosses, other triplet lines; closed circles, singlet lines.

tween the two curves, which we shall call Z, may be interpreted as being due to a smaller total number of helium atoms available for absorbing the ultraviolet lines. This weakening of the ultraviolet lines with respect to those on the red side of λ 3647 is the principal observational result of this study and is shown in the fourth column of Table 3. The sixth column lists the luminosity classifications which, with the exception of those in parentheses, are taken from Williams.[7] In the seventh column are the measures of the so-called Balmer discontinuity, D, in the continuous spectrum,[8] where

$$D = \log_{10} \frac{\text{Int } (3647 + \epsilon)}{\text{Int } (3647 - \epsilon)} .$$

[7] *Op. cit.*, p. 305.

[8] Cf. the papers in the *Annales d'astrophysique* by Arnulf, Barbier, Chalonge, *et al.*

That the cause of Z is the depression of the continuous background in the Balmer continuum becomes obvious upon examination of Figure 3, which correlates Z with the D of Chalonge and his collaborators.[8] The increase of Z with D indicates that this is the primary correlation.

TABLE 3

SUMMARY OF RESULTS

STAR		V	Z	SPEC.	LUM.	D*
HD	Name					
886	γ Peg	0.38	0.98	B2	i	+0.13
2905	κ Cas	.12	0.71	Bo	(g)	+ .03
3360	ζ Cas	.38	0.98	B3	i	+ .12
5394	γ Cas	.46	0.68	Bop	(g)	− .19
36512	ν Ori	.32	0.45	Bo	(d)	.....
36822	ϕ Ori	.41	0.64	Bo	(d)	.....
36861	λ Ori (br)	.25	0.50	Oe5	i	+ .03
44743	β C Ma	.35	0.56	B1	i	+ .08
52089	ϵ C Ma	.28	0.51	B1	(i)	+ .07
53138	σ^2 C Ma	.17	0.71	B5p	(g)	+ .08
91316	ρ Leo	.30	0.44	Bop	g	+ .04
149438	τ Sco	.43	0.59	Bo	d	+ .05
157056	θ Oph	.34	0.65	B3	(d)	.....
160762	ι Her	.40	1.36	B3	i	+ .17
164353	67 Oph	.17	0.94	B5p	g	+ .13
166182	102 Her	.35	0.91	B3	(i)	.....
180163	η Lyr	.22	1.26	B3	(i)	.....
193237	P Cyg	.05	0.54	B1p	(g)	− .02
198478	55 Cyg	.15	0.60	B2	g	+ .04
205021	β Cep	.44	0.88	B1	i	+ .08
206165	9 Cep	.20	0.90	B2p	g	+ .06
214680	10 Lac	0.41	0.46	Oe5	i	+0.04

* From the papers by Arnulf, Barbier, Chalonge, *et al.* in *Annales d'astrophysique*.

In a study of lines of *Ti* II in the Balmer continuum Struve and Sherman[9] have observed a similar weakening. They have shown that the weakening, expressed as numbers of atoms, is to be interpreted as a change in the continuous absorption coefficient. This will be true in our case, provided there is no stratification of helium with respect to hydrogen. We have calculated the relative populations of the helium level, 2^1P, as a function of the optical depth, following Swings

[9] *Ap. J.*, **91**, 428, 1940. We are grateful to the authors for the opportunity of examining this paper in manuscript.

and Chandrasekhar,[10] on the assumption of an effective temperature of 20,000° K. Upon comparing these results with those of Swings

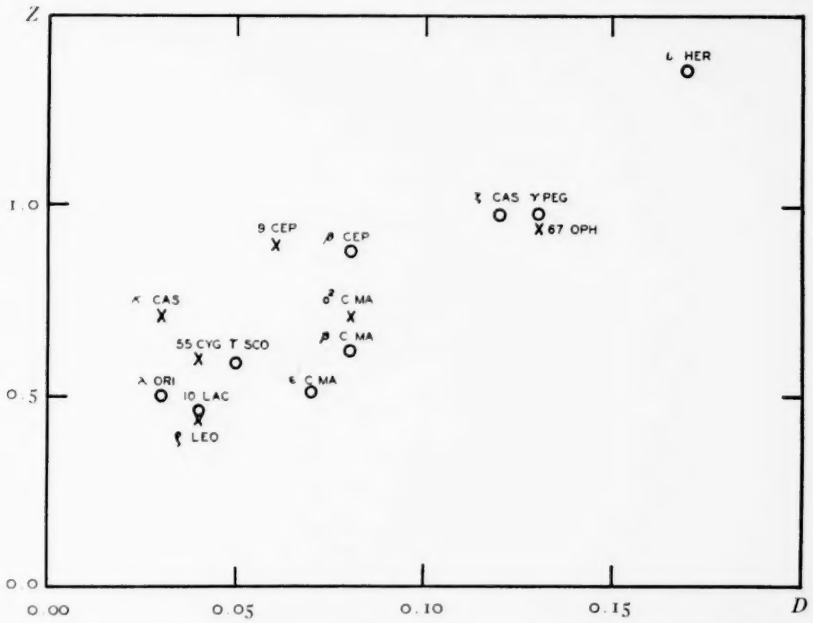

FIG. 3.—The observed weakening in the Balmer continuum plotted against *D*. The points for P Cyg and γ Cas are not included. The symbol code is the same as for Fig. 4.

TABLE 4

Spectral Class	Mean *Z*	Spectral Class	Mean *Z*
Oe5	0.48	B3	1.03
B0	.59	B5	0.82
B1	.62	A0	1.07*
B2	0.83		

* The value of *Z* for A0 is from Struve and Sherman (*Ap. J.*, **91**, 428, 1940). Their measures for η Leo, α Cyg, and α Lyr are included in the mean.

and Chandrasekhar for hydrogen, we obtain the entries of Table 5. It is immediately apparent that the relative stratification is negligible for normal and giant stars and is very small for dwarfs, so that

[10] *M.N.*, **97**, 24, 1936.

we are justified in assuming that the ratio, η, of the mass absorption coefficient within the line, $\kappa_\nu + \sigma_\nu$, to the mass absorption coefficient for continuous radiation, κ, does not vary with optical depth.

If we employ the nomenclature of Struve and Sherman,[9] we have

$$\eta = \frac{\kappa_\nu + \sigma_\nu}{\kappa} = \frac{N(\kappa_{at} + \sigma_{at})}{\kappa},$$

where N is the number of active atoms per gram of gas. Hence, while we have observed an effect which has been interpreted as $\Delta \log N$,

TABLE 5

RATIO OF ABUNDANCE: HYDROGEN (BALMER) TO HELIUM (2^1P) FOR $T_e = 20{,}000°$ K

τ (Optical Depth)	Intermediate	Giant	Dwarf
0.01	5.389	5.371	6.095
0.02	5.385	5.371	6.781
0.05	5.446	5.400	7.282
0.10	5.400	5.380	7.325
0.20	5.398	5.382	6.849
0.50	5.360		6.159
0.666	5.152		5.683
1.0	5.373		5.661
1.5	5.392		5.541
2.0	5.462		5.553
3.0	5.354		5.401
4.0	5.362		5.391

or Z, the cause of the measured apparent *decrease* in N is an actual *increase* in the mass absorption coefficient, κ, due to the photoionization of hydrogen.

The observed Z of this paper may, therefore, be compared with the theoretical value of the increase in the mass absorption coefficient at the Balmer head. Unsöld[11] has computed this increase for pure hydrogen (his Table 30, p. 127) and for a ratio of hydrogen atoms to metallic atoms of 13.7:1 (his Table 28, p. 121). In Figure 4 are shown our observations, together with the two curves from Unsöld, as a function of $\theta(=5040/T)$. With the exception of two high points

[11] *Physik der Sternatmosphären*, Berlin: Julius Springer, 1938.

(η Lyrae and ι Herculis) the observed data scatter about the curve for pure hydrogen. In principle, it should be possible to determine in this manner the percentage of hydrogen in stellar atmospheres, especially if the weakening of lines in the continuum is measured for

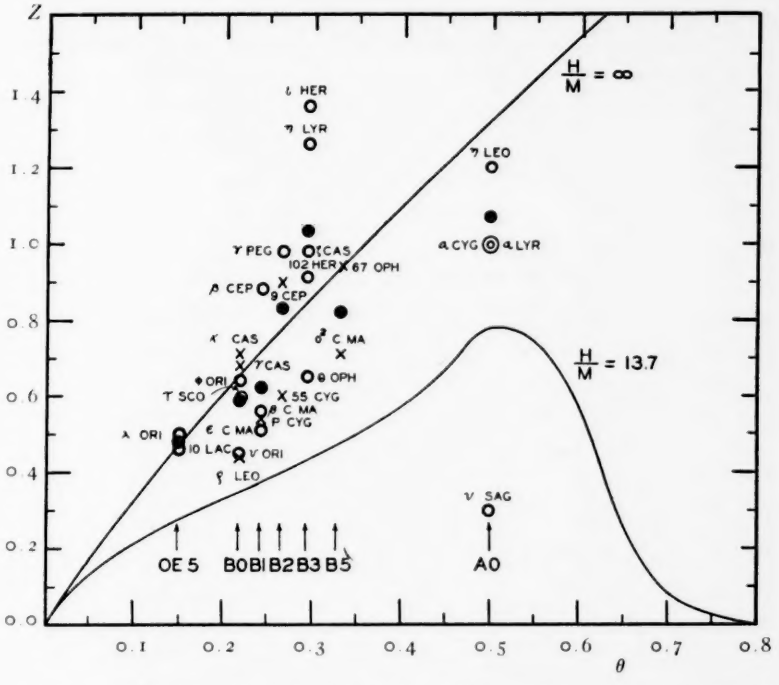

FIG. 4.—The observed weakening in the Balmer continuum as a function of θ ($=5040/T$). Open circles designate dwarfs and intermediates; crosses, giants; closed circles, the means by spectral class. The data for α Cyg, α Lyr, η Leo, and υ Sag are from Struve and Sherman.[9] The two solid lines are from Unsöld's calculations of the increase of the continuous absorption coefficient in the Balmer continuum; the upper curve is for pure hydrogen; the lower, for $H/M = 13.7$.

stars of spectral classes later than Ao. From our data, together with the points from the paper by Struve and Sherman, omitting υ Sagittarii, we have also plotted the averages by spectral class (solid circles). The results favor a much higher hydrogen content than $H/M = 13.7$.

Those points which fall considerably above the mean curve, as those for η Lyrae and ι Herculis, are of particular interest. That

these points are associated with a Stark effect is ruled out, since there is, in general, no correlation of the weakening with absolute magnitude, a result which is impossible if Stark effect is involved.[12]

On the other hand, the vertical displacements of our curves of growth, V, are definitely functions of luminosity. The mean value of V for the dwarfs and the intermediate stars is 0.35, and for the giants, 0.20. Goldberg's[2] Figure 5 indicates the same result, and he suggests that "in the low-luminosity groups the value of V is a measure of the average Stark broadening in the diffuse series, while in the giants V measures the degree of turbulence in the stellar atmosphere."

Attention is called to the stars P Cygni and γ Cassiopeiae. For these stars the Balmer continuum is found to be emission rather than absorption: D is negative. Nevertheless, we find appreciable values of Z, about the average for the respective spectral classes. This is not unexpected: the continuous absorption of hydrogen within the shells of these stars should produce a weakening of *He*-lines if the latter are also produced in the shell.[13]

We are indebted to Miss Frances Sherman, who made a number of the microphotometer tracings for us at the Yerkes Observatory. We wish to express our appreciation also to the McDonald Observatory and to Dr. Struve for lending us the spectrograms for this study, and to acknowledge the value of discussions of the problem with Dr. Struve.

STEWARD OBSERVATORY
AND
DEPARTMENT OF PHYSICS
UNIVERSITY OF ARIZONA
March 1940

[12] The role of Stark effect in the calculations of his theoretical curves of growth of B-type stars was discussed by Goldberg.[2] He assumed an average Stark broadening for all the diffuse series lines; whereas a rigorous solution should consider the increase of Stark broadening with serial number. It is apparent that if Stark broadening is significant it should enhance the equivalent widths of the higher members of the series and thus produce an effect the opposite of that which we have observed.

[13] Struve, *Proc. Nat. Acad. Sci.*, **26**, 117, 1940.

HETEROCHROMATIC SURVEYS OF INFRARED VARIABLE STARS

CHARLES HETZLER

ABSTRACT

Seven late M-type variables—T Cep, R Cas, R Leo, R Aql, *o* Cet, X Oph, and R Aqu—are included in this first of a series of papers on the heterochromatic photometry (particularly at 8500 A) of about forty infrared variable stars. The average relative magnitude ranges are 4.94, 4.29 (first two stars only), 4.73, 2.43, and 1.95 in the ultraviolet, photographic, visual, 8500 A, and 9100–9250 A regions, respectively.

The tri-color condition for a black star is shown to be that the plot (designated as "slope-index") of any two color indices gives a straight line whose slope depends only on the wave lengths and which passes through the origin. The indices involving the ultraviolet and infrared magnitudes come closest to meeting this condition, and temperatures from these indices are therefore considered most reliable. Using these temperatures (averaging 2800° at maximum and 2100° at minimum), the differential absorption in the visual region between maxima and minima is calculated for each of the variables, being least for R Cas and R Leo, and around 2 mag. for each of the others, the average being 1.4 mag.

It is shown that, for a black variable, star magnitudes at any wave length plotted against those at any other give a straight line of slope equal to the ratio of the wave lengths. Plots of visual against 8500 A magnitudes give straight lines (except for curvature near the maxima of stars having a delayed infrared drop and near the minima of stars having companions) of medial slopes 1.92, 1.87, 1.82, 1.94, 1.95, 1.80, and 1.92 for the seven stars, respectively, averaging 1.89, as compared to the theoretical value 1.54. The delayed infrared drop and the steeper slopes near maxima, particularly in *o* Ceti, are interpreted as an effect of band absorption which is not synchronous with, or proportional to, the temperature change; and the generally steeper slopes are due primarily to a superposition upon the black-body slope of an absorption which, on the average, increases linearly toward minimum; but changes of diameter would also contribute to this effect. The ultraviolet magnitudes plotted against the infrared magnitudes give straight lines of slopes near the theoretical value of 2.3; hence, band absorption is probably the chief factor of departures in the visual region. The *y*-intercepts give the radii and possible changes in radii, if we know the individual absolute magnitudes.

Extrapolation of the medial straight-line portions of the visual *minus* infrared and ultraviolet *minus* infrared slope-index curves yield the visual and ultraviolet magnitudes, and hence the colors, of the companions to *o* Cet, X Oph, and R Aqu.

In previous articles[1] the instruments and methods of heterochromatic photometric surveys, particularly in the infrared, have been briefly described. The filter and emulsion combinations and the resulting effective wave lengths have already been indicated. This is the first of a series of articles which will give the magnitude tables and corresponding curves of about forty infrared (long-period) varia-

[1] *Ap. J.*, **82**, 75, 1935; **83**, 372, 1936; **86**, 509, 1937.

bles, particularly at 8500 A, but also to some extent at 9100 A and 9250 A and at 3725 A, with visual-curves of the A.A.V.S.O. (kindly furnished by Professor Leon Campbell, of Harvard Observatory) and, for a few stars, with photographic-curves by Müller.[2] In this paper we present the data for the variables T Cep, R Cas, R Leo, R Aql, *o* Cet, X Oph, and R Aqu. Since all of these stars have spectra of late M type, it is of interest to compare them; and since the last three have known or suspected companions, certain deductions can be drawn from any departures from regularities found in the other four.

Although it is generally recognized that stars do not radiate at their surfaces strictly as black bodies because of absorption bands, particularly of *TiO* in M stars and of *CN* in N stars, the amount and individual behavior of these deviations are little known, and comparison with some standard is fundamental in understanding them. The equation for the absolute magnitude of a black star at any wave length is (to an approximation accurate enough for our purpose):[3]

$$M_\lambda = C_\lambda + \frac{1.560}{\lambda T} - 5 \log R . \qquad (1)$$

The absolute visual magnitude of the sun, for which R is taken as 1, is known; hence we may readily compute C_λ for the effective wave length of the eye, about 5300 A for the sun. Having determined the visual constant, C_v, the constants for other effective wave lengths can be computed by considering that for Ao stars, for which T is fairly well established at around 11,000°, all absolute magnitudes are equal. The values of C for the various wave lengths we are considering (adopting 5500 A for the visual for red stars) are: $C_{37} = -1.23$, $C_{42} = -0.72$, $C_{53} = -0.08$, $C_{55} = 0.02$, $C_{85} = 0.93$, $C_{91} = 1.04$, and $C_{93} = 1.07$, the subscripts defining the spectral region in hundreds of angstroms. The difference in magnitude at any two wave lengths is an index of the color and temperature. For various combinations of magnitudes at different effective wave lengths the tempera-

[2] *Pub. Ap. Obs. Potsdam*, **29**, 2, 1938.

[3] Russel, Dugan, and Stewart, *Astronomy*, p. 733, 1927.

ture indices are readily transformed into the following temperatures:

$$\left.\begin{aligned} T &= \frac{7200^\circ}{I_{42-53} + 0.64} : T = \frac{18{,}350^\circ}{I_{42-85} + 1.65} : T = \frac{10{,}000^\circ}{I_{55-85} + 0.91} : \\ T &= \frac{23{,}800^\circ}{I_{37-85} + 2.16} : T = \frac{25{,}000^\circ}{I_{37-91} + 2.27} : T = \frac{25{,}300^\circ}{I_{37-93} + 2.30} . \end{aligned}\right\} \quad (2)$$

These equations will be used in our considerations of the empirical indices from the data of the curves.

Starting again with the general equation (1), it is readily seen that for the two wave lengths, λ_1 and λ_2,

$$M_{\lambda_1} = \frac{\lambda_2}{\lambda_1} M_{\lambda_2} + \left[C_{\lambda_1} - 5 \log R - \frac{\lambda_2}{\lambda_1} (C_{\lambda_2} - 5 \log R) \right] \quad (3)$$

and

$$R = \text{antilog} \left[\frac{\lambda_1(y\text{-intercept}) + \lambda_2 C_{\lambda_2} - \lambda_1 C_{\lambda_1}}{5(\lambda_2 - \lambda_1)} \right] . \quad (4)$$

These equations are independent of the temperature. Thus, a plot of the absolute magnitudes of a "perfect variable" at two wave lengths is a straight line of slope equal to the ratio of the wave lengths. The *y*-intercept of this straight line depends upon the radius as well as upon the wave lengths. Such plots for actual stars will be designated as "*bi-color*," or 2λ, *slope-indices*. Changes of radius mean different intercepts at different points, amounting to an overall change of slope; but the slope-index curves would still be straight if the change in radius is uniform. The radii and changes of radii can be determined from the intercepts if the absolute magnitudes are known, as they are for a few long-period variables, such as *o* Ceti. This star is the only one whose radial velocity has been measured, showing a range from 64 to 52 km/sec, the greatest velocity of approach being at minimum. Differential band absorption in actual variables would also alter the ideal slopes, since both absorption and radii increase toward minimum; and only if the amount of the one is known, as in *o* Ceti (if the change in radius is real), can the effect of the other be inferred.

It is evident that some criterion independent of the radius is needed to decide between changes of radius and of absorption, since disagreement of the slope with the ratio of the wave lengths does not necessarily mean deviation from a black body if the radius changes with the temperature, nor does agreement indicate radiation like a black body if absorption and changes in radius compensate one another. Considering again equation (1), this time at three wave lengths, we have

$$M_{\lambda_2} - M_{\lambda_1} = C_{\lambda_2} - C_{\lambda_1} + \frac{C}{T}\left(\frac{1}{\lambda_2} - \frac{1}{\lambda_1}\right)$$

and

$$M_{\lambda_3} - M_{\lambda_1} = C_{\lambda_3} - C_{\lambda_1} + \frac{C}{T}\left(\frac{1}{\lambda_3} - \frac{1}{\lambda_1}\right).$$

The left-hand members of these equations are the color indices, I_{21} and I_{31}. For an Ao star the color index is zero between any two wave lengths. Thus, at the temperature T_{Ao},

$$I_{Ao} = o = C_{\lambda_2} - C_{\lambda_1} + \frac{C}{T_{Ao}}\left(\frac{1}{\lambda_2} - \frac{1}{\lambda_1}\right) = C_{\lambda_3} - C_{\lambda_1} + \frac{C}{T_{Ao}}\left(\frac{1}{\lambda_3} - \frac{1}{\lambda_1}\right).$$

Subtracting these equations from those preceding, we have

$$I_{21} = C\left(\frac{1}{T} - \frac{1}{T_{Ao}}\right)\left(\frac{1}{\lambda_2} - \frac{1}{\lambda_1}\right) \quad \text{and} \quad I_{31} = C\left(\frac{1}{T} - \frac{1}{T_{Ao}}\right)\left(\frac{1}{\lambda_3} - \frac{1}{\lambda_1}\right),$$

whence

$$I_{21} = \frac{\left(\frac{1}{\lambda_2} - \frac{1}{\lambda_1}\right)}{\left(\frac{1}{\lambda_3} - \frac{1}{\lambda_1}\right)} I_{31}. \tag{5}$$

The tri-color condition for black-body radiation is, therefore, that a plot of any two color indices as ordinate and abscissa yield a straight line passing through the origin with a slope involving only the wave lengths, independently of R and T. We shall apply this *tri-color slope-index* to our observational color indices.

Figures 1–3 show the heterochromatic-curves for the seven variables. The corresponding data are given, together with the comparison stars and their adopted magnitudes, in Tables 1–20. As indicated in the notes to the tables, the earlier portions of the curves at 8500 A (*P*-emulsions) and the earlier points at 9250 A (*Q*-emulsions) are from data obtained with the 30-inch refractor of the Allegheny Observatory. All other observations were made with the 24-inch reflector of the Yerkes Observatory. With the *Q* and *M* emulsions (effectively at 9250 A and 9100 A), because of their wide range of sensitivity, the bluer stars are of significantly shorter effective wave length, particularly with a reflector where there are no focal differences. This makes the bluer comparison stars systematically too bright, for these wave-length regions,[4] relative to the variables. Most of the comparison star magnitudes at 8500 A were obtained by direct or indirect comparison with Vega, but at the other wave lengths they have been largely computed from visual magnitudes of the *Henry Draper Catalogue*. Supposing the bluer comparison-star magnitudes to be correctly computed for 9100 A and 9250 A, the variable-star magnitudes will be relatively too faint; but since the values adopted for the comparison stars are somewhat uncertain, no corrections for differences in effective wave length were attempted. The ranges of the variables are independent of the comparison stars whenever the same ones are always used. The streakiness and poor keeping qualities and possible differences in different batches of the *M* and *Q* emulsions are also to be considered as contributing to any, otherwise unexplainable, irregularities in the results.

The magnitudes at 9100 A, at 8500 A, in the visual, and in the ultraviolet are shown as solid circles, while those at 9250 A and the photographic magnitudes of Müller are shown as open circles. The weights of the points are indicated in the tables. The visual points are ten-day means which tend to smooth those observations. There are a number of instances where observations at 8500 A which depart from the curves are associated with similar departures in the ultraviolet or at 9100 A and 9250 A, and possibly many of the irregular fluctuations are real. These fluctuations, however, are relatively insignificant.

[4] *Ap. J.*, **86**, 511, 1937.

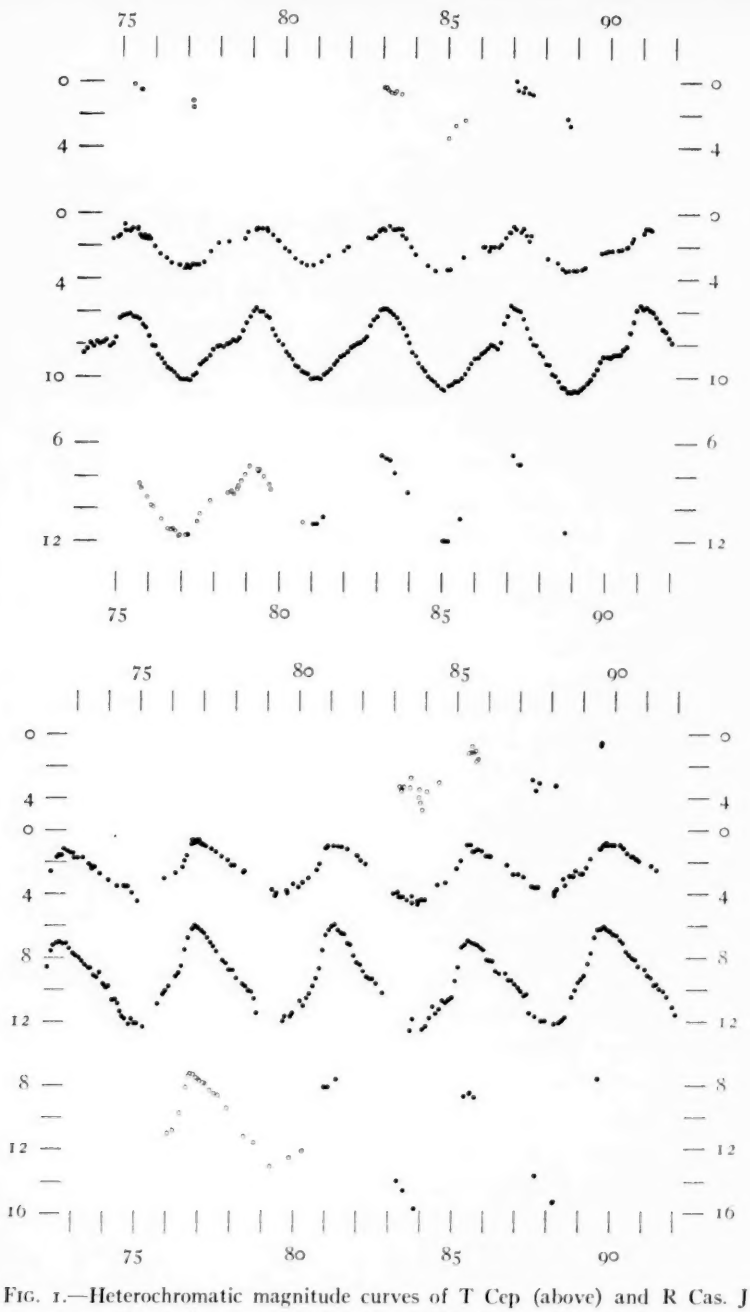

FIG. 1.—Heterochromatic magnitude curves of T Cep (above) and R Cas. JD 2427200–9200. *Top to bottom:* 9200 A infrared (M plates solid and Q plates open circles), 8500 A infrared, visual (A.A.V.S.O. ten-day means), 3700 A uv (solid) and ptg. (open) by Müller (see Tables 1–6).

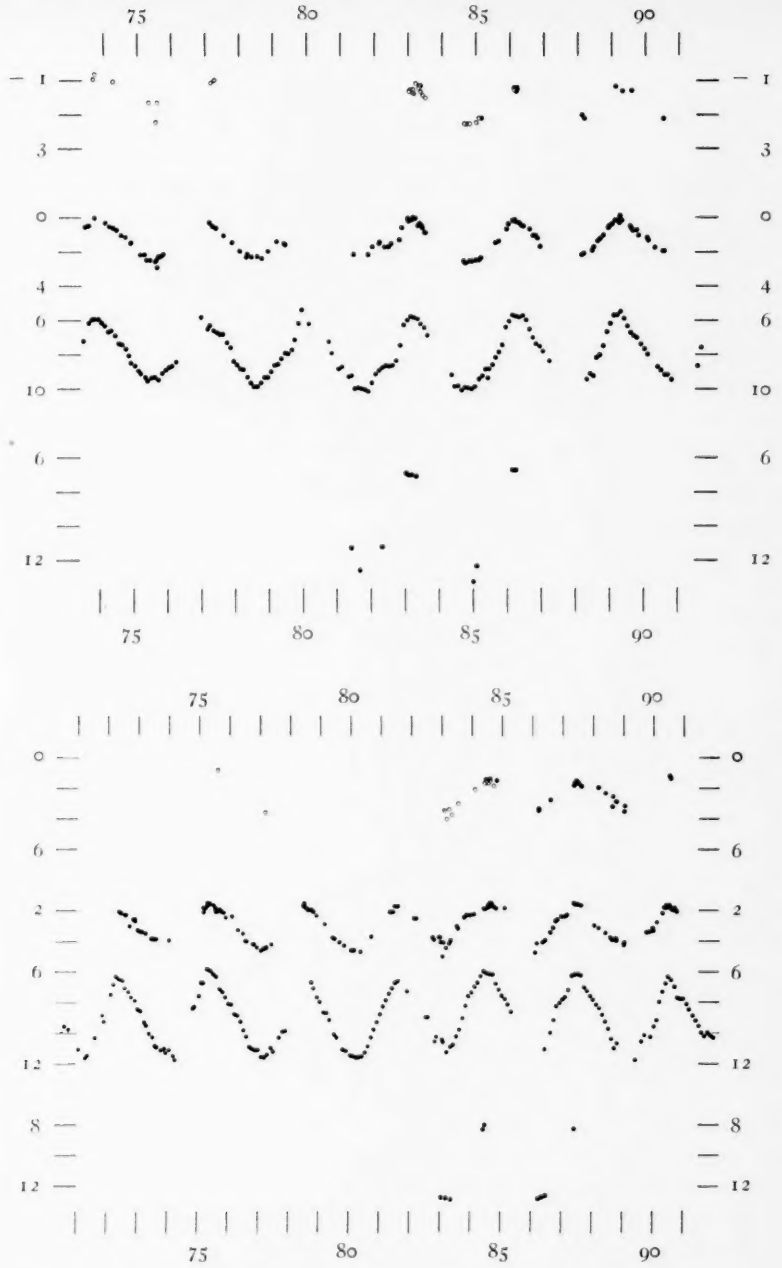

FIG. 2.—Heterochromatic magnitude curves of R Leo (above) and R Aql. JD 2427200–9200. *Top to bottom:* 9200 A infrared (M plates solid and Q plates open circles), 8500 A infrared, visual (A.A.V.S.O. ten-day means), and 3700 A uv (see Tables 10–15).

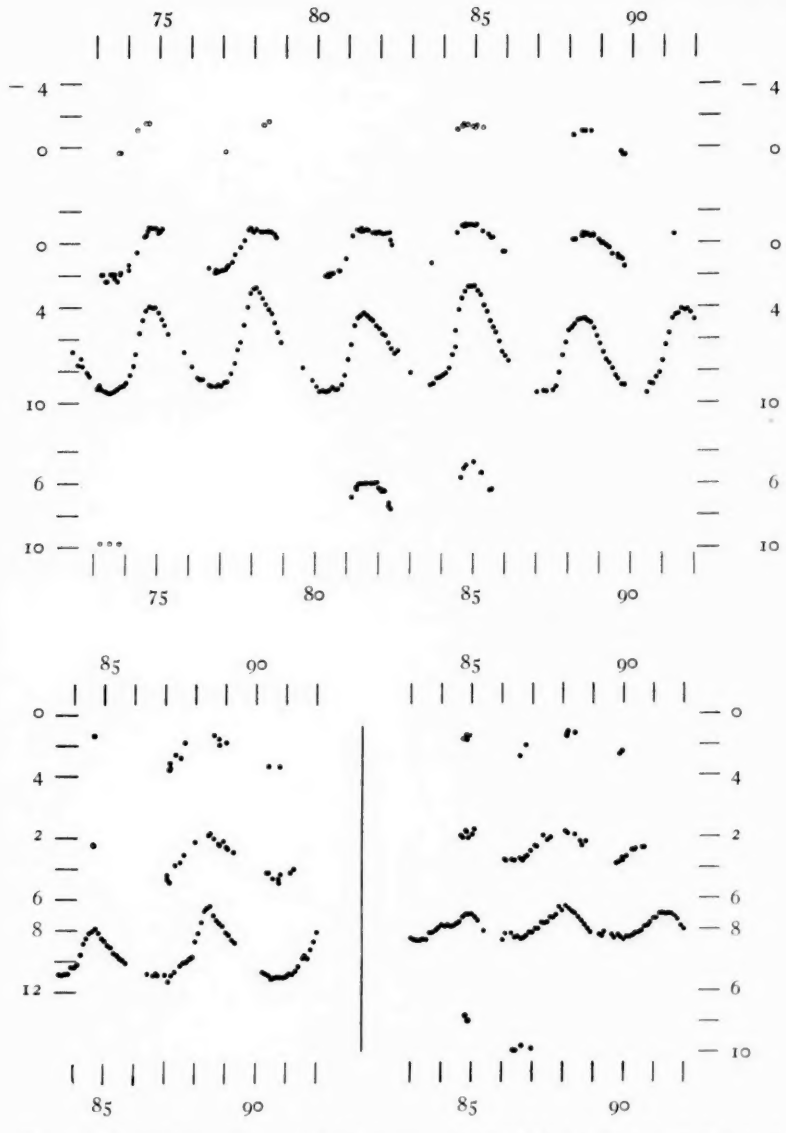

FIG. 3.—Heterochromatic magnitude curves of *o* Cet (*above*), R Aqu (*left, below*) and X Oph. JD 2427300–9200. *Top to bottom:* 9200 A infrared (M plates solid and Q plates open circles), 8500 A infrared, visual (A.A.V.S.O. ten-day means), and 3700 A uv (see Tables 7–9 and 15–20).

TABLE 1

T Cephei at 8500 A

JD 242+	Mag.	Quality	JD 242+	Mag.	Quality
7475	1.58	g	8282	1.29	f
490	1.41	vg	293	1.06	f
498	1.29	g	294	0.97	g
512	0.65	fg	303	0.87	g
514	1.06	g	310	0.96	vg
516	1.09	g	324	0.72	fg
527	1.06	p	335	0.91	vg
530	0.99	g	336	0.91	g
537	0.87	g	344	0.93	pf
549	0.93	g	351	0.90	g
558	1.29	g	362	0.93	g
565	1.48	f	363	1.29	g
570	1.38	g	377	1.48	g
571	1.29	g	391	2.01	g
575	1.47	f	404	2.44	g
581	1.58	f	443	3.15	g
584	1.40	pf	468	3.45	g
589	1.58	g	502	3.41	f
602	2.01	g	514	3.39	vg
620	2.44	fg	552	2.63	f
639	2.73	g	614	2.01	g
654	3.00	g	619	2.01	vg
679	3.16	vg	633	2.23	f
680	3.15	g	637	1.99	vg
692	3.45	f	647	2.02	g
698	3.32	g	661	2.03	f
701	3.14	g	669	1.86	fg
705	3.23	fg	682	1.44	vg
709	3.31	fg	695	1.13	vg
719	3.15	fg	697	1.13	p
727	3.15	g	707	0.76	g
739	3.11	pf	714	0.87	vg
757	2.96	f	730	1.09	vg
777	2.31	f	738	0.88	g
799	1.90	g	746	1.29	g
820	1.71	g	754	1.64	g
861	1.29	p	761	1.30	g
880	1.53	g	813	2.73	vg
888	1.11	vg	842	2.96	vg
915	0.96	vg	858	3.32	vg
915	0.88	fg	868	3.48	fg
921	0.87	g	878	3.45	vg
934	0.86	g	893	3.45	vg
947	0.87	vg	902	3.47	g
948	0.99	g	918	3.39	g
964	1.25	g	926	3.24	g
979	1.61	fg	979	2.38	fg
985	1.63	vg	991	2.31	fg
8002	2.11	vg	999	2.24	fg
016	2.31	g	9011	2.23	fg
034	2.73	fg	029	2.20	fg
053	2.96	vg	041	2.15	fg
068	3.12	vg	055	2.01	fg
090	3.15	vg	059	2.00	vg
114	2.89	vg	070	1.71	fg
138	2.54	fg	077	1.48	fg
184	2.24	g	109	1.19	g
197	2.02	p	112	0.75	fg
199	2.01	f	120	0.85	fg
259	1.44	?	125	0.87	fg
271	1.49	g	132	0.95	g

The Allegheny 30-inch refractor was used through JD 2428068; thereafter the Yerkes 24-inch reflector. The comparison star was α Cep (2.01 mag.).

TABLE 2

T Cephei at 3700 A

JD 242+	Mag.	Quality	JD 242+	Mag.	Quality
8101	10.91	fg	8502	11.99	f
114	10.91	g	503	11.97	fg
131	10.48	f	517	11.97	fg
311	6.76	fg	552	10.61	f
323	6.90	f	715	6.70	fg
335	7.03	vg	730	7.29	f
351	7.78	g	738	7.26	vg
391	8.97	f	878	11.44	g

The comparison stars with their computed ultraviolet magnitudes were: HD 201731 A2 6.76; 201684 A3 7.95; 202614 A0 8.28.

TABLE 3

T Cephei at 9250 A and at 9100 A

JD 242+	Mag.	Quality & Comp.	JD 242+	Mag.	Quality & Comp.
7537	0.16	p 1	8502	3.42	fg 2
558	0.45	f 1	523	2.64	g 2
559	0.45	f 1	552	2.33	vg 3
717	1.27	f 1	709	-0.09	fg 1
718	1.51	fg 1	715	0.46	fg 1
8304	0.33	f 2	730	0.57	f 1
310	0.32	fg 2	737	0.31	p 1
316	0.47	fg 2	746	0.62	g 1
324	0.62	fg 2	761	0.76	g 1
336	0.66	fg 2	868	2.23	fg 1
341	0.53	fg 2	878	2.62	g 1
357	0.72	f 2			

The Allegheny refractor was used through JD 2427718; thereafter the Yerkes reflector. Q plates (9250A) were used through JD 2428552; thereafter M plates (9100A). The comparison stars were: 1 = α Cep (2.30 mag. for the refractor and 1.90 mag. for the reflector); 2 = α Lyr (0.00 mag.) and 3 = α Aur (-0.74 mag.).

TABLE 4

R Cassiopeiae at 8500 A

JD 242+	Mag.	Quality & Comp.	JD 242+	Mag.	Quality
7227	2.57	pf 1	7375	2.72	vg
238	1.69	f 2	404	3.15	g
245	1.57	f 2	430	3.55	g
255	1.57	f 2	453	3.56	g
261	1.15	pf 3	457	3.55	vg
272	1.29	g 3	464	3.57	f
282	1.43	fg 3	477	3.95	pf
290	1.44	fg 3	495	4.45	vp
291	1.71	fg	581	3.03	f
300	2.01	pf	614	2.72	f
306	1.72	fg	637	2.31	g
322	1.73	vg	643	1.90	g
341	2.13	vg	651	1.59	vg
351	2.43	fg 3	667	0.86	f
352	2.30	g	669	0.66	g
359	2.31	g	672	0.64	g

TABLE 4 (continued)

R Cassiopeiae at 8500 A

JD 242+	Mag.	Quality	JD 242+	Mag.	Quality
7677	0.77	g	8443	3.44	vg
680	0.65	vg	466	3.25	g
687	0.57	g	501	2.39	fg
690	0.76	g	514	1.89	g
698	0.87	fg	534	0.87	g
701	0.86	g	544	0.87	pf
709	0.96	g	552	1.29	g
727	1.16	f	556	1.30	g
741	1.34	fg	566	1.16	vg
758	1.59	g	580	1.29	vg
777	1.89	g	594	1.59	g
790	2.22	pf	602	1.60	g
799	2.21	fg	609	1.58	g
830	2.61	f	661	2.16	g
832	2.54	vg	682	2.54	g
919	3.72	vg	697	2.73	vg
931	4.13	g	715	2.92	g
934	3.96	vg	740	3.49	vg
964	3.78	vg	752	3.56	g
966	3.95	g	761	3.56	vg
985	3.39	pf	813	4.09	g
8002	3.55	fg	814	3.87	vg
016	3.28	g	820	3.68	pf
034	3.05	g	840	3.03	g
044	3.04	f	847	3.44	vg
062	2.50	vg	858	2.83	vg
068	2.12	fg	870	2.85	vg
088	1.13	vg	879	2.44	g
090	1.10	f	893	2.54	fg
094	1.02	vg	902	2.54	f
113	0.99	vg	911	2.31	fg
128	0.97	vg	925	1.75	fg
140	1.06	p	954	1.06	fg
156	1.16	vg	957	1.06	fg
186	1.60	p	964	0.87	f
187	1.59	g	969	0.88	fg
197	1.89	g	975	0.76	fg
213	2.12	pf	981	0.86	g
303	3.99	g	994	0.87	pf
316	3.90	g	998	1.21	pf
319	4.15	vp	999	0.87	fg
324	4.14	vg	9019	0.85	f
332	4.14	vg	029	1.01	fg
345	4.39	vg	041	1.40	fg
362	4.15	vp	055	1.65	fg
363	4.56	f	059	1.64	f
379	4.64	pf	069	1.73	fg
381	4.44	g	078	1.86	fg
391	4.38	g	116	2.22	fg
404	4.38	g	133	2.45	fg

The Allegheny refractor was used through JD 2428068; thereafter the Yerkes reflector. The comparison star was β Cas (1.59 mag.) except: 1 = α Lyr (0.00 mag.); 2 = α Aql (0.43 mag.); and 3 = α And (2.01 mag.).

TABLE 5

R Cassiopeiae at 3700 A

JD 242+	Mag.	Quality	JD 242+	Mag.	Quality
8092	8.11	f	8345	14.65	f
105	8.14	fg	381	15.68	f
131	7.62	f	534	8.69	fg
325	14.00	f	550	8.53	fg

TABLE 5 (continued)

R Cassiopeiae at 3700 A

JD 242+	Mag.	Quality	JD 242+	Mag.	Quality
8552	8.48	fg	8819	15.30	f
566	8.70	f	820	15.25	f
761	13.65	f	957	7.58	f

The comparison stars with their assumed or derived ultraviolet magnitudes were: BD +50° 4208 = HD 224648 B9 7.17; BD +50° 4198 = HD 224456 B9 8.82; BD +50° 4200 10.98 (faint companion to R Cas); BD +50° 4202 9.42.

TABLE 6

R Cassiopeiae at 9250 A and at 9100 A

JD 242+	Mag	Quality & Comp.	JD 242+	Mag.	Quality & Comp.
7380	1.93	fg 1	8545	1.14	fg 4
8317	3.24	f 2	547	0.72	g 3
324	3.53	pf 3	552	1.11	g 4
332	3.26	fg 3	556	0.97	fg 4
352	3.29	f 3	559	1.64	fg 4
353	2.68	f 3	566	1.54	g 4
378	3.94	fg 3	740	2.83	g 1
381	3.44	pf 4	752	3.59	vg 1
384	4.26	fg 4	761	3.07	vg 1
391	4.71	f 4	813	3.22	f 1
405	3.58	f 4	814	3.22	fg 1
443	3.00	fg 3	954	0.70	g 1
534	1.14	g 3	957	0.52	fg 1

The Allegheny refractor was used for JD 2427380. Q emulsion was used through JD 2428566; thereafter M emulsion. The comparison stars were: 1 = β Cas (1.93 mag.); 2 = η Aql (0.49 mag.); 3 = α Lyr (0.00 mag.) and 4 = α Aur (-0.74 mag.).

TABLE 7

o Ceti at 8500 A

JD 242+	Mag.	Quality	JD 242+	Mag.	Quality
7315	1.94	g	7485	-0.90	g
322	1.84	vg	489	-0.93	g
333	2.35	pf	496	-0.69	g
335	2.38	pf	498	-0.77	g
345	2.19	f	503	-0.75	f
346	1.95	f	511	-0.92	g
349	1.93	vg	657	1.46	fg
357	2.17	g	677	1.81	pf
358	1.96	pf	679	1.75	fg
367	2.37	vp	680	1.65	vg
374	1.94	f	687	1.75	f
377	1.81	g	698	1.63	p
404	1.37	g	701	1.67	g
405	1.65	p	709	1.60	f
430	0.52	f	713	1.46	f
454	-0.43	g	719	1.37	fg
458	-0.49	g	731	1.15	f
464	-0.80	g	740	0.68	f
467	-1.03	f	757	0.23	f
477	-0.92	vp	769	-0.20	g
483	-0.92	g	782	-0.86	g

TABLE 7 (continued)

o Ceti at 8500 A

JD 242+	Mag.	Quality	JD 242+	Mag.	Quality
7789	-0.96	pf	8460	-1.08	fg
799	-0.77	fg	466	-1.18	fg
807	-0.92	g	468	-1.03	fg
820	-0.75	fg	471	-1.15	vg
827	-0.78	g	477	-1.12	g
840	-0.77	vg	481	-1.17	g
846	-0.76	f	491	-1.15	g
853	-0.75	g	501	-1.11	g
865	-0.58	vg	506	-1.15	vg
870	-0.39	fg	524	-0.73	vg
8027	2.03	vg	544	-0.55	g
034	2.08	g	552	-0.39	pf
039	1.94	vg	557	-0.40	g
040	2.04	g	590	0.52	g
043	1.89	vg	595	0.50	g
052	1.90	f	813	-0.20	vg
070	1.74	vg	814	-0.20	vg
072	1.76	pf	820	-0.18	g
094	0.94	vp	840	-0.43	pf
113	-0.46	fg	842	-0.63	vg
128	-0.83	g	846	-0.43	g
140	-0.75	fg	849	-0.57	g
141	-0.92	f	858	-0.58	g
147	-0.77	f	861	-0.50	g
156	-0.63	p	867	-0.45	g
157	-0.86	fg	868	-0.43	vg
162	-0.82	vg	877	-0.50	fg
177	-0.63	vg	878	-0.43	g
183	-0.60	g	893	-0.20	vg
187	-0.65	g	902	0.03	g
194	-0.73	fg	907	0.00	g
199	-0.62	f	918	0.17	g
208	-0.63	g	926	0.33	fg
209	-0.63	g	936	0.68	pf
220	-0.65	g	954	0.75	fg
230	-0.60	?	957	0.94	g
232	-0.20	g	964	0.95	f
237	0.10	g	970	1.05	fg
363	1.24	?	975	1.46	fg
444	-0.63	fg	9133	-0.57	fg

The Allegheny refractor was used through JD 2428072; thereafter the Yerkes reflector. The comparison star was α Cet (-0.20 mag.).

TABLE 8

o Ceti at 3700 A

JD 242+	Mag.	Quality	JD 242+	Mag.	Quality
7300			8199	6.31	fg
to	9.8	g	208	6.43	fg
7350			209	6.50	fg
8115	6.92	g	220	6.56	fg
128	6.29	vg	232	7.50	f
129	6.37	f	233	7.27	fg
138	6.11	g	237	7.66	p
147	6.08	f	460	5.65	fg
157	6.07	f	468	5.07	fg
162	6.10	fg	477	4.89	fg
177	6.08	g	501	4.70	fg
183	6.08	fg	524	5.35	g
187	6.03	fg	552	6.46	f
194	6.05	fg	557	6.41	fg

Notes to Table 8:
The comparison star for all observations except those of 1933 was HD 18884 for which the magnitude 5.65 was adopted, based upon an adopted ultraviolet magnitude of 4.93 for HD 18883. The 1933 magnitude was based upon observations at Allegheny (Ap. J. 82, 84, 1935) plus an adopted ultraviolet magnitude of 9.90 for BD -3°357 A3.

TABLE 9

o Ceti at 9250 A and at 9100 A

JD 242+	Mag.	Quality	JD 242+	Mag.	Quality
7372	0.32	g	8477	-1.43	vg
377	0.30	g	492	-1.33	g
430	-1.12	vp	501	-1.23	g
458	-1.54	vg	506	-1.35	fg
467	-1.55	fg	524	-1.25	g
709	0.23	g	814	-0.76	fg
830	-1.44	f	841	-1.05	fg
846	-1.65	pf	849	-1.07	fg
8444	-1.12	g	858	-1.04	g
460	-1.35	fg	964	-0.26	fg
466	-1.46	g	970	0.47	fg
471	-1.45	g	975	0.45	vg

The Allegheny refractor was used through JD 2427846; thereafter the Yerkes reflector. Q plates (9250 A) were used through JD 2428524; thereafter M plates. A value of -0.40 mag. was adopted for α Cet, the comparison star, at this wave length.

TABLE 10

R Leonis at 8500 A

JD 242+	Mag.	Quality	JD 242+	Mag.	Quality
7349	0.52	f	7827	2.25	f
358	0.43	fg	828	2.14	vg
361	0.43	g	841	2.25	vg
377	0.00	g	858	2.25	g
407	0.27	f	871	2.36	g
408	0.28	fg	888	1.95	g
420	0.47	g	914	1.38	vg
431	0.57	f	924	1.49	vg
442	0.70	f	940	1.57	pf
456	1.00	pf	8141	2.15	g
468	1.14	pf	185	2.14	f
482	1.48	fg	190	1.43	pf
484	1.42	fg	198	1.72	fg
513	2.14	g	217	1.55	fg
525	2.15	f	218	1.42	vg
530	2.44	vg	231	1.72	f
542	2.43	g	245	1.70	fg
556	2.57	fg	252	1.57	g
561	2.46	pf	275	1.30	fg
562	2.90	f	284	0.57	vg
566	2.23	pf	301	0.05	f
573	2.26	fg	302	0.21	g
581	2.14	fg	303	0.16	g
715	0.28	vg	307	0.14	g
727	0.47	g	314	-0.14	g
735	0.56	fg	317	0.01	g
758	0.99	fg	321	0.05	pf
783	1.43	f	323	0.05	g
806	1.95	f	331	0.47	g

TABLE 10 (continued)

R Leonis at 8500 A

JD 242+	Mag.	Quality	JD 242+	Mag.	Quality
8334	0.47	g	8682	1.18	fg
335	0.37	fg	691	1.69	g
341	0.45	g	813	2.14	g
343	0.56	vg	820	2.08	g
350	0.85	g	845	1.91	f
352	0.87	g	848	1.69	g
466	2.51	g	860	1.36	g
471	2.63	vg	867	1.19	g
481	2.52	vg	878	1.00	fg
489	2.50	g	891	0.57	fg
502	2.45	g	894	0.47	vg
510	2.44	?	904	0.37	g
518	2.31	g	912	0.15	fg
560	1.43	fg	925	0.17	f
568	1.37	vg	927	-0.14	?
592	0.63	fg	931	0.15	vg
597	0.37	g	955	0.47	vg
609	0.15	g	959	0.57	f
618	0.15	g	965	0.70	vg
619	0.19	g	975	0.70	fg
630	0.28	g	992	0.98	f
635	0.43	fg	9007	1.16	f
642	0.50	g	010	1.30	fg
660	0.63	g	030	1.71	fg
670	1.00	f	054	1.95	fg
677	0.99	vg	057	1.95	fg

The Allegheny refractor was used through JD 2428252; thereafter the Yerkes reflector. The comparison star was α Leo (1.00 mag. at 8500 A).

TABLE 11

R Leonis at 3700 A

JD 242+	Mag.	Quality	JD 242+	Mag.	Quality
8141	11.28	g	8330	7.07	fg
166	12.60	fg	500	13.25	fg
231	11.22	fg	511	12.17	fg
301	6.92	g	614	6.70	f
307	7.00	fg	625	6.69	f
317	7.00	g			

The fundamental comparison stars and their adopted ultraviolet magnitudes were: HD 84748 F0 6.33 and HD 84561 K5 8.33.

TABLE 12

R Leonis at 9250 A and at 9100 A

JD 242+	Mag.	Quality	JD 242+	Mag.	Quality
7372	-1.07	g	8303	-0.35	g
376	-1.38	g	305	-0.44	vg
430	-0.93	g	314	-0.30	g
535	0.28	g	316	-0.48	fg
558	1.43	p	317	-0.24	fg
561	0.28	vp	323	-0.85	f
718	-0.85	f	331	-0.55	fg
727	-1.01	f	334	-0.71	fg

TABLE 12 (continued)

R Leonis at 9250 A and at 9100 A

JD 242+	Mag.	Quality	JD 242+	Mag.	Quality
8335	-0.71	fg	8618	-0.44	vg
337	-0.37	fg	614	-0.57	fg
343	-0.15	fg	619	-0.41	f
352	-0.02	fg	620	-0.56	fg
460	1.53	pf	813	1.00	p
471	1.54	vg	820	1.22	vg
483	1.53	g	912	-0.66	vg
502	1.43	fg	931	-0.41	fg
510	1.19	fg	959	-0.42	f
518	1.15	?	9054	1.19	fg
614	-0.50	fg			

The Allegheny refractor was used through JD 2427727; thereafter the Yerkes reflector. Q plates (9250 A) were used through JD 2428618 except that on JD 2428614 both Q and M plates were used; thereafter M plates were used. The value 1.00 was adopted for the magnitude of the comparison star, α Leo, at these wave lengths.

TABLE 13

R Aquilae at 8500 A

JD 242+	Mag.	Quality	JD 242+	Mag.	Quality
7238	2.09	f	7691	4.42	p
245	2.17	vg	704	4.63	p
258	2.28	vg	714	4.52	g
261	2.26	vg	718	4.40	p
272	2.99	pf	723	4.23	g
283	2.57	f	844	1.72	g
288	2.55	vg	847	1.57	p
290	2.70	vg	855	1.85	g
291	2.71	vg	861	1.95	f
299	3.29	f	871	1.95	g
306	3.39	f	880	2.08	fg
312	3.42	f	888	2.33	fg
325	3.52	vg	915	2.86	vg
345	3.85	fg	941	3.72	g
352	3.86	fg	948	3.80	g
359	3.84	f	964	4.02	vg
402	3.94	pf	980	4.28	g
516	1.87	f	8002	4.57	pf
517	2.15	f	003	4.55	pf
522	1.86	pf	014	4.60	pf
527	1.58	p	034	4.68	vg
530	1.69	g	069	3.66	vg
538	1.61	f	129	2.09	vg
548	1.69	g	140	2.09	g
556	1.87	f	146	1.74	g
557	2.09	fg	157	1.73	vg
560	2.07	fg	210	2.48	pf
568	1.94	g	218	2.49	p
575	2.09	g	271	3.72	f
582	2.16	fg	276	4.63	p
589	2.44	fg	277	3.90	f
609	2.40	g	293	3.70	g
628	3.29	pf	294	3.73	f
645	3.52	f	298	4.04	g
654	4.01	pf	303	4.99	fg
658	4.00	f	308	4.10	vg
679	4.23	fg	315	4.44	f
680	4.20	f	324	4.15	pf

TABLE 13 (continued)

R Aquilae at 8500 A

JD 242+	Mag.	Quality	JD 242+	Mag.	Quality
8331	3.93	f	8737	1.53	g
351	3.01	f	740	1.59	g
353	3.15	g	745	1.60	fg
377	2.44	g	750	1.57	g
383	2.28	vg	761	1.66	g
395	2.27	g	813	2.94	g
409	2.25	vg	818	3.09	fg
441	1.87	g	841	3.45	f
442	1.87	g	858	3.76	f
444	1.85	fg	863	3.88	g
453	1.71	f	864	3.86	fg
457	1.78	vg	877	3.82	vg
460	1.57	g	878	3.95	vg
465	1.55	fg	902	4.21	g
471	1.76	g	903	4.12	fg
481	1.87	vg	976	3.37	vg
509	1.84	vg	986	3.33	g
610	4.77	f	998	3.10	f
614	4.10	g	999	3.29	fg
633	4.05	f	9011	2.75	fg
643	3.90	g	029	2.15	vg
660	3.40	vg	035	1.81	fg
669	3.10	g	041	1.80	pf
678	2.67	f	043	1.67	fg
683	2.57	g	053	1.65	fg
695	2.38	f	055	1.81	f
709	2.38	vg	063	1.96	fg
715	2.25	vg	069	1.84	fg
			077	2.06	fg

The Allegheny refractor was used through JD 2428069; thereafter the Yerkes reflector. The comparison stars were: α Aql (mag. 0.43, JD 7238 through 7740 and 8069 through 8610); α Cyg (mag. 1.00, JD 7844 through 8043) and HD 184406 (mag. 3.10, JD 8614 and after).

TABLE 14

R Aquilae at 3700 A

JD 242+	Mag.	Quality	JD 242+	Mag.	Quality
8303	12.76	fg	8444	8.00	fg
319	12.79	fg	622	12.81	fg
334	12.86	fg	636	12.71	fg
441	8.28	fg	647	12.67	fg
			740	8.28	fg

The fundamental comparison stars and their adopted ultraviolet magnitudes were: HD 178162 B9 9.00 and HD 178216 G0 10.10

TABLE 15

R Aquilae at 9250 A and at 9100 A

JD 242+	Mag.	Quality	JD 242+	Mag.	Quality
7560	0.79	f	8323	3.35	pf
718	3.58	f	331	3.68	f
8308	3.42	fg	353	2.98	f
317	4.00	pf	409	2.03	fg

TABLE 15 (continued)

R Aquilae at 9250 A and at 9100 A

JD 242+	Mag.	Quality	JD 242+	Mag.	Quality
8441	1.63	f	8745	1.53	g
442	1.40	fg	750	1.63	vg
444	1.51	fg	761	1.89	fg
453	1.63	fg	818	1.96	fg
459	1.40	g	841	2.34	fg
460	1.52	vg	863	3.20	fg
471	1.82	vg	864	2.56	fg
481	1.51	g	877	2.85	fg
620	3.42	p	878	2.85	f
621	3.35	fg	902	3.53	f
660	2.77	fg	903	3.16	fg
737	1.81	f	9053	1.21	pf
740	1.63	g	055	1.36	fg

The Allegheny refractor was used through JD 2427718; thereafter the Yerkes reflector. Q plates were used through JD 2428471, and M plates thereafter. The magnitude adopted for the comparison star, α Aql, was 0.49.

TABLE 16

X Ophiuchi at 8500 A

JD 242+	Mag.	Quality	JD 242+	Mag	Quality
8465	1.94	fg	8737	1.96	f
471	2.11	g	750	2.23	g
481	1.63	g	761	2.04	g
483	1.76	fg	813	1.66	vg
490	2.09	g	818	1.79	g
502	1.87	g	841	1.88	g
509	1.54	pf	858	2.33	g
610	3.52	g	864	2.57	vg
614	3.53	g	877	2.33	vg
633	3.47	fg	976	3.73	vg
643	3.53	f	986	3.63	fg
660	3.40	g	998	3.40	pf
669	3.51	g	999	3.53	fg
678	3.33	fg	9011	3.29	g
683	3.26	g	029	2.87	fg
695	2.94	g	035	2.91	fg
709	2.62	g	041	2.80	pf
715	2.67	g	063	2.73	fg
			069	2.73	fg

The Yerkes reflector was used throughout. The comparison stars were: α Aql (0.43 mag.) through JD 2428610; thereafter HD 184406 (3.10 mag.)

TABLE 17

X Ophiuchi at 3700 A

JD 242+	Mag.	Quality	JD 242+	Mag	Quality
8481	7.62	fg	8647	9.91	g
490	7.98	g	665	9.61	g
636	9.90	g	695	9.81	g

The fundamental comparison stars and their adopted ultraviolet magnitudes were: HD 172400 K0 8.44; HD 172522 A2 7.11; HD 172588 A3 7.41.

TABLE 18

X Ophiuchi at 9250 A and at 9100 A

JD 242+	Mag.	Quality	JD 242+	Mag.	Quality
8471	1.63	g	8812	1.44	pf
481	1.53	vg	813	1.32	fg
481	1.37	fg	818	1.15	fg
483	1.68	fg	841	1.25	g
660	2.77	f	986	2.63	g
678	2.03	fg	993	2.42	fg

Q plates were used through JD 2428481; thereafter M plates (9100 A). The comparison star was α Aql (mag. 0.49).

TABLE 19

R Aquarii at 8500 A

JD 242+	Mag.	Quality	JD 242+	Mag.	Quality
8464	2.46	fg	8849	1.76	g
465	2.50	fg	861	2.08	fg
707	4.43	f	877	2.42	g
708	4.78	vg	878	2.51	vg
715	4.94	f	893	2.28	vg
735	3.80	fg	902	2.66	g
751	3.61	fg	907	2.78	f
763	3.17	fg	925	2.97	vg
814	2.30	vg	9035	4.33	f
844	1.87	f	041	4.35	g

TABLE 19 (continued)

R Aquarii at 8500 A

JD 242+	Mag.	Quality	JD 242+	Mag.	Quality
9055	4.69	f	9078	4.40	f
072	4.75	fg	112	4.33	fg
073	4.97	f	124	4.06	g

The Yerkes reflector was used throughout. A field comparison star, HD 222643 K2, was assumed to be of magnitude 3.80 at 8500 A.

TABLE 20

R Aquarii at 9250 A and at 9100 A

JD 242+	Mag.	Quality	JD 242+	Mag.	Quality
8465	1.37	f	8861	1.32	g
712	3.60	f	877	1.59	pf
714	3.17	f	878	1.98	f
715	3.47	fg	902	1.80	fg
735	2.63	f	9041	3.37	f
751	2.81	vg	078	3.41	fg
763	1.80	f			

The Yerkes reflector was used throughout. M plates were used except on JD 2428465. The comparison star, HD 222643 K2, was assumed to have a magnitude of 3.60 at 9100 A.

T Cephei.—The curve (Fig. 1) at 8500 A is very similar to the visual-curve, but the average magnitude ranges from five maxima and four minima are 2.56 and 4.63, respectively. All infrared maxima attain about the same value, while the one visual maximum which is conspicuously lower is rather broader, so that the area under the curve from a magnitude below maximum is of the same order as for other maxima. Two minima are definitely lower visually and correspondingly at 8500 A. Over two maxima and three minima the ultraviolet-curve practically parallels the visual, the ranges being 4.75 and 4.70. The photographic range by Müller is less than the visual in the ratio 3.22:3.67 over two cycles, probably because band absorption in the visual more than compensates for the temperature change. The ranges at 9100 A and 9250 A are 2.0 and 1.9, as compared with 2.6 at 8500 A.

T Cep obviously does not everywhere radiate like a black star. Since the ultraviolet-, photographic-, and visual-curves are practically parallel, some of the color indices will differ only by a constant giving a 45° line not passing through the origin. The ultraviolet-*minus*-8500 A and the ultraviolet-*minus*-9100 A indices, however, give a slope of index 0.92, passing through the origin. The theoretical value of the slope is 0.94. The temperatures from the various indices derived from formulae (2) are as shown in the accompanying table. If 2975°

Wave Lengths	Indices		Temperatures	
	Max.	Min.	Max.	Min.
5500–8500	4.98 (5)	7.15 (4)	1700°	1240°
3700–8500	5.87 (2)	8.12 (3)	2975	2320
4200–8500	6.85 (2)	8.02 (2)	2160	1900
3700–9100	6.50 (1)	8.95 (1)	2860	2235
3700–9300	6.40 (1)	9.10 (1)	2920	2230

at maximum and 2320° at minimum are chosen as most probable, the visual magnitude range for a black body is 2.72, corresponding to 4.87 observed and indicating a differential absorption between maximum and minimum of 2.15 mag., provided there are no changes in radius and no band absorption in the ultraviolet and at 8500 A.

In the plot of visual and 8500 A magnitudes (Fig. 4) the points for

the ascending branches of the curves lie near the slope of index 2.00, while those of the descending branches indicate 1.83, averaging 1.92. Since the infrared maxima are flatter, particularly following the visual maxima, both branches are perhaps best represented by the slope-indices 2.33 and 1.78 toward maximum and minimum, respectively, for the ascending branches, and 2.44 and 1.60 for the descending branches. Thus, toward the minima the slope-indices are nearest the theoretical value of 1.55, indicating little change in absorption, but a nearly uniform graying; but toward the maxima the absorption lessens more or less linearly, but not always in phase with the temperature change. The ultraviolet-*minus*-8500 A slope-index of 2.1 is near the theoretical value of 2.3. The photographic-*minus*-8500 A index of 1.75, compared to the theoretical value of 2.0, might indicate an increase of diameter toward maximum, but probably differential band absorption also obtains in the photographic region.

R Cassiopeiae.—The infrared maxima are rather less variable than the visual maxima, and the average magnitude ranges from five maxima and four minima are 3.07 and 5.65, respectively (Fig. 1). As in T Cep, the photographic range (Müller) is less than the visual in the ratio 4.80:5.40, while the ultraviolet is greater than the visual in the ratio 7.22:5.80. The ranges at 9100 A and at 9250 A are 2.6 and 2.9, to 3.6 at 8500 A. The plot of the ultraviolet-*minus*-8500 A and visual-*minus*-8500 A indices does not pass through the origin, and the slope-index is 1.5, compared to the theoretical value of 2.4; but the line formed by the ultraviolet-*minus*-8500 A and the ultraviolet-*minus*-9100 A indices passes through the origin with a slope

Wave Lengths	Indices		Temperatures	
	Max.	Min.	Max.	Min.
5500–8500	5.49 (5)	8.07 (4)	1560°	1110°
3700–8500	6.90 (3)	11.2 (2)	2050	1800
4200–8500	6.60 (1)	9.10 (1)	2240	1715
3700–9100	7.05 (1)	12.0 (1)	2700	1750
3700–9300	7.45 (1)	12.05 (1)	2600	1800

equal to the theoretical value of 0.94. Indices from these spectral regions should therefore give the best temperature estimates. Choos-

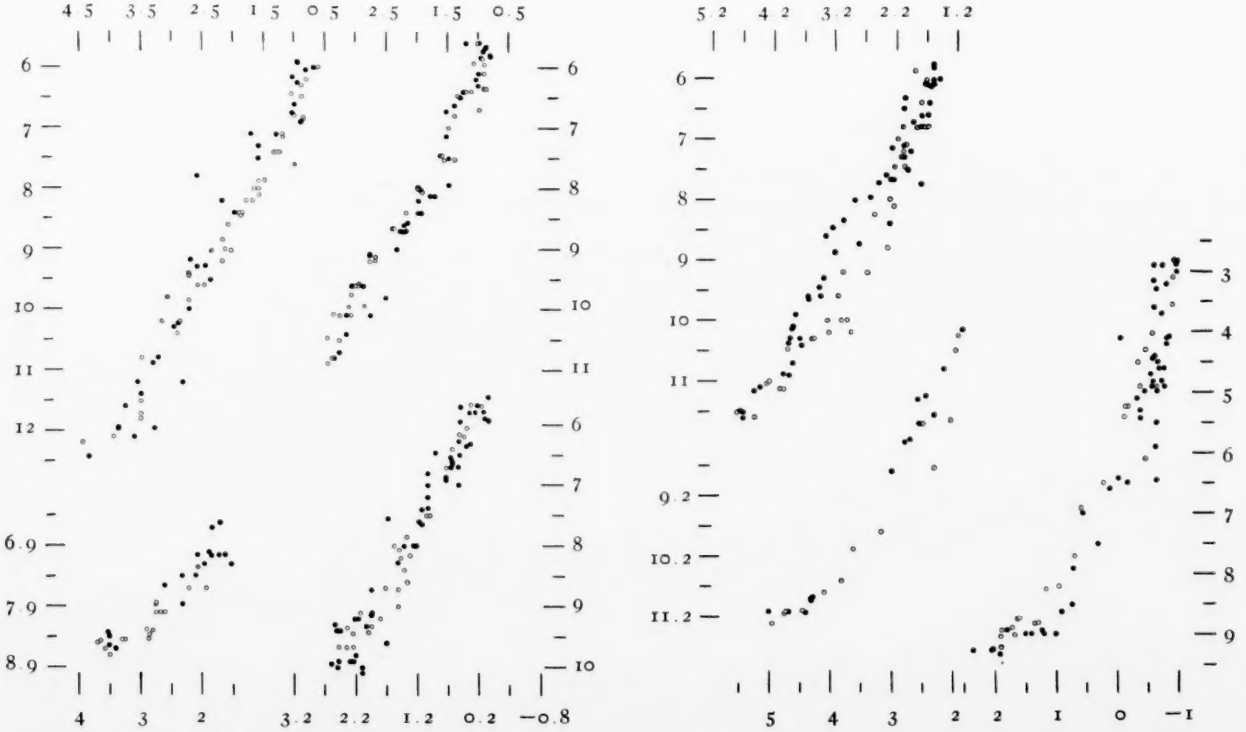

FIG. 4.—Infrared—visual slope index curves. *Left group:* R Cas and T Cep (*left to right, above*) and X Oph and R Leo (*below*). *Right group:* R Aql (*above*) and R Aqu and *o* Cet (*right*). Apparent visual magnitudes vertical, infrared horizontal.

ing 2650°–1800° as most probable, the black-body visual range would be 5.10 mag., which corresponds to 5.90 observed, showing a differential absorption of 0.80 mag.

The visual-*minus*-8500 A plot (Fig. 4) gives 1.95 as the slope-index of the ascending branches and 1.80 as the slope of the descending branches of the curves, the average of 1.87 being close to that for T Cep. But there is no indication of curvature, as with that star. The photographic-*minus*-8500 A slope-index of 1.85 and the ultraviolet-*minus*-8500 A index of 2.1 (in exact agreement with T Cep) are fairly near the theoretical values of 2.0 and 2.3; and possibly only slight, if any, radial changes are indicated.

R Leonis.—The average magnitude ranges from five maxima and five minima at 8500 A and in the visual region are 2.16 and 3.83, the curves being very similar (Fig. 2). Over two cycles the ultraviolet and visual ranges are in the ratio 6.05:4.22, while the ranges at 9100 A and at 9250 A average 1.70 and 1.52, to 2.00 at 8500 A. The ultraviolet-*minus*-8500 A index plotted against the visual-*minus*-8500 A index intercepts below the origin and has a slope of 1.9, compared to the theoretical value of 2.4; the line formed from the ultraviolet-*minus*-8500 A and the ultraviolet-*minus*-9100 A indices passes through the origin with a slope of 0.93, in agreement with T Cep, R Cas, and the theoretical value. The temperatures from the various indices are given in the accompanying table. The temperatures of

Wave Lengths	Indices		Temperatures	
	Max.	Min.	Max.	Min.
5500–8500	5.79 (5)	7.30 (5)	1490°	1220°
3700–8500	6.75 (2)	10.60 (2)	2670	1860
3700–9300	7.30 (2)	11.45 (1)	2650	1850

2670° at maximum and 1860° at minimum would give a black-body visual range of 4.18, in practically exact agreement with the corresponding value of 4.20 observed over the same cycles as for the temperatures, the differential absorption being zero.

The plot of visual and 8500 A magnitudes (Fig. 4) for both ascending and descending branches gives the slope 1.82 without much scat-

ter or definite indication of curvature: the ultraviolet-*minus*-8500 A slope is 2.71; and the ultraviolet-*minus*-9250 A slope is 3.2. These are all greater than the theoretical values of 1.55, 2.3, and 2.5; and our data would indicate that, since there is no differential absorption, but merely a uniform graying in the visual region, the star expands toward minimum, the amount being readily derived by equation (4), if absolute magnitudes are determined.

R Aquilae.—The average magnitude ranges at or near maxima and minima over seven cycles are 4.76 visually and 2.31 at 8500 A (Fig. 2). Over two cycles the ultraviolet range is less than the visual in the ratio 4.55:4.81, while for three maxima and two minima at 9100 A and for one cycle at 9250 A the ranges are 1.92 and 1.86, respectively, to 2.40 at 8500 A. The visual curve practically parallels the ultraviolet curve, but the ultraviolet-*minus*-8500 A against the ultraviolet-*minus*-9100 A slope passing close to the points and through the origin is again the theoretical 0.94. The temperatures from the various indices are as shown in the accompanying table.

Wave Lengths	Indices		Temperatures	
	Max.	Min.	Max.	Min.
5500–8500	4.59 (7)	7.00 (7)	1820°	1265°
3700–8500	6.45 (2)	8.70 (1)	2775	2200
3700–9100	6.60 (2)	9.40 (1)	2830	2150
3700–9300	6.50 (1)	9.20 (1)	2890	2200

Adopting 2800° at maximum and 2200° at minimum the blackbody visual range would be 2.76 mag., as against 4.81 observed over the same cycles as for the temperatures, the differential absorption being 2.05 mag. in the visual region, if the others have none.

The visual-*minus*-8500 A line (Fig. 4) has an average slope of 1.94; but toward maximum the slope is more nearly 2.4 for both branches, while toward minimum it is about 1.3 for the ascending branches and 2.0 for the descending. The ultraviolet-*minus*-8500 A slope is 2.0, and the ultraviolet-*minus*-9100 A slope is 2.3. Probably there are radial changes as well as absorption changes; and since the latter two slopes are less than the theoretical values of 2.3 and 2.5,

respectively, there are indications of an increase in diameter toward maximum, as was already suggested for T Cep and R Cas, while R Leo apparently expands toward minimum. Probably the present data are insufficient for a final decision, but they suggest that there are striking differences in the infrared variables.

The four variables thus far considered—T Cep, R Cas, R Leo, and R Aql—are all of similar spectra, M5–M8. Plots of visual and ultraviolet magnitudes against infrared magnitudes give straight lines, particularly toward minima. This feature can be used in considering three further stars of similar type—*o* Cet, X Oph, and R Aqu—of which the visual and ultraviolet magnitudes toward minima are affected by the presence of known or suspected companions. Extrapolation of the straight lines beyond the points where they become curved because of the companions gives the true visual and ultraviolet magnitudes of the variables for any particular total magnitude; hence, it also gives the visual and ultraviolet magnitudes, or the colors, of the companions.

o Ceti.—Many of the maxima (Fig. 3) show a delayed drop of the infrared points, a feature already noticeable, though less conspicuous, in T Cep. The infrared maxima overlie the projection of the visual-curve a magnitude or so below maxima, over which the visual peak is usually, but not always, displaced to the left.[5] The visual peak shows more fluctuation in range, as well as in position, than the infrared. The effect upon the visual-infrared plot (Fig. 4) is an upbending toward maximum. There is also a decided upbending toward minima, which is interpreted as being caused by the known companion, since it does not occur in the stars already considered. Extending the line toward minimum of slope 1.60, which presumably is affected neither by the differential maxima nor by the companion, the visual magnitude of the variable for total visual magnitude 9.2 is 9.7, giving 10.3 as the visual magnitude of the companion. This is in agreement with the average estimates of 9.8 by Joy,[6] of 9.6 by Pettit and Nicholson,[7] and of 11.1 by Van Biesbroeck.[8]

In the ultraviolet we use our observations obtained at the 1933

[5] *Pub. A.A.S.*, **9**, 124, 1937.
[6] *Ap. J.*, **63**, 281, 1926.
[7] *Ap. J.*, **78**, 327, 1933.
[8] *Ap. J.*, **82**, 84, 1935.

minimum at the Allegheny Observatory[7] with the same filter as that used over two maxima at the Yerkes Observatory. Extending the ultraviolet-*minus*-8500 A line of slope 2.0, we obtain 11.3 as the ultraviolet magnitude of Mira, corresponding to a total ultraviolet magnitude of 9.8. Hence, the ultraviolet magnitude of the companion, based upon an adopted ultraviolet magnitude of 9.90 for the A_3 star BD $-3^\circ 357$, is 10.1. Adopting the values in the following table for the magnitudes of the two comparison stars used at Yerkes and at Allegheny, the results for *o* Ceti A and B are:

Star	Magnitude		
	Ultraviolet	Photographic	Visual
BD $-3^\circ 357$ (A_3)	9.90	9.85	9.77
BD $-3^\circ 355$ (Ma)	11.34	9.65*	9.08
o Ceti (A+B)	9.8	9.75	9.2
o Ceti A	11.3	10.7	9.7
o Ceti B	10.1	10.3	10.3

* Derived from the preceding star and differing from the HD estimate of 10.4 assumed at Allegheny.

These magnitudes are all interrelated; and the values are fairly consistent, except possibly in the photographic region, where the magnitudes have been rederived from the few observations at Allegheny.[7] In this region the A and B components were nearly equal, so that 10.3 and 10.7 are about the limits corresponding to total magnitude 9.75.

The temperatures from the various indices, after correction for the effect of the companion, are as shown in the accompanying table.

Wave Lengths	Indices		Temperatures	
	Max.	Min.	Max.	Min.
5500–8500	4.70 (6)	7.6 (3)	1800°	1175°
4200–8500	.....	8.7 (1)	.....	1770
3700–8500	6.38 (2)	9.3 (1)	2800	2035
3700–9300	6.00 (1)	10.9 (1)	3000	1915

Temperatures of 2800°–2035° would give a visual-magnitude range of 3.3. The corrected visual range from six maxima and five minima is 5.66, as compared to 2.52 at 8500 A. The visual range corresponding to these temperatures is about 6.1, but the various maxima are extremely variable and the indicated differential absorption of 2.8 mag. is doubtless also variable. The very steep slope of 3.7 of the visual-*minus*-8500 A line toward maxima probably indicates a rapidly changing absorption; but the medial slope of 1.95 is similar to that of the other stars. The star *o* Cet most resembles T Cep; and, except near maxima, the various slopes of the two stars are practically identical.

X Ophiuchi.—This variable has a companion of K-type spectrum for which Pettit and Nicholson deduced a visual magnitude of 8.9.[7] The points at 8500 A (Fig. 3) have almost as great a range between maxima and minima as the visual, and the infrared-curve may rise while the visual-curve maintains a constant minimum. Extending the line of slope-index 1.80 of the visual-*minus*-8500 A plot (Fig. 4), the visual magnitude of the variable is 10.0 (in general agreement with Van Biesbroeck, as against Pettit and Nicholson[7]) for total apparent magnitude 8.6, giving 8.9 as the visual magnitude of the companion. The ultraviolet-*minus*-8500 A line of slope 2.1 gives 11.2 for the variable, corresponding to a total apparent magnitude of 9.6, or to 9.9 for the ultraviolet magnitude of the companion. The temperatures from the various corrected indices are given in the accompanying table. Possibly 2900°–2400° is fairly close to the actual

Wave Length	Indices		Temperatures	
	Max.	Min.	Max.	Min.
5500–8500	5.10 (2)	6.4 (2)	1666°	1370°
3700–8500	6.0 (1)	7.7 (1)	2920	2410
3700–9100	6.1 (1)	8.8 (1)	3000	2250

temperature range of the variable. The corrected visual range corresponding to the infrared range (8500 A) of 1.7 mag. is 3.0 mag., while for a black body it would be 2.1 mag., indicating a differential ab-

sorption of 0.9 mag. The ranges at 8500 A and 9100 A are 1.8 and 1.1, respectively, from two cycles.

R Aquarii.—Our observations definitely indicate the presence of a companion by the strong curvature of the visual-*minus*-8500 A plot (Fig. 4) toward minimum. Extending the line of slope 1.92, the visual magnitude of the variable corresponding to a total visual magnitude of 11.2 is 12.8, making the visual magnitude of the companion 11.5. This cannot be far off, although Pettit and Nicholson obtained 10.0.[7] Unfortunately, few ultraviolet observations of this star were obtained; hence the color remains unknown. The magnitude range at 9100 A is 2.2 mag., as compared to 2.5 mag. at 8500 A.

YERKES OBSERVATORY
September 1939

CONTRIBUTIONS TOWARD A PHYSICAL MODEL OF γ CASSIOPEIAE

RALPH B. BALDWIN

ABSTRACT

The light-curve and the temperature-curve of γ Cassiopeiae are correlated in a peculiar manner. An explanation is that the photosphere of the star is variable in size and that a reduced color temperature depends on an increase in the extent of the radiating surface relative to the available energy.

The law of conservation of angular momentum may be used to explain these correlations. The broad absorption lines are observed to change in width; and if this is interpreted as a change in the velocity of rotation, we immediately have relative radii of the star for all dates covered by measures of the absorption width. The original absolute magnitude and the light-curve permit computation of a temperature-curve, which is found to be in agreement with the observed temperature-curve.

This principle allows a determination of the radii of the layers of emission. It is found that the atmosphere is stratified and that it pulsates in a manner similar to the photosphere but with a moderate lag.

Equivalent widths of certain sharp absorption lines of helium and hydrogen have been measured, and the method of Struve and Wurm has been applied to give the distance from the photosphere to the "shell" in which the lines were produced. The results are consistent with the radii determined from the broad absorption and emission lines; the sharp absorption lines are produced in the outermost layers.

Variations in the emission intensity ratios of the two components of the lines of ten elements are shown to exist and are discussed.

The 216 spectrograms of γ Cassiopeiae on which this study is based cover the period 1926–1938. Most of the plates are on Process emulsion and were taken with the Michigan one-prism spectrograph; the dispersion is 40 A/mm at $H\gamma$. Because of the unusual transparency of this glass prism the ultraviolet spectrum was photographed beyond the limit of the Balmer series.

THE LUMINOSITY

Many observers have discussed the problem of the luminosities of stars of classes B and Be, and they generally agree that the Be stars are slightly brighter. Mean absolute magnitudes of Bo stars range from $-2^{m}5$ to $-3^{m}4$, according to the work consulted. However, space absorption is not considered in the earlier estimates. Including the effect of space absorption, Stebbins, Huffer, and Whitford[1] find a mean absolute magnitude of Bo stars of $-3^{m}9$. E. G. Williams'[2]

[1] *Ap. J.*, **90**, 209, 1939. [2] *Ap. J.*, **83**, 305, 1936; *Mt. W. Contr.*, **541**, 29, 1936.

value of the absolute magnitude of γ Cassiopeiae, derived from interstellar line intensities, is $-2^{m}.5$. The original color excess[1] was $+0^{m}.11$, at least part of which is an intrinsic property of the star; the remainder is due to space reddening. The dimming of any star by continuous interstellar absorption ($A \sim \lambda^{-1}$) is $7E$ on the visual-magnitude scale.[1] Consequently, the uncorrected absolute magnitudes found for γ Cassiopeiae must be decreased by a quantity between $0^{m}.00$ and $0^{m}.77$. A direct trigonometric parallax[3] yields $-0^{m}.03$, which seems too faint. In the following discussion the absolute magnitude will be considered as $-2^{m}.5$.

THE BROAD ABSORPTION LINES

HISTORICAL

In 1932 Struve[4] showed that the broad absorption wings which flank the emission lines of hydrogen in Be stars have the contours of normal absorption lines which have been abnormally broadened by rapid axial rotation. Struve did not specify what actual velocities were present for each star, but showed only that the wing contours were of the form to be expected if rotational velocities were large. If we make any reasonable assumption for the mass and density of a Boe star, the maximum velocity of rotation which could obtain is of the order of 300 km/sec, derived from Jeans's criterion for liquid bodies.[5]

It is not established that the laws found for liquid bodies are applicable to the gaseous and compressible materials of stars. It may be that even higher rotational velocities would not disturb the stability of the average Boe star where centrifugal force does not become equal to gravity until the velocity is greater than 500 km/sec.

The first measurable part of the $H\beta$ wing of γ Cassiopeiae is displaced 16 A from the center on microphotometer tracings;[4] and if this were to be interpreted as a Doppler effect, it would correspond to nearly 1000 km/sec. Obviously then, a measure of the displacement of any definite point in the wing of a line will not, by itself, give the rotational velocity but will give a velocity which is proportional to, and larger than, the rotational velocity.

[3] Schlesinger, *General Catalogue of Stellar Parallaxes*, 6, 1935.

[4] *Ap. J.*, **76**, 309, 1932. [5] *Astronomy and Cosmogony*, 198, 1928.

THE MEASURES

In general, the structure at any strong line is that of a double reversal. The continuous spectrum is weakened by many very broad absorption lines. An emission line approximately bisects each of the the broad absorption lines and is in turn divided into two components by a sharp absorption line (Fig. 1).

As described by several authors,[6-11] the spectrum of γ Cassiopeiae was relatively constant from 1911 to 1928, when slight changes began. The star has passed through three increasingly violent cycles

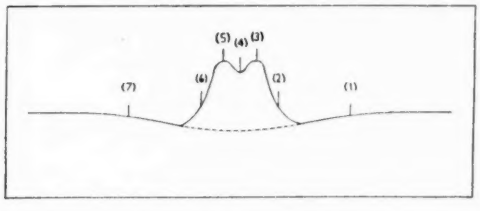

FIG. 1.—Ideal cross-section through a complex line, showing a broad absorption line bisected by an emission structure, and the latter, in turn, divided by a central "absorption" dip. The indicated points are the places at which the seven velocity-curves of Fig. 2 were measured.

of change since 1928[12-24] and is at present (1939) beginning a fourth. In each cycle the two emission components varied oppositely in intensity (V/R variation), while the emission and absorption lines grew narrower; and the components of the former even blended in 1934 and 1937 (single-line stages). During the latter cycle the color temperature first dropped 5500° K from 13,500° K and then returned

[6] Curtiss, *Pub. Obs. U. of Michigan*, **2**, 1, 1916.
[7] *Ibid.*, **3**, 1, 1923.
[8] *Ibid.*, p. 16.
[9] *Ibid.*, p. 256.
[10] Lockyer, *M.N.*, **93**, 362, 1933.
[11] Cleminshaw, *Ap. J.*, **83**, 495, 1936.
[12] Baldwin, *Ap. J.*, **87**, 573, 1938.
[13] *Ibid.*, **89**, 235, 1939.
[14] *Ibid.*, **90**, 204, 1939.
[15] Lockyer, *M.N.*, **96**, 2, 1935.
[16] *Ibid.*, p. 679.
[17] McLaughlin, *Ap. J.*, **84**, 235, 1936.
[18] *Ibid.*, **85**, 181, 1937.
[19] Heard, *J.R.A.S. Canada*, **32**, 353, 1938.
[20] Heard, *Ap. J.*, **81**, 341, 1935
[21] Cherrington, *Pop. Astr.*, **46**, 183, 1938.
[22] Cherrington, *Pub. A.S.P.*, **49**, 91, 1937.
[23] *Perkins Obs. Contr.*, No. 11, 1938.
[24] Cherrington, *Perkins Obs. Contr.*, No. 12, 1939.

nearly to normal.[25-31] The light fluctuated[32] in an irregular manner, although minimum brightness occurred at minimum color temperature. The number of visible emission lines increased markedly during this cycle.

In none of the earlier investigations had anyone studied the behavior of the broad underlying absorption lines. Inspection of the plates disclosed that throughout the entire series there were broad lines of hydrogen, helium, and ionized iron, while ionized magnesium, ionized silicon, and, surprisingly, ionized nickel appeared in absorption near the single-line phase of the 1937 cycle.

Complete measures were made for width of *Hδ*, *He* I 4026, *Fe* II 4233, *Si* II 3863, *Mg* II 4481, and *Ni* II 4067. The point of setting was, of course, rather arbitrary; but an attempt was made to measure the first point where the wing could be distinguished from the continuous spectrum except at *Hδ*. At this line there seemed to be a more or less definite break in the contour of each wing, a sudden dip; and the settings were made on these points and not in the extreme wings. As a result, *Hδ* is usually given as narrower than *Fe* II 4233, although it is really broader. These features are actually parts of the *Hδ* wings and are not to be attributed to *N* III 4097 and *N* III 4103. If γ Cassiopeiae is in class Bo, these lines will be present, but they should not show the measured changes of radial velocity.

The individual measures for each line of all elements scattered considerably from plate to plate, but this is only what would be expected in view of the diffuseness of the absorption. Nevertheless, when the measures from the two hundred odd plates are compared, it is seen immediately that definite trends are present. Prior to JD 2426900 in 1932, the absorption widths at *Hδ* were apparently constant. There are not enough plates covering the 1928 cycle to show possible small changes in absorption width.

[25] Greaves, *Observatory*, **62**, 252, 1939.

[26] *M.N.*, **98**, 435, 1938; *Observatory*, **61**, 118, 1938. Temperatures by Greenwich observers. I have adjusted their scale.

[27] Hunter, Martin, *Observatory*, **62**, 237, 1939.

[28] *C.R.*, **203**, 1329, 1936.

[29] *Observatory*, **60**, 329, 1937.

[30] *Observatory*, **62**, 76, 1939.

[31] Williams, University of Michigan, unpublished.

[32] Huffer, *Ap. J.*, **89**, 139, 1939.

Plates taken after the middle of 1932 tell an entirely different story. The broad absorption line, $H\delta$, gradually sharpened until in the latter part of 1934 it was more than 200 km/sec narrower than formerly. This narrowing was essentially in phase with the narrowing of the emission lines in the 1934 cycle. The absorption then widened at a more rapid rate than that of the narrowing and came approximately to the original width at the beginning of 1936. This was followed by a rapid decline in absorption width to a value 400 km/sec less than normal during the 1937 cycle.

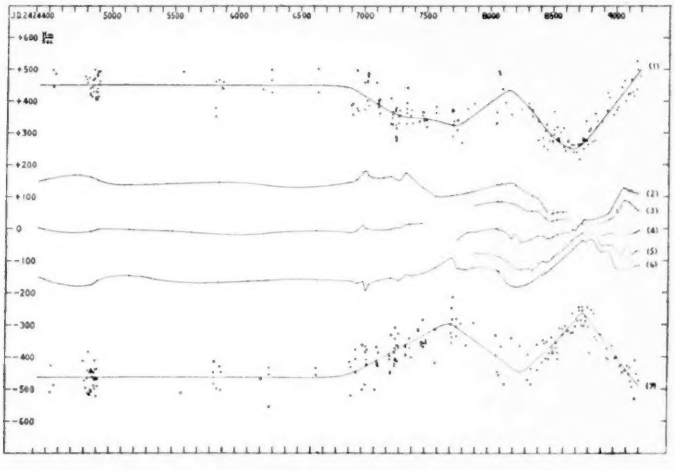

FIG. 2.—Velocity-curves for absorption and emission structures at $H\delta$. (1) and (7) are the curves for the red and violet absorption wings, respectively; (2) and (6) are for the red and violet emission edges; (3) and (5) are for the red and violet emission maxima; (4) is the central "absorption" velocity-curve.

In an earlier paper[13] it was pointed out that the red emission velocities were slightly out of phase with the violet emission velocities. The absorption edges were also out of phase, but each edge was in phase with the emission-curve for the corresponding side (Fig. 2). The narrowest absorption came at the time of the single-line emission state; and the absorption widened as the emission widened, until in 1938 the absorption was even broader than it was originally.

Complete measures of the lines *He* I 4026 and *Fe* II 4233 indicate a slight, but real, decrease in velocity width at the 1934 cycle and a much more prominent narrow stage during the 1937 cycle. The

Mg II, *Si* II, and *Ni* II lines were not visible until 1936 but thereafter were unanimous in showing a narrowing and subsequent widening. The mean curves of Figure 3 are simply plots of the average absolute values of the velocity displacements of each edge of each line for each plate. Even though the edge curves of *Hδ* are slightly out of phase, they have been combined in this manner for comparison purposes. The *Hδ* curve in the 1937 phase passes through its changes slightly

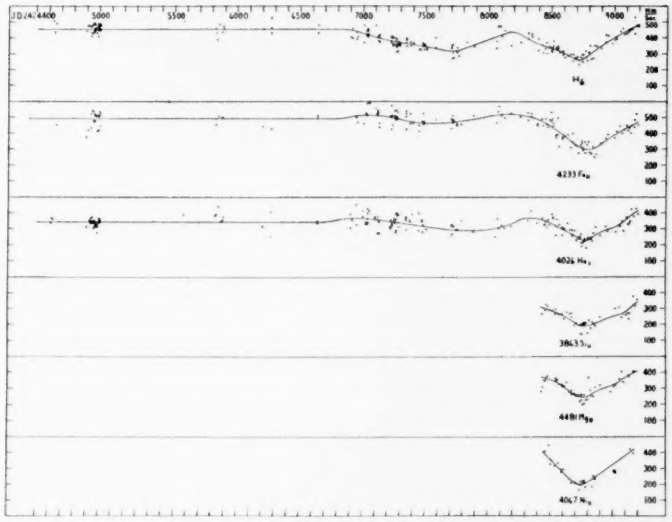

FIG. 3.—Mean velocity half-widths of six broad absorption lines

earlier than do the curves of the other elements, and the *He* I maximum width in 1936 comes a bit later. Otherwise, the six mean curves are different only in the amount of narrowing.

A complication is found for *Hδ* (and other *H* lines), namely, that there is a *V*/*R* variation of relative absorption-wing intensities which is essentially in phase with the *V*/*R* curves for the *Hδ* emission (Fig. 4). The absorption is strengthened on the side adjacent to the stronger emission component, an effect similar to one discovered in the spectrum of 25 Orionis by Miss Dodson.[33] The absorption edge on the side of the weaker emission component apparently is not affected until the emission components reverse intensities. This

[33] *Ap. J.*, **84**, 180, 1936.

additional absorption may be at least a partial explanation of the lack of agreement in phase of the absorption edges of $H\delta$. The normal state at this line is one in which the violet absorption component is slightly stronger than the red.

A general weakening of the absorption lines could produce an apparent narrowing. Such a diminution of strength is present during 1937 but not in 1934. It is suggestive of general absorption in the extensive atmosphere but does not appear large enough to account for the observed changes of line widths.

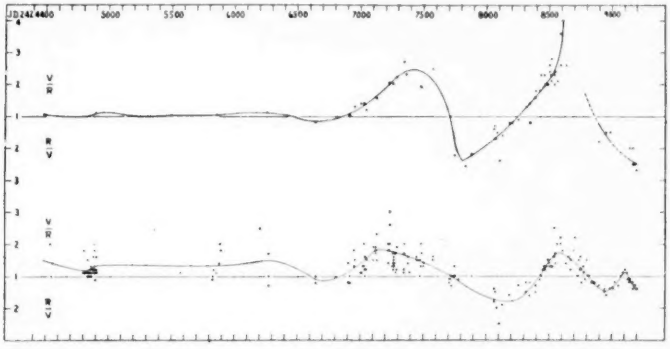

FIG. 4.—Emission V/R curve (*top*) and absorption-wing V/R curve (*bottom*). Note subcycle in latter curve near JD 2429100. The emission V/R curve is not well defined near this time.

If the widths of the diffuse absorption lines are caused by Doppler effect, they will vary linearly with wave length; whereas Stark effect and other widening influences are not linear with wave length. Stark effect is symmetrical for hydrogen only and scarcely affects the lines of the ionized metals. As these lines are also very broad and symmetrical, it follows that the widening process is not Stark effect.

On two plates chosen at random near the single-line stage, measures were made on the Balmer lines as far as $H\mu$. The results indicate a constant velocity width. The essential similarity of phenomena in the broad metallic absorptions and in the hydrogen wings suggests a rapid rotation as the broadening agent.

INTERPRETATIONS

In earlier paragraphs it was shown that the great widths of the metallic absorption lines, and probably those of hydrogen and heli-

um, are due to rotation of the star. A change of line width implies either a change in the rotational velocity or an increased general absorption in the shell. The latter mechanism was undoubtedly present, particularly in 1937. In 1934 a sharp decrease in line width occurred practically independent of an increase in the general absorption. In addition, the absorption and emission widths are closely related. It seems probable that the rotational interpretation is the more logical hypothesis. In this view, a decrease in the rate of rotation is dependent upon an increase in the radius. This is a necessary result of the principle of conservation of angular momentum in a closed rotating system. An increase in the line-width, then, is indicative of a contraction of the photosphere. As these fluctuations in line-width do occur, we infer a correspondingly variable apparent surface.

Fortunately, we can check this line of reasoning observationally. A brightness range of about one magnitude was measured photoelectrically.[32] Correlated with the light-curve is a temperature-curve[25-31] which at one point was 5500° K lower than normal. An explanation of this temperature drop in terms of superimposed Paschen continuous emission[34] has been shown to be untenable.[13] The only theory which seems capable of explaining simultaneous changes of light and heat is one in which the photosphere itself is alternately large and small. The necessary range of photospheric radii is less than 2.

Kosirev[35] offers a logical explanation of the anomalous conditions obtaining in stars with extended atmospheres where the color temperature is very much lower than the ionization temperature. He shows that the energy distribution from a star with a deep, tenuous atmosphere will depart greatly from that of a black body, in the sense that the star will be rich in ultraviolet radiations. We can think of Kosirev's energy distribution as coming from a *raised* photosphere, although the usual concept of a photosphere is not really applicable. The "photosphere" in the terminology of this paper simply refers to some average layer within the greatly extended layers of the star which produce continuous absorption.

If we disregard such effects as general absorption would produce on the broad lines, and interpret the measured widths as pure Dop-

[34] Woolley, *M.N.*, **95**, 115, 1934. [35] *M.N.*, **94**, 430, 1934.

pler effect of rotation, we may then apply the law of conservation of angular momentum.

The true velocity of rotation ($v \sin i$) cannot be determined by measures of apparent width. However, the theoretical contours of absorption lines for all rapid rotational velocities are similar; thus, the measures of apparent widths must be nearly proportional to the actual rotational velocities, and in a computation involving relative velocities we may substitute the measured line-widths.

In any closed rotating system angular momentum must be conserved according to the formula.

$$RV = \text{Constant} . \tag{1}$$

Thus, if the effective radius is increased, the velocity of rotation must decrease proportionally. Chandrasekhar[36] has suggested that angular momentum is conserved in the atmospheric layers of an individual, nonpulsating star; i.e., the outer layers rotate more slowly.

The measured line-widths may now be substituted into equation (1), and relative radii may be determined for every date from 1926 to 1938.

If, for any time, the actual photospheric radius can be determined, the photospheric radii at all other dates are known. To find the initial value, we go to the light-curve for the apparent magnitude and the temperature-curve for a temperature of corresponding date. At JD 2428800, $m = +2.03$ and $T = 8400°$ K. The original apparent magnitude was $+2.25$, and an original absolute magnitude of -2.5 has been measured by Williams.[2] Consequently, the absolute magnitude at JD 2428800 was -2.72. These quantities may be introduced into the well-known formula

$$\log R = \frac{5900}{T} - 0.20\, M_v - 0.02 , \tag{2}$$

and the radius for this date found in terms of the radius of the sun as a unit. This value is 10.3 $\odot$. Greaves[25] states that the radius of a star determined from its color temperature and absolute magnitude may be in error by as much as a factor of 2 or 3 because the stellar radiation may differ decidedly from black-body distribution in the

[36] *Ap. J.*, **88**, 106, 1938.

inaccessible parts of the spectrum. However, this should not seriously affect the *relative* radii determined for γ Cassiopeiae at different times. The constants in equation (2) are adjusted by observation on the sun, and several observers have shown that γ Cassiopeiae radiated energy with black-body distribution in the spectral range of

TABLE 1

COMPUTED RADII AND TEMPERATURES

JD 242+	Velocity Width	m_V	M_V	R	T
	km/sec				
5500	454	$+2^m.25$	$-2^m.50$	10.3 ⊙	11,050° K
6500	454	+2.18	−2.57	10.3	11,350
7000	427	+2.07	−2.68	11.0	11,250
7100	405	+2.04	−2.71	11.6	10,900
7200	377	+2.02	−2.73	12.4	10,400
7300	364	+1.99	−2.76	12.8	10,250
7400	359	+1.97	−2.78	13.0	10,200
7500	354	+1.95	−2.80	13.2	10,150
7600	342	+1.92	−2.83	13.7	10,000
7700	329	+1.90	−2.85	14.2	9,800
7800	302	+1.87	−2.88	15.5	9,300
7900	336	+1.84	−2.91	13.9	10,150
8000	368	+1.82	−2.93	12.7	10,950
8100	402	+1.79	−2.96	11.6	11,950
8200	441	+1.77	−2.98	10.6	13,100
8300	377	+1.75	−3.00	12.4	11,500
8400	342	+1.72	−3.03	13.7	10,750
8500	302	+1.70	−3.05	15.5	9,850
8600	273	+1.63	−3.12	17.1	9,350
8660	260	+1.57	−3.18	18.0	9,250
8700	260	+1.62	−3.13	18.0	9,100
8775	270	+1.92	−2.83	17.3	8,500
8800	278	+2.03	−2.72	16.8	8,400
8860	311	+2.46	−2.29	15.0	8,000
8900	338	+2.33	−2.42	13.8	8,700
9000	391	+2.30	−2.45	12.0	9,700
9100	433	+2.17	−2.58	10.8	10,950
9200	477	+2.25	−2.50	9.8	11,500

4000–6300 A during all stages.[26, 31] From the above value of the radius the radii at all dates were computed and listed in Table 1. Then, with the computed radii and the absolute magnitudes derived from the observed light-curve, we may re-enter equation (2) and solve for the temperature at each date.

The computed temperatures agree within the errors of measurement with the observed temperature-curve for the 1936–1938 cycle, although

there is a possible slight phase lag of computed curve over the measured temperature-curve. If real, this means that the photosphere went through its changes ahead of the reversing layer. For 1938 the computed temperature is very slightly too low; and the original temperature, 1926, is found to be 11,050° K against a measured value of 13,500° K.[26] These discrepancies are in the right direction, however. If the reversing layers were larger in proportion to the photosphere in those times than in the period of great change, the difference is easily explained. It requires a relative decrease of only 12 per cent in the size of the photosphere to account for the 2500° K original difference. The reversing layer would have to be largest relatively when the photosphere was smallest absolutely.

A similar result could probably have been obtained on the assumption of an increase in general absorption in the atmosphere, but the fact that good agreement is found by the former method is considered significant.

For the numerical work the velocities used were those of $H\delta$, but with this limitation: because of the excess absorption strength on the side of the stronger emission component, it was felt that the velocities there might be affected. Therefore, the velocities were read from the smooth curve drawn through the points on the weak side only, thus shifting from side to side with the V/R curve. This precaution was hardly necessary, as a temperature-curve derived from the mean widths of the absorption velocity-curve was in excellent agreement with the adopted curve.

Huffer's photoelectric light-curve[32] and the observed and computed temperatures are shown in Figure 5. The observed temperatures are from three observatories and are reduced to the scale of R. C. Williams,[37] of the University of Michigan. We have added 0.15 and 0.12 to the Greenwich gradients[25-27] and to those of Chalonge and Safir,[28] respectively. Observations have been made by Vanderkerkhove[29, 30] on the Greenwich scale but are not shown in the figure because of their relatively large scatter. The general agreement is good. The measured temperatures could have been reduced to the Greenwich scale equally well for such a computation.

The temperatures, of course, can be computed accurately for only

[37] *Pub. Obs. U. of Michigan*, **7**, 159, 1939.

those times when a light-curve is available. Thus, we are confined to dates after JD 2428400. Fortunately, the largest temperature variations must have occurred after this date. Regardless of this, we may compute approximate temperatures for earlier dates. The apparent magnitude of γ Cassiopeiae during the period 1931–1936 is not known; had it been of outstanding brilliance as in 1936, it would almost certainly have been noticed. Likewise, it could not have been very subnormal, or this too would have been seen. The star was

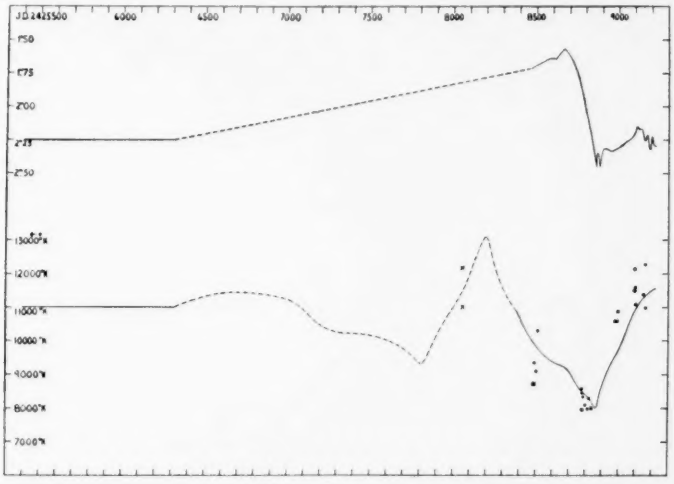

FIG. 5.—Photoelectric light-curve by Huffer (*top*) and theoretical temperature-curve (*bottom*). Published measured temperatures are shown. Crosses (×) are by Chalonge and Safir; open circles, by R. C. Williams; filled circles, by Greenwich observers.

often used as a standard of comparison for the variable α Cassiopeiae. Therefore, it has been assumed in the calculation that the brightness rose gradually, but continually, from 1931 to 1936, and a temperature-curve was computed on that basis. This curve shows a secondary dip in temperature at the time of the 1934 cycle, an effect which might have been suspected after the observed drop in the corresponding 1937 cycle but which certainly was not measured. If we assume that the apparent magnitude was normal in the interim, we also get a temperature dip, but deeper than on the above assumption. In any event, a mild drop in temperature for the weak 1934

spectroscopic cycle is indicated, and a larger decrease for the radical 1937 phase.

A change in the original absolute magnitude changes the absolute values of the computed radii but not the relative values, and consequently the temperatures are independent of the absolute magnitude.

COMPUTED RADII OF THE EMITTING LAYERS

Possibly the principle may be carried one step farther. On this rotational model the width of a spectral feature determines the radius or height at which it is formed, unless the lines are affected by radial motion. In a later section of this paper it will be shown that no significant pulsational velocities (greater than 60 km/sec) were present during a period of nearly two years. Consequently, we may deduce the general extent of the emitting layers by comparing their velocity widths with any reasonable assumed original velocity of rotation of the photosphere. This has been done for an original velocity of 300 km/sec, with the results listed in Table 2. If the original velocity were not 300 km/sec, the radii of the emitting layers will be in error by a constant proportionality factor.

In Table 2 the radii for the different elements are derived from the measured edge displacements of each emission component.[13] The hydrogen components are decidedly asymmetric, and the degree of asymmetry may depend on the depth in the atmosphere from which the Balmer emission can escape. If we can see down only to the photosphere in the Balmer wave lengths, the displacement of the red component will be measured too small in the case of an actual atmospheric expansion. It may be necessary to invoke some such mechanism to explain the observed velocities and thus the emission asymmetry, and therefore the unequal extent of hydrogen emission on the approaching and receding sides of the star may be illusory.

The hydrogen radii of Table 2 are shown in Figure 6, along with the V/R curve of emission intensity ratio for $H\delta$. It is found that the violet emission component is stronger than the red when the emitting layers are increasing in size, and that the red component is stronger during a decrease in the volume effective in emission. It is probably an apparent change of volume rather than a bodily shift of material, as the velocities are not observed to change sign. The

atoms are probably continually streaming through the emitting layers, and the apparent size of the envelope changes as the density and radiative flux vary.

The only apparent exception to this rule comes about JD 2429100; but then the emission structure is complex, and neither the emission

TABLE 2

RADII OF THE EMITTING LAYERS

JD 242+	R_p	Abs. V/R	Em. V/R	Hydrogen		*Fe* II	*He* I	*Si* II	*Mg* II	*Ni* II
				R	V					
4500	10.3 ⊙	1.5	1.05	18 ⊙	20 ⊙	.....	.....	.....	.....	.....
5000	10.3	1.3	1.07	20	21	.....	.....	.....	.....	.....
5500	10.3	1.3	1.03	21	20	.....	.....	.....	.....	.....
6000	10.3	1.3	1.08	21	20	.....	.....	.....	.....	.....
6500	10.3	1.2	1.07*R*	22	20	.....	.....	.....	.....	.....
7000	11.0	1.4	1.37	17	20	.....	.....	.....	.....	.....
7100	11.6	1.7	1.44	18	20	.....	.....	.....	.....	.....
7200	12.4	1.8	1.93	18	21	.....	.....	.....	.....	.....
7300	12.8	1.7	2.35	18	21	.....	.....	.....	.....	.....
7400	13.0	1.6	2.25	19	22	.....	.....	.....	.....	.....
7500	13.2	1.4	2.08	24	24	.....	.....	.....	.....	.....
7600	13.7	1.2	2.25	29	28	.....	.....	.....	.....	.....
7700	14.2	1.1	1.18	28	36	.....	.....	.....	.....	23 ⊙
7800	15.5	1.2*R*	2.45*R*	27	26	.....	.....	.....	.....	.....
7900	13.9	1.5*R*	2.13*R*	24	27	20 ⊙	27 ⊙	.....	.....	.....
8000	12.7	1.7*R*	1.68*R*	22	27	19	.....	.....	.....	.....
8100	11.6	1.8*R*	1.72*R*	21	22	19	.....	23 ⊙	.....	22
8200	10.6	1.8*R*	1.31*R*	21	17	19	.....	22	.....	23
8300	12.4	1.6*R*	1.18	27	19	21	18	22	22 ⊙	21
8400	13.7	1.1*R*	1.75	33	21	22	23	26	23	22
8500	15.5	1.4	2.24	56	26	27	29	30	25	25
8600	17.1	1.7	2.70	52	37	34	28	40	30	38
8700	18.0	1.4	.....	.....	64	69	70	84	66	55
8800	16.8	1.0	.....	88	110	58	84	107	52	81
8900	13.8	1.4*R*	1.40*R*	70	48	53	51	62	50	53
9000	12.0	1.4*R*	1.90*R*	32	30	26	29	30	41	40
9100	10.8	1.1	?	24	26	23	23	22	20	26
9200	9.8	1.4*R*	2.57*R*	27	30	22	27	22	23	23

widths nor the V/R ratio estimates are reliable. There is an indication of a subcycle in the proper direction in the absorption V/R curve, and the emission curve of V/R is usually in phase with that of the absorption.

On McLaughlin's hypothesis[38] we should find the opposite condi-

[38] *Proc. Nat. Acad. Sci.*, **19**, 44, 1933.

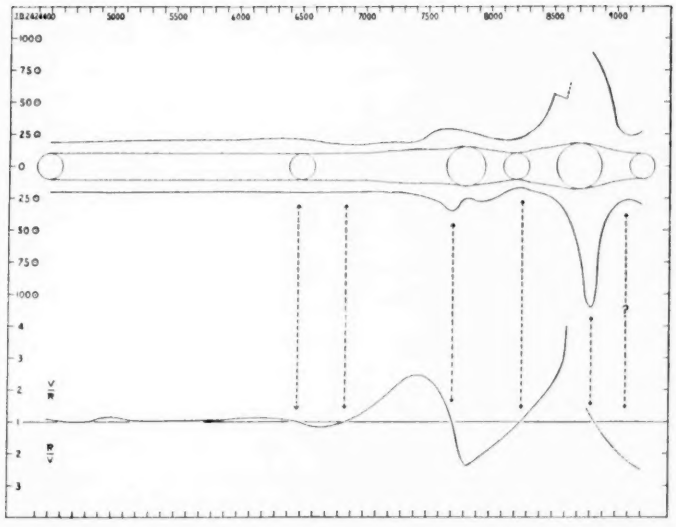

FIG. 6.—Computed changes of photospheric radius and extent of emitting layers of hydrogen in the atmosphere (*top*). *Hδ* emission V/R curve (*bottom*). Note that, when the violet emission component is stronger than the red, the hydrogen atmosphere is expanding, and vice versa. The hydrogen asymmetry may not be real.

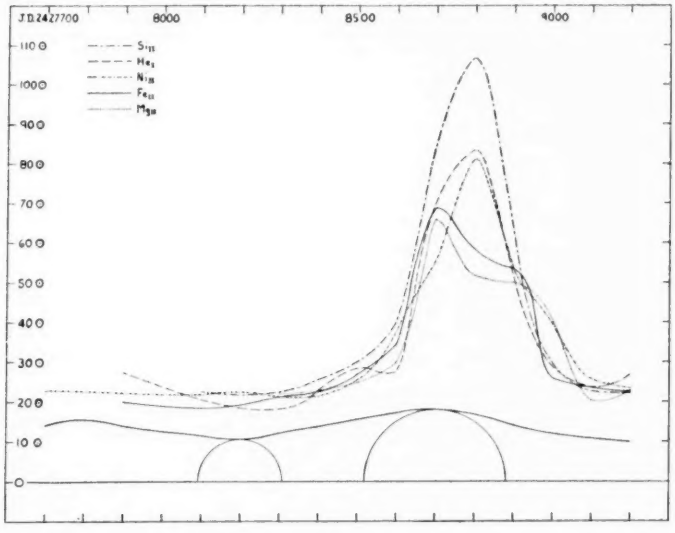

FIG. 7.—Extents of emitting layers of five elements and variations in radius of the photosphere. Each of these layers appears to be symmetrical.

tions to obtain, the red component theoretically being the stronger one during an actual expansion of the atmosphere, while the violet is strong during a collapse.

Figure 7 shows the changes in the radii of the emitting layers for the remaining elements of Table 2. The velocity-curves[13] of the edges of the emission components of these elements are nearly symmetrical so that mean radii only are given.

If average values of the width, or height, of the emitting layers are taken for the period JD 2428300–2429200, the elements appear to be stratified as follows: *Si* II highest, then *H*, with *Ni* II, *He* I, and *Mg* II grouped, and *Fe* II lowest. Similarly, the lines of the elements present in diffuse absorption suggest stratification. The *Si* II lines are narrowest, followed by *He* I, *Ni* II, and *Mg* II, which are grouped, with *Fe* II last. Hydrogen cannot be listed with the latter because of the slightly different manner in which the lines were measured. It should be borne in mind that a weak absorption line, or a line on an overexposed or underexposed plate, will be measured too narrow, while an emission line in the violet is apparently narrower than one in the blue because of slit effects. Attempts have been made to eliminate these effects, but both may still be operative, and thus the stratification may be somewhat other than that given.

THE SHARP ABSORPTION LINES

An outstanding and entirely unexpected set of spectral changes occurred between JD 2427880 and 2428500. These changes have been described by Lockyer,[15, 16] McLaughlin,[17] and in the second paper of this series.[13] Briefly, the *He* I lines, which are normally broad and dish-shaped, developed strong, sharp absorption cores. The first line to appear was λ 3889 (2^3S-3^3P), which arises from a metastable lower level. Soon other *He* I lines appeared, including λ 5015 (2^1S-3^1P), λ 3965 (2^1S-4^1P), and λ 3614 (2^1S-5^1P), which also possess a common metastable lower level. The last line was the only measurable feature in the region of the Balmer emission continuum. There were six other *He* I lines visible in more or less strength, as well as the Balmer lines of hydrogen. Several of the stronger lines of *Fe* II and λ 4067 of *Ni* II were also present, although they were

extremely weak. The 2S level of hydrogen is metastable, as are the lower levels of the *Fe* II and *Ni* II lines.

DATES OF APPEARANCE

These sharp absorption lines appeared just after a red maximum of the emission V/R curve prior to the 1937 cycle. A search was then instituted on plates taken at the corresponding phase before the previous cycle. Suggestions of absorption cores at λλ 3889, 3965, and 4026 of *He* I, and at $H\delta$ were found. Thus, the absorption before the 1934 phase was weak, and this set of spectroscopic changes was not of great significance. The absorption lines suddenly became strong just before the 1937 cycle, and this was the most radical ever seen for any Be star. At present, in the fall of 1939, the emission V/R curve is just past a red maximum, and the sharp absorption lines have returned in greater strength and numbers than ever before. Many lines never until now seen in a "shell" spectrum are present.

Two years after the 1937 cycle came the beginning of a fourth cycle of spectroscopic changes. Thus far the shorter the period between cycles the stronger have been the changes; the strength of the spectrum of the "shell" also seems to be an indication of the nature of the subsequent variations. Therefore, it seems likely that the 1937 phase is about to be repeated, possibly in more cataclysmic form than before, i.e., in an increase in light and a corresponding decrease in color temperature.

THE VELOCITIES

All of the "shell" lines which appeared before the 1937 cycle were extremely sharp, and even on microphotometer tracings showed practically no wings. Because of their signal sharpness, velocity measures were made on the two edges and centers of all lines. The results are given in Table 3. The helium and hydrogen velocities were similar but not identical. Irregular, though real, changes were found from plate to plate, and the *He* I lines varied more than did the hydrogen lines. They are shown in Figure 8. Emission structures at the *He* I lines were present, but not measurable, on early plates of this period. Emission velocity measures for *He* I were made on some of the later plates, and for hydrogen they were made on all plates.

When the hydrogen absorption-line velocities are plotted over the emission structure, it is seen that they lie in the normal central dip of the emission line. However, when the helium absorption lines are plotted over the helium emission, it is seen that the absorption

TABLE 3

HYDROGEN AND HELIUM VELOCITIES*

JD 242+ (1)	Hydrogen					Helium					
	EE (2)	EM (3)	VAE (4)	CA (5)	RAE (6)	VAE (7)	CA (8)	RAE (9)	VAE (10)	CA (11)	RAE (12)
7885	− 2	− 4	.....	−11	.....	.....	+10	.....	.....	.....	.....
806	+10	+11	.....	+ 2	.....	.....	−14	.....	.....	.....	.....
806	+ 4	− 8	.....	− 1	.....	.....	−27	.....	.....	.....	.....
807	0	0	.....	+ 2	.....	− 64	−27	+ 6	.....	.....	.....
808	+ 1	− 3	.....	− 6	.....	− 57	−16	+23	.....	.....	.....
810	−10	− 9	.....	− 8	.....	− 56	−17	+22	.....	.....	.....
812	− 7	− 7	.....	−10	.....	− 33	− 4	+32	.....	.....	.....
8182	−22	−27	−85	−35	+10	− 83	−40	+ 3	.....	.....	.....
8206	−16	−16	−70	−17	+34	− 66	−12	+41	.....	.....	.....
8256	−32	−35	−83	−42	+ 2	− 86	−44	− 2	.....	.....	.....
8315	−32	−32	−71	−32	+ 3	− 75	−41	− 9	.....	.....	.....
8315	−30	−31	−78	−35	+ 1	− 77	−38	0	.....	.....	.....
8340	−32	−39	−84	−35	+12	− 79	−37	+ 5	.....	.....	.....
8342	−38	−40	−97	−48	− 6	−109	−63	−16	.....	.....	.....
8391	−27	−25	.....	−26	.....	− 95	−56	−16	−60	−21	+16
8392	−29	−30	−70	−20	+30	−103	−65	−26	.....	−33	.....
8426	−35	−32	.....	−28	.....	−106	−67	−31	.....	− 7	.....
8432	−35	−32	.....	−24	.....	.....	−63	.....	.....	− 7	.....
8450	−40	−35	.....	−25	.....	−106	−66	−25	.....	−13	.....
8461	−42	−36	.....	−31	.....	.....	−54	.....	.....	.....	.....
8468	−43	−38	.....	−32	.....	.....	−75	.....	.....	.....	.....

* All velocities are in kilometers per second. EE stands for mean emission edge velocity; EM, mean emission maxima velocity; VAE, violet absorption edge velocity; CA, central absorption velocity; RAE, red absorption edge velocity.

Values in columns 7, 8, and 9 prior to JD 2428342 are mean velocities from all helium lines. After this date these columns give the velocities found for the lines λ 3889 and λ 3965. The last three columns give the measured velocities for λλ 3820, 4026, and 4472.

gradually shifts until it partly *overlies* the violet emission component. Because there is no diminution of absorption intensity on the violet side, i.e., the emission is almost completely absorbed, we have additional proof that the sharp lines of helium, and consequently of hydrogen, originate in layers of atmosphere more remote from the photosphere than do the emission lines. The *He* I absorption velocities show secondary changes superimposed on a constant accelera-

tion by which the velocity changes from +10 to −60 km/sec in the six hundred days prior to JD 2428500.

Peculiarly enough, the helium lines arising from metastable levels, λ 3889 and λ 3965, show this continuous acceleration throughout the entire period. The remaining *He* I lines do not possess metastable lower levels, and they all show the acceleration until JD 2428342,

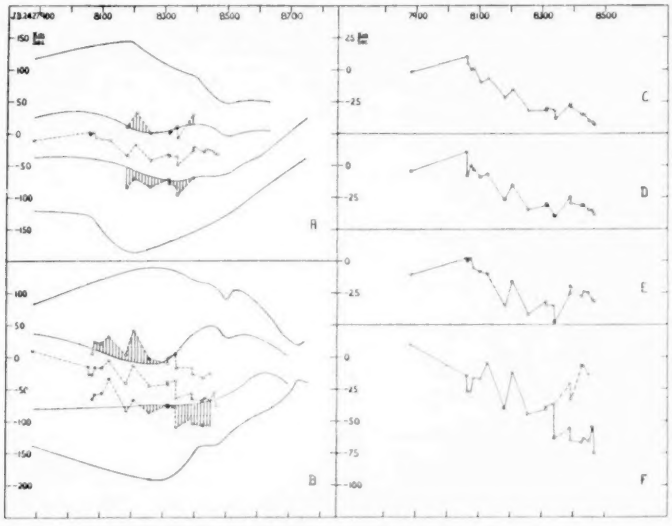

FIG. 8.—*A:* Relation between sharp absorption (dotted lines) and the two emission components of hydrogen. The two edges and center of the absorption line are given. Shaded regions show portions of emission which have been absorbed by the outer "shell" gases. *B:* Similar structure in lines of helium, showing an even greater overlapping of absorption over emission. *C:* Mean velocities of the hydrogen emission edges. *D:* Mean velocities of the hydrogen emission maxima. *E:* Mean velocities of the hydrogen sharp absorption lines. *F:* Mean velocities of the helium sharp absorption lines. From JD 2427885 to 2428340 the velocities are the means of all lines. After the latter date the solid lines represent λ 3889 and λ 3965, which arise from metastable lower levels. The dotted line is for the normal lines λλ 3820, 4026, and 4472.

when they break off sharply to lower velocities. The hydrogen lines also veer off, but not as far as the helium lines. This may possibly be a consequence of the partial metastability of the 2S level of hydrogen under the conditions of electron density to be found in the upper atmosphere.

An odd fact is noticed in this and other Be variables. The mean

velocities of the emission edges or emission maxima practically duplicate the velocities of the central dip in the emission. Here the hydrogen emission edge velocities were almost identical with those measured for the *sharp* absorption, which arose in another layer, even to the secondary changes. This arises through a decided emission asymmetry. The mean emission velocity curves are also shown in Figure 8.

THE EQUIVALENT WIDTHS

Through the kindness of Dr. J. F. Heard, of the David Dunlap Observatory, who made microphotometer tracings of plates of γ Cassiopeiae taken during the second absorption-line stage, it has been possible to measure the equivalent widths of the sharp absorption lines of helium and hydrogen over the entire sequence.

The measured equivalent widths of these lines are listed in Table 4. The unit is one-thousandth of an angstrom. The column headed "3889 *Hζ*" marks the intensity of the blend of the helium and hydrogen lines. If, as seems probable, the hydrogen line is produced lower in the atmosphere than λ 3889, the effective continuous spectrum reaching the helium atoms is reduced, and consequently the helium line is stronger than a simple subtraction of intensities of blend *minus Hζ* would indicate. The probable intensity of *Hζ* may be interpolated from the intensities of *Hγ*, *Hδ*, *Hε*, and *Hη*. A preliminary computation suggests that *He* I 3889 is nearly of the same equivalent width as the measured width of the blend. Therefore, the intensity of the blend is a first approximation to the intensity of λ 3889. The ratio of the strength of the blend to λ 3965 is given in column 11. The measured mean ratio is 4.76. The theoretical ratio of strengths of λλ 3889–3965 is 5. Consequently, the lines are produced in a region so close to the photosphere that the dilution factor is not extremely small, and the difference in metastability of the 2^3S and 2^1S levels is not yet apparent. With dilution factors such as are found in the Orion nebula the ratio of strengths may be very large.

Unexpectedly, it was found that the λ 3889-*Hζ* blend appeared to be weakest, relative to λ 3965, when the remaining hydrogen lines were strongest.

DISCUSSION

Because the 2^1S and 2^3S levels of helium are metastable and the 2^1P and 2^3P levels are not, it is possible to compute the dilution factor by using relative intensities of absorption lines arising from these levels in "shell" stars and in normal stars. The method has been completely described by Struve and Wurm.[39]

TABLE 4

EQUIVALENT WIDTHS OF THE SHARP ABSORPTION LINES IN THE SPECTRUM OF γ CASSIOPEIAE

JD 242+	Helium										Hydrogen			
(1)	3820 (2)	3889 $H\zeta$ (3)	3965 (4)	4026 (5)	4144 (6)	4388 (7)	4472 (8)	5016 (9)	5876 (10)	$\frac{3889}{3965}$ (11)	$H\gamma$ (12)	$H\delta$ (13)	$H\epsilon$ (14)	$H\eta$ (15)
8063	....	119	....	....	....	....	....	....	....	....	....	....	....	....
806.	....	80	....	....	....	....	....	....	....	....	....	....	....	....
8075	....	177	34	28	....	....	38	....	....	5.21	57	29	62	....
808.	....	332	37	42	....	....	55	....	....	8.97	47	28	46	....
8105	....	235	48	30	....	....	47	....	....	4.90	65	42	36	47
8128	....	225	33	33	....	....	61	....	....	6.82	89	42	56	....
8182	260	585	133	154	....	16	235	....	....	4.40	202	166	98	149
8206	....	625	257	206	....	49	357	....	....	2.43	406	473	275	....
8256	304	923	239	252	56	53	459	....	....	3.86	511	511	322	278
8315	125	495	80	68	....	30	120	....	....	6.19	262	155	177	87
8315	103	535	84	123	....	14	112	....	....	6.37	214	171	232	133
8340	....	569	143	135	....	15	113	151	200	3.98	185	189	98	....
8342	235	811	300	278	31	52	316	....	....	2.70	449	276	252	183
8301	82	253	65	116	....	....	59	....	....	3.89	97	57	29	48
8302	90	324	89	95	....	....	106	....	....	3.64	145	92	125	55
8426	....	134	29	38	....	....	19	....	....	4.62	40	59	47	26
8434	....	132	38	23	....	....	28	....	....	3.57	21	66	87	51
8450	....	34	....	....	....	....	....	....	....	....	....	....	....	....
8461	....	74	....	....	....	....	....	....	....	....	....	....	....	....

In order to maintain homogeneity of the measures, a plate of γ Pegasi, taken with the Michigan spectrograph, was run on the David Dunlap Observatory microphotometer. The resultant equivalent widths were assumed to be those of a normal star and were used in the computation. They are comparable to the values determined by Williams.[40] Rudnick[41] has also measured equivalent widths of lines in the spectrum of γ Pegasi; they show fair agreement with measures

[39] *Ap. J.*, **88**, 84, 1938.

[40] *Ap. J.*, **83**, 279, 1936; *Mt. W. Contr.*, No. 540, 1936.

[41] *Ap. J.*, **83**, 439, 1936.

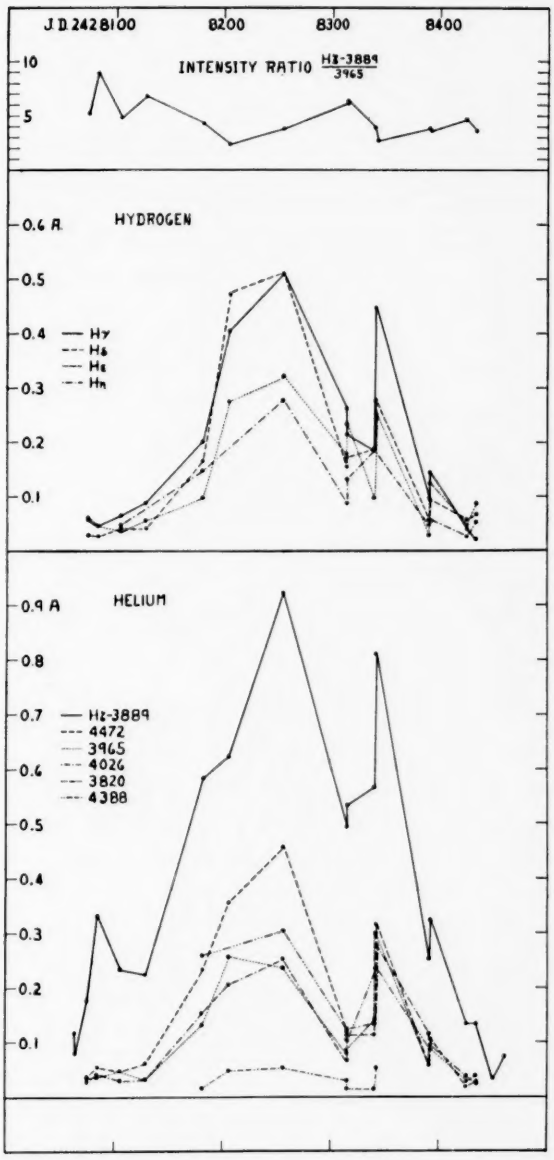

FIG. 9.—Equivalent widths of the sharp hydrogen and helium absorption lines

by Williams and the author for the weak lines but are systematically smaller for strong lines. Table 5 lists twelve lines whose equivalent widths have been measured. The unit of equivalent width is one-hundredth of an angstrom.

From the dilution factor we may compute the radius of the helium shell relative to that of the photosphere, and if the radius of the photosphere is known, we shall have the absolute radius of the shell. This procedure is subject to rather large experimental error; nevertheless, it should give an approximate value of the radius of the shell.

TABLE 5

EQUIVALENT WIDTHS OF STANDARD LINES IN THE SPECTRUM OF γ PEGASI

Line	Baldwin	Williams	Rudnick	Line	Baldwin	Williams	Rudnick
He I 3820	134	166	.....	*H*γ	482	436	232
3965	18	18	26	*H*δ	449	460	182
4026	121	143	98	*H*ϵ	409	510	.....
4121	38	36	34	*H*ζ-3889	391	529	.....
4144	74	83	69	*H*η	396	544	.....
4388	98	80	92				
4472	149	118	142				

It should be recalled here that this process depends on the dilution of black-body photospheric radiation at a particular color temperature. For the stars discussed by Struve and Wurm[39] this method should give fair approximations to the real radii. In the atmosphere of γ Cassiopeiae the case is different; there is definite emission in helium lines whose lower levels have $n = 2$. Consequently, there will be strong emission at the transition $2^1P - 1^1S$. This line is emitted below the shell and thus will disturb both the effective color temperature of the radiation reaching the shell and the dilution factor. Therefore, the computed radius of the shell will be too small, and we shall determine only a lower limit of size.

The radii of the photosphere are derived earlier in this paper; the values of the minimum relative radii of the shell, computed from the measured dilution factors, are given in Table 6, as are the minimum absolute radii. When the changes of radius of the shell are plotted on the same time scale as the mean intensity-curve of the sharp heli-

um absorption lines, they are seen to give nearly a reflected curve; i.e., the stronger the line, the closer to the photosphere it is produced.

In making the computations the intensity ratios of λλ 3965–4388, 3965–4144, 3889–4026, and 3889–4472 were used. The assigned weights were 4, 2, 1, and 1, as λ 4144 was weaker than λ 4388, and since λ 3889 could not be observed independently. The value of the equivalent width used for λ 3889 was five times the observed width of λ 3965; so we are really comparing λ 3965 with λ 4026 and λ 4472.

TABLE 6

CHANGES OF THE RADIUS OF THE SHELL

JD 242+	Radius of Photosphere	Relative Radius of Shell	Radius of Shell
8075	11.9 ⊙	3.1	37 ⊙
8084	11.8	3.6	42
8105	11.6	3.3	38
8128	11.4	3.0	34
8182	10.8	3.0	32
8206	10.7	2.4	26
8256	11.6	2.4	28
8315	12.6	2.4	30
8315	12.6	2.9	37
8340	12.9	3.4	44
8342	12.9	2.7	35
8391	13.6	2.2	30
8392	13.6	2.4	33
8426	14.2	3.1	44
8434	14.3	3.1	44

In each case the value was close to the measured equivalent width of the *Hζ*-3889 blend.

Earlier in the paper it was shown that changes in the effective volume of the atmosphere in which emission occurred could be found by comparing emission velocities at different times with an original photospheric velocity of rotation. Part of Figure 6 is repeated in Figure 10, with the minimum values of the radii of the shell superimposed. It is seen that the minimum distance of the shell from the photosphere comes at the time when the emitting layer has reached minimum size. The shell is shown to be definitely outside, and its radius changes in a manner which is roughly proportional to the changes in size of the layers of emission.

The displacements of the *He* I lines show a continuous increase in negative, or expansional, velocity. In spite of this, the shell apparently approached the photosphere and then receded. Probably the shell is merely an optical effect produced by atoms streaming through a region where conditions are right for the production of sharp absorption lines. The irregular nature of the intensity curves near JD 2428340 is strong evidence against a discrete shell hypothesis.

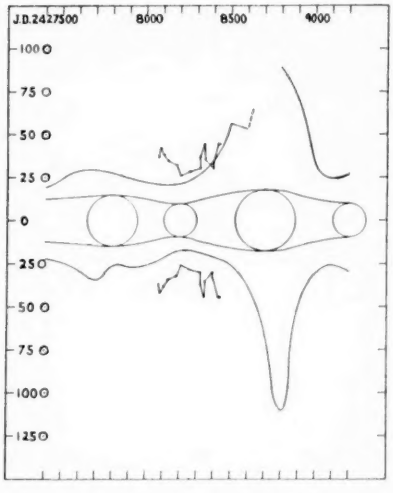

FIG. 10.—Computed radii of the helium "shell," compared with the radii of the hydrogen emitting layers. The helium layer of emission is very similar to the hydrogen layer, except that it appears to be symmetrical.

The shell layers are certainly exterior to the emitting layers, and yet the $n = 2$ levels of helium are highly populated. This means that radiation of wave length shorter than λ 584.4, $1^1S - 2^1P$, is penetrating the layers where emission is produced. Thus, the Lyman continuous absorption is not complete.

The sharp absorption lines were present about a year and a half. In that time the maximum velocity of expansion was approximately 60 km/sec, and the average was about 30 km/sec. During this period, then, it is clear that there were no expansional components of motion comparable to that of the rotation. The emission and absorption V/R curves meanwhile changed sign. In both cases the red component was originally stronger, while the violet components gained as the red lost intensity, and were the more prominent features at the end of the shell stage. This seems to indicate that the expansional component of the motion of the atmosphere is not the factor which controls the V/R changes and that future models of the Be stars must be built on a modification of Struve's rotational hypothesis.[42]

[42] *Ap. J.*, **73**, 93, 1931.

THE V/R CHANGES OF THE EMISSION LINES

B stars with emission lines are relatively rare; yet they actually total over four hundred established cases. In a large percentage of those which have been observed intensively the hydrogen emission lines are double and undergo cyclical V/R changes. However, in all the V/R variables only five stars are known to the author to show similar changes in the lines of any other element. They are β Monocerotis,[43] where the variation is undoubted, ϕ Persei,[44] ϵ Capricorni,[43] the Be component of VV Cephei[45] where the variation is suspected, and γ Cassiopeiae. In the first three cases it is only the strongest line or two of *Fe* II which shows V/R changes similar to those of hydrogen. For the companion of VV Cephei the H and K lines may vary, although the origin of these emission lines is not definitely established as in the atmosphere of the Be star. In the spectrum of γ Cassiopeiae lines of at least ten different elements show the V/R transpositions. They are: *H*, *Fe* II, *Si* II, *Mg* II, *Ca* II, *Ni* II, *Cr* II, *Na* I, *He* I, a line tentatively assigned to *Mg* I, and the unidentified line λ 6444.

The V/R curves for $H\gamma$ and $H\delta$, three multiplets of *Fe* II, *Si* II, and *Mg* II, have been given for the period March 23, 1935—October 24, 1938, in the second paper of this series.[13] Estimates of the V/R ratios were made later for the K line of *Ca* II, *Ni* II 4067, and occasionally *Cr* II 4558, when it could be distinguished from *Fe* II 4556. Dr. Cherrington of the Perkins Observatory kindly sent several spectrograms of the visual region covering the time when the emission lines were narrowing, and on these it was found that the D lines of *Na* I also showed the expected variations and that the range was larger than for any other element except hydrogen. The number of plates was not sufficient to give complete curves. Estimates were also made of λ 6318, which is possibly produced by *Mg* I, the D_3 line of *He* I, and λ 6444 of unknown origin. The latter line appears to be blended with another emission feature, as the V/R estimates were not dependable.

Estimates of the ratios of intensities of the two emission com-

[43] McLaughlin, *Pub. Obs. U. of Michigan*, **4**, 175, 1932.

[44] Dustheimer, *Pub. Obs. U. of Michigan*, **7**, 171, 1939.

[45] Goedicke, *Pub. Obs. U. of Michigan*, **8**, 1, 1939.

ponents have been made for all Balmer lines from $H\beta$ to $H\lambda$. From these, two general conclusions may be reached. The lines of shorter wave length show a smaller range of V/R, and the changes at any line precede those of the line of next longer wave length by an interval which increases toward the long-wave end of the series. The phase differences for lines of shorter wave length than $H\eta$ are not noticeable. They are, roughly, 30, 60, and 80 days between $H\epsilon$ and $H\delta$, $H\delta$ and $H\gamma$, and $H\gamma$ and $H\beta$, respectively, while Cherrington's estimates[46] indicate a lag of the order of 300 days for $H\alpha$ relative to $H\beta$.

In the rising part of the V/R curve for the 1934 and the 1937 cycles, $H\delta$ preceded $H\gamma$; but in the descending part of the 1934 curve, $H\gamma$ preceded $H\delta$ and therefore passed through its changes more rapidly. An effect of the same nature is indicated for the descending branch of the latter cycle, but this cannot be proved, as $H\gamma$ was not completely resolvable until near maximum width was reached.

Numerous emission lines of *He* I appeared after the 1934 cycle and possessed both components. With the single exception of the D3 line in the visual spectrum, these components remained almost exactly equal in intensity. The D3 line showed changes similar in nature and direction to those of the other elements.

The amplitudes of the V/R curves for all elements were much less than those of the hydrogen lines. In spite of the relatively small variations, real changes could be detected and estimated. These changes for all lines are shown graphically in Figure 11. For most elements the curves continue to rise until approximately the beginning of the single-line stage. The exact date of maximum is usually hard to determine; yet the *Si* II lines and the lines of the $b^4F - z^4D^o$ multiplet of *Fe* II reached maxima of V/R during the narrowing stage and then approached equality before the components blended.

CORRELATIONS

All the curves for the ionized metals are related to each other. Correlations may be made which suggest that the process producing

[46] *Pub. A.A.S.*, **9**, 2, 34, 1937.

the V/R changes is the same for all. The hydrogen, helium, and neutral metals give curves which are not as accordant.

Only two elements are represented in the latter group—sodium and probably magnesium. Both the D lines of sodium are weak, and the blends caused by atmospheric absorption lines make estimates of V/R difficult.

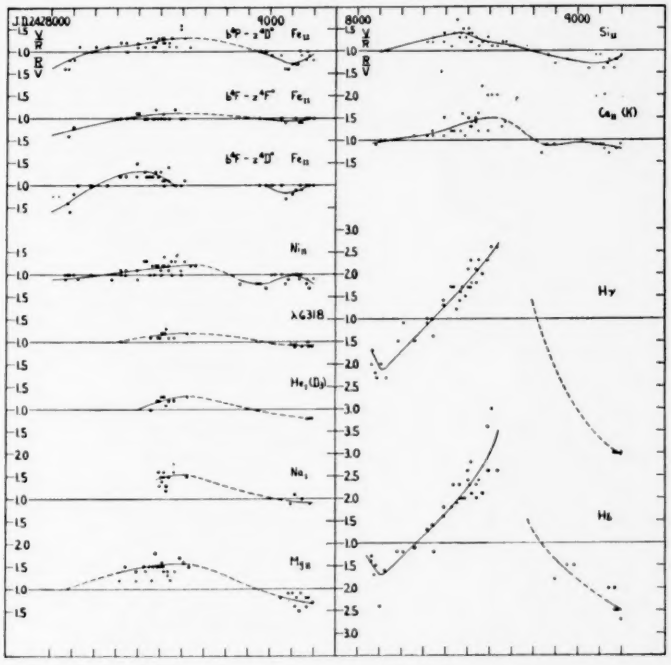

FIG. 11.—Emission V/R curves

If we take the maximum values of the V/R ratios for the period JD 2428300–700 as determined from smooth curves drawn through the estimated points, it is to be expected that the accidental errors of estimation will largely cancel out and that an index of the true changes will be formed. This period of time corresponds to the narrowing phases when V was greater than R. The second period shown in Figure 11 is after the single-line stage, when R was greater than V. The latter values are not used in the discussion, as a second pair

of emission lines blended with the original components of several lines, perhaps with all, and seriously affected the accuracy of the estimates. The above-mentioned maximum V/R values are given in column 2 of Table 7; columns 3, 4, and 6 are self-explanatory; while column 5 lists the date when the two emission components became equal after R had been stronger than V.

It is seen that when the range of V/R is plotted against the ionization potential there is a weak relationship. The elements which have

TABLE 7

DATA CONCERNING THE EMISSION LINES

Element	Maximum V/R Range	Ionization Potential Volts	Atomic Weight	Date of Equality JD 242+	Date of Maximum V/R JD 242+
Hγ	.....	13.54	1.008	8350	?
Hδ	.....	13.54	1.008	8280	?
He I	1.05	24.47	4.000	?	?
He I (D_3)	1.33	24.47	4.000	8400	8625
Na I	1.56	5.12	23.00	.....	8600
Mg II	1.55	14.97	24.32	8070?	8620
Si II	1.43	16.27	28.06	8110	8475
Ca II	1.50	11.82	40.07	8150	8635
Cr II	1.35	16.6	52.01	.....	.....
Fe II*	1.31	16.16	55.84	8175	8625
Fe II†	1.10	16.16	55.84	8325	8600
Fe II‡	1.30	16.16	55.84	8200	8435
Ni II	1.25	18.4	58.69	8215	8625
Mg I? (6318)	1.20	7.61	24.32	8300?	8625

* $b^4P-z^4D^o$. † $b^4F-z^4F^o$. ‡ $b^4F-z^4D^o$.

the higher ionization potentials exhibit, in general, smaller V/R ranges. On this chart the hydrogen values are not accordant (Fig. 12, *A*).

The atomic weights are also related to the range of V/R in that, excepting helium, the heavier elements are least variant. Hydrogen again shows too great a range to fit the curve, while the other residuals are within the errors of estimation (Fig. 12, *B*).

An additional correlation may be noted. If the range of V/R is plotted against the Julian day when the emission components became equal after having had the red component stronger, there is a relationship for all elements, again excepting hydrogen. The ele-

ments which showed the greatest range of V/R reached equality first. The dates for *Mg* II λ 4481 and *Mg* I 6318 are extrapolations.

The value for the line at λ 6318 falls beautifully on the last correlation curve; but if the other two are used to predict the atomic weight and ionization potential, we arrive at extremely improbable results. It seems that the first two curves are valid only for the ionized metals and that the placing of the values for the D lines is fortuitous. If the relationships shown in the charts are due to physical causes and are not purely chance coincidences, they lend added sup-

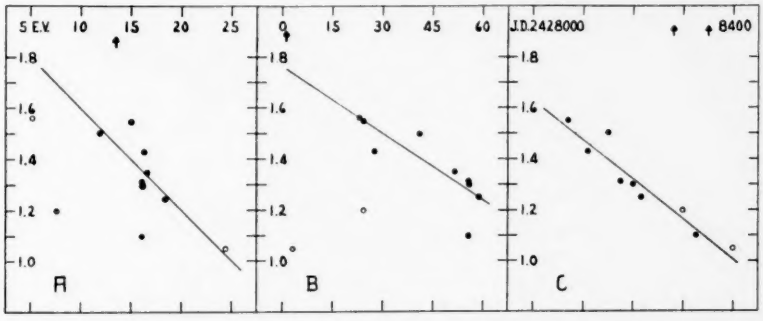

FIG. 12.—Correlations with emission V/R ratios. *A:* V/R — Ionization potential. *B:* V/R — Atomic weight. *C:* V/R — Time when emission components became equal. Filled circles are for ionized metals; open circles are for neutral elements. Hydrogen values are indicated by arrows. The correlations appear valid for only the ionized metals.

port to Cherrington's identification[23] of λ 6318 as a line of a neutral metal.

DISCUSSION

In attempting to get a better picture of the structure of such a star as γ Cassiopeiae from the above data, let us recall that Goedicke[45] has shown for the Be companion to VV Cephei that the hydrogen emission is stratified. $H\beta$ is emitted with measurable intensity over a much larger volume than is $H\gamma$, and $H\gamma$ over a larger volume than $H\delta$. As the V/R lags suggest a stratification effect in γ Cassiopeiae, it is probably valid to assume that such is the case, and thus for hydrogen the range of V/R and the phases of the V/R curves are functions of the effective level of emission.

The existence of the strong and broad *He* I absorption lines in the

earlier stages suggests an original high excitation temperature, probably higher than the observed original color temperature of 13,500° K. As the color temperature dropped to 8000° K, the ionization temperature rose considerably. The recent presence and increasing strength of the helium emission lines indicate that the atoms were ionized and then underwent recombination. The ionization of the neutral helium atom requires nearly 25 volts, or a temperature of the order of 20,000° K. The increase in the emission strength[14] of the hydrogen lines and continuum appears to be correlated with the change at the helium lines. Swings, Edlén, and Grandjean[47] have identified four of the emission lines measured by the author during the single-line stage as due to *Fe* III. If their identifications are correct, the iron atoms must first be doubly ionized and then excited to produce the observed emission. The weakness of the lines suggests that they are produced by excitation rather than by recombination. The presence of the *Fe* III lines probably is indicative of a high ionization temperature of the star during the period when the color temperature was very low.

The production of emission lines of *Fe* III and *He* I may be reconciled with the presence of the emission lines of neutral metals, such as *Na* I and *Mg* I, by the theory of Kosirev.[35]

To say that the atmosphere of γ Cassiopeiae appears to be stratified does not mean that the atoms themselves are confined to any given region. They may, and probably do, stream through these regions all together, as is shown by the similarities of their velocity-curves. In this view they would be stratified in the sense that they produced emission from definite layers in a manner similar to the Balmer lines.

SUMMARY

In conclusion it may be said that, although a complete physical model of γ Cassiopeiae cannot now be constructed, the data presented point toward the fact that such a model must be based on rotational motions with pulsational velocities superimposed. The principle of conservation of angular momentum gives a satisfactory explanation of the correlations and dissimilarities between the observed light- and temperature-curves.

[47] *Ap. J.*, **90**, 378, 1939.

The size of the detectable atmosphere is greatly variable, and the emitting and absorbing layers are probably stratified. Certain absorption lines characteristic of a "shell" spectrum are produced in regions outside the emitting layers. The conception of a discrete shell of hydrogen and helium must be discarded, as the atoms are observed to stream through a nearly stationary region in which the absorption lines are produced.

The V/R changes of the emission lines of ten elements are similar but show real differences which seem to be related to the atomic weights and the ionization potentials of the elements. Any future model must explain, for instance, why the curves for the lines of the three multiplets of *Fe* II are not identical, and why elements whose velocity-curves are similar show V/R curves going in opposite directions at the same time. A typical example of the latter point is found before the single-line stage, when the *Si* II lines were approaching equality after reaching a maximum of V/R, while lines of *Ca* II, *Mg* II, etc., were still showing an increasing ratio of intensities.

I wish to express my appreciation to Dr. D. B. McLaughlin, of the University of Michigan Observatory, for lending me the long series of spectrograms of γ Cassiopeiae and to Dr. Ernest Cherrington, Jr., of the Perkins Observatory, for lending me several spectrograms of the visual region. Dr. J. F. Heard, of the David Dunlap Observatory, rendered invaluable aid by making microphotometer tracings of the spectrograms taken during the "shell" stage. The page copy has been made possible by a subsidy from the Research Council of the Graduate School of Northwestern University.

DEARBORN OBSERVATORY
December 14, 1939

THE KINETIC TEMPERATURE OF THE SOLAR REVERSING LAYER

PEARL J. RUBENSTEIN

ABSTRACT

A redetermination of the curve of growth for the sun by means of least squares has resulted in a value of the temperature of the solar reversing layer for iron atoms

$$T = 5400^\circ \pm 1300^\circ \text{ (m.e.)}$$

and a value of the damping constant

$$\frac{\Gamma}{\nu} = 1.7 \times 10^{-6} \pm 0.40 \times 10^{-6} \text{ (m.e.)} .$$

In a series of recent papers[1, 2, 3] the theoretical expression for the curve of growth has been derived and compared with Allen's[4] observations of the equivalent widths of lines in the solar spectrum. The present note concerns a further investigation of the same material and of the new tables by Allen,[5] which extend the observations to 3924 A. A least-squares solution gave the theoretical curve which best fits the observational data.

Theory shows that W/λ can be given as a function of X_0, the optical depth at the center of the line. For small values of X_0,

$$\log \frac{W}{\lambda} = \tfrac{1}{2} \log \pi + \log \frac{v}{c} + \log X_0 + \log \left(1 - \frac{X_0}{\sqrt{2}} + \frac{X_0^2}{\sqrt{3}} \ldots . \right) .$$

For intermediate values of X_0,

$$\log \frac{W}{\lambda} = \log X_0 \frac{v}{c} \sqrt{\pi} - \tfrac{1}{2} \log (1 + X_0) - \frac{\tfrac{1}{2} \log 4\sqrt{\pi} \dfrac{v}{c} \dfrac{\nu}{\Gamma}}{1 + 15 e^{-2 \log X_0}} ;$$

and for large X_0,

$$\log \frac{W}{\lambda} = \tfrac{1}{4} \log \pi - \log 2 + \tfrac{1}{2} \log \frac{v}{c} + \tfrac{1}{2} \log X_0 + \tfrac{1}{2} \log \frac{\Gamma}{\nu_0} ,$$

[1] *Ap. J.*, **84**, 462, 1936.

[2] *Ap. J.*, **84**, 474, 1936.

[3] *Ap. J.*, **87**, 81, 1938.

[4] *Mem. Comm. Solar Obs.*, **1**, No. 4, 1934.

[5] *Ibid.*, **2**, No. 6, 1938.

where

$$X_0 = \left[3.510 \times 10^{-12} \frac{N_a}{b(T)} \sqrt{\frac{\mu}{T}}\, \varphi\right] S \frac{s}{\Sigma s} e^{-X_{J'}/kT}.$$

Since $X_{J'}$, the excitation potential, is essentially constant for lines of a given multiplet, all the lines have been plotted on a single diagram with an arbitrary zero point for log X_0. Various multiplets are combined on the diagram by sliding the log X_0 zero point until the

TABLE 1

log X_0	log $\frac{W}{\lambda}$	N	σ	O−C
−0.92	−5.98	4	0.101	+0.10
−0.68	−5.82	14	.242	+ .04
−0.53	−5.74	24	.121	− .01
−0.32	−5.52	17	.142	+ .02
−0.12	−5.48	17	.148	− .14
+0.68	−5.02	30	.132	− .06
+0.87	−4.95	36	.149	− .06
+1.08	−4.84	25	.117	.00
+1.26	−4.81	28	.071	− .02
+1.44	−4.75	21	.067	+ .01
+1.65	−4.71	22	.131	.00
+1.84	−4.65	29	.078	+ .02
+2.05	−4.58	20	.081	+ .03
+2.43	−4.46	25	.097	+ .08
+2.64	−4.37	8	.136	+ .07
+2.75	−4.47	4	.071	− .09
+3.00	−4.18	7	.147	+ .08
+3.13	−4.20	2	.119	− .01
+3.41	−4.03	3	0.050	+0.02

best fit with an assumed master-curve is obtained. The master-curve used in this study was that given by Menzel, Baker, and Goldberg.[3]

The resulting graph was divided into equal parts along the log X_0 axis, and all the points in each strip were averaged to give the normal points for the least-squares solution. The first and second columns of Table 1 give the co-ordinates of the normal points; the third column, the number of observations; and the fourth, the mean error obtained from the combined dispersions in the two co-ordinates. The last column gives the difference between the observed and computed values of log (W/λ) for given log X_0, computed with

the least-squares values of the constants. Figure 1 shows the normal points with their mean errors in the log (W/λ) co-ordinate and the final theoretical curve.

A least-squares solution was carried out to determine the best values of the constants v/c and Γ/ν. An attempt to solve for both Γ/ν and Γ/ν_0 separately resulted in values which differed insignificantly from each other, in view of the large mean errors. In the final solution Γ/ν was therefore set equal to Γ/ν_0. The curve was

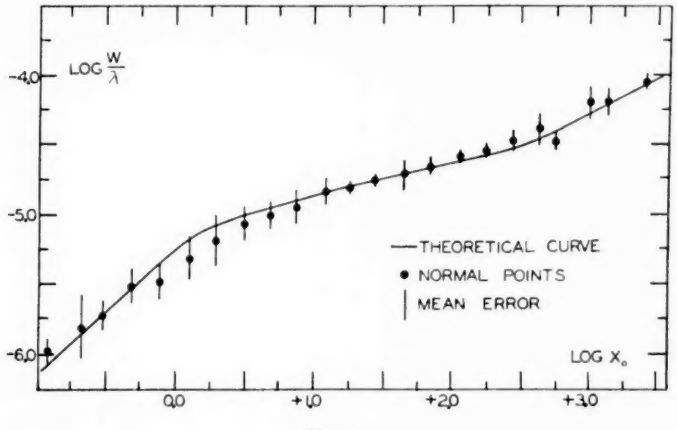

FIG. 1

divided into three parts, corresponding to the three theoretical expressions; and points in the transition regions were omitted.

Using the relation

$$v = 1.289 \times 10^4 \sqrt{\frac{T}{\mu}},$$

where μ is the atomic weight, one arrives at the following value of the temperature for iron atoms:

$$T = 5400^\circ \pm 1300^\circ \text{ (m.e.)}.$$

The solution also gives

$$\frac{\Gamma}{\nu} = 1.7 \times 10^{-6} \pm 0.40 \times 10^{-6} \text{ (m.e.)}.$$

From Figure 1 it is seen that the normal points fit very well on the theoretical curve determined with two constants. The temperature derived in the solution is not the same as that previously found, but the mean error is so large that one can draw no certain conclusions from the differences. One can merely state that the temperature falls within the range of values determined by various other methods. The value of Γ/ν agrees well, within the limit of error, with that found by Menzel.[1]

I wish to express my appreciation to Dr. D. H. Menzel and Dr. T. E. Sterne for their kind assistance and many suggestions in connection with this paper.

HARVARD COLLEGE OBSERVATORY
February 12, 1940

RECENT EVIDENCE ON THE NUCLEAR REACTIONS IN THE CARBON CYCLE

H. A. BETHE

ABSTRACT

New experimental results provide better estimates of the probabilities of nuclear reactions involved in the carbon cycle than those available previously. The lifetimes of C^{12} and N^{14} are found to be almost equal, namely, 2.5×10^{6} years and 4×10^{6} years, respectively. The abundances of C^{12} and N^{14} should be similar in main-sequence stars. The combined abundance of C and N should be about 1 per cent by weight—in sufficient agreement with observational evidence. The ratio $N^{14}:N^{15}$ in the sun should be $2\times10^{5}:1$, considerably greater than on earth ($260:1$).

In the last months several experimental investigations have been published which permit more accurate estimates of the probability of the nuclear reactions involved in the carbon cycle.[1] Curran and Strothers[2] have observed the radiative capture of protons by N^{14} and have measured its cross-section. Burcham and Smith[3] have found the reaction $N^{15} + H^{1} = C^{12} + He^{4}$, and Holloway and Bethe[4] have measured its cross-section. The other reactions involved, viz., the radiative capture of protons by C^{12} and C^{13}, had already been measured[5,6] when the theory of the carbon cycle was put forward.

The reaction

$$N^{15} + H^{1} = C^{12} + He^{4} \qquad (1)$$

has been found to be exceedingly probable. The measured cross-section is compatible with the assumption that *all* protons hitting the N^{15} nucleus produce reaction (1). The effective width Γ used in "I" as a measure of the probability of nuclear reactions (cf. I, eqs. [4], [7], and [11] and Table V) comes out[4] to be 1.0×10^{7} e.v. (electron volts), while only 10^{5} e.v. was assumed in I, Table V. The reaction

[1] H. A. Bethe, *Phys. Rev.*, **55**, 434, 1939 (quoted as "I").

[2] *Nature*, **145**, 224, 1940.

[3] *Nature*, **143**, 795, 1939.

[4] *Phys. Rev.*, **57**, 747, 1940.

[5] R. B. Roberts and N. P. Heydenburg, *Phys. Rev.*, **53**, 374, 1938.

[6] P. I. Dee, S. C. Curran, and V. Petrizilka, *Nature*, **141**, 642, 1938.

is therefore one hundred times more probable than was assumed in I, which reduces the mean life of a N^{15} nucleus at the center of the sun to 20 years. At the same time it means that the reaction $N^{15} + H^1 = C^{12} + He^4$ is presumably about 10^6 times more probable than the radiative capture of the proton, $N^{15} + H^1 = O^{16} + \gamma$, because the "width," Γ, is of the order of 10 e.v. for most radiative capture reactions. Of a million C^{12} nuclei undergoing the transformations of the carbon cycle, on the average only one will be transformed into O^{16}, while all the others will return to C^{12}. In I, the ratio was assumed to be only 10^4, which was already quite sufficient to insure the conservation of practically all the carbon and nitrogen in the star.

The measurement of the reaction

$$N^{14} + H^1 = O^{15} + \gamma \qquad (2)$$

is even more important. Curran and Strothers[2] find that about 1.5×10^{-11} nuclei O^{15} are formed in a thick Na_3N target by protons of 960 kv. (kilovolts) initial energy. The excitation curve shows indications of resonances, so that conclusions from the high-energy (500–900 kv.) cross-section on the probability of thermonuclear reactions (proton energy, a few kilovolts) are not very certain. From the curve given in footnote 2, the cross-section comes out to be 1.8×10^{-30} cm^2 between 890 and 940 kv. proton energy, and 0.33×10^{-30} cm^2 between 550 and 650 kv. From either measurement we obtain $\Gamma = 60$ e.v., using equation (11) of I. This is a very high probability for a radiative capture reaction which is equaled only by the reaction:[7] $Li^7 + H^1 = Be^8 + \gamma$. If we assume the same Γ for low proton energy (which may not be justified because of the resonances), the probability of the thermonuclear reaction (2) will be twelve times greater than was assumed in I, and therefore the mean life of a N^{14} nucleus at the center of the sun will be reduced to 4×10^6 years (the previous value was 5×10^7).

Including the carbon isotopes for which we take over the values obtained in I, we have for the lifetimes of the nuclei involved in the

[7] W. A. Fowler, E. R. Gaerttner, and C. C. Lauritsen, *Phys. Rev.*, **53**, 628, 1938.

carbon cycle at the center of the sun (assumed density, $\rho = 80$; hydrogen content, 35 per cent; temperature, 2×10^7 degrees):

$$\left.\begin{array}{ll} C^{12} \ldots\ldots\ldots & 2.5 \times 10^6 \text{ years} \\ C^{13} \ldots\ldots\ldots & 5 \times 10^4 \\ N^{14} \ldots\ldots\ldots & 4 \times 10^6 \\ N^{15} \ldots\ldots\ldots & 20 \end{array}\right\} . \tag{3}$$

All these values may easily be wrong by about a factor of 3 either way. The main conclusions to be drawn from the figures are:

1. The lifetimes of C^{12} and N^{14} are now almost equal, whereas previously the life of N^{14} was assumed to be twenty times longer than that of C^{12}. This means that C^{12} and N^{14} should be about equally abundant in main-sequence stars, which seems to be in agreement with the astrophysical evidence, in contrast to the previous assumption (N^{14} twenty times as abundant as C^{12}).

2. The total time required for a complete carbon cycle is now only 6×10^6 years, as against 5×10^7 years previously assumed. Therefore, in order to obtain the same energy evolution as before, we can now assume the combined abundance of carbon and nitrogen to be only one-tenth of the value assumed in I. This means a combined abundance of about 1 per cent by weight, or about 0.5 per cent for each of the two elements, C and N. This again seems to be in sufficient agreement with astrophysical data, whereas the abundance of 10 per cent for nitrogen, assumed in I, appeared to be much too high.

3. The ratio of the abundances of the two nitrogen isotopes in the sun should be $N^{14}:N^{15} = 2 \times 10^5 : 1$. This is very much greater than the abundance ratio on earth,[8] viz., 260:1. It is, of course, not yet quite certain whether our values for the lifetimes of N^{14} and N^{15} in the sun are correct, but the value for N^{15} seems rather well established from the nuclear observations, while that for N^{14} seems well substantiated by the astrophysical evidence (points 1 and 2 above). If we assume the lifetimes to be correct, there is certainly a very great discrepancy between the abundance ratios $N^{14}:N^{15}$ at the

[8] A. L. Vaughan, J. H. Williams, and J. T. Tate, *Phys. Rev.*, **46**, 327, 1934.

center of the sun and on the earth. This makes it likely that the earth was separated from the sun when the equilibrium between the elements in the carbon cycle was not yet established and the sun was still at a lower temperature.

Similar discrepancies have previously been found[9] in the abundance ratio of the hydrogen isotopes and in the existence of lithium on the earth. The ratio $H^1:H^2$ is about 5000:1 on the earth, while it must be at least 10^{18}:1 at the center of the sun. *Li* is found in some quantity on the earth and must be exceedingly rare at the center of the sun—of the same order as deuterium. In all cases mentioned (N^{15}, H^2, and $Li^{6,7}$), nuclei which should be very rare in the sun, because they undergo rapid nuclear reactions, are found in some abundance on the earth. The simplest explanations would be that either (*a*) the earth was separated from the sun when the sun was much cooler than now and the respective nuclear reactions had not yet destroyed the H^2, *Li*, and N^{15} nuclei originally present or (*b*) the earth originated from some region of the sun near the surface which was cool enough to retain approximately its original chemical composition. Assumption (*b*) requires that there be very little mixing of the various parts of the sun, so that concentration gradients can persist. Even though this may be true ordinarily, it seems not very likely at the time of a catastrophe such as the formation of the planetary system. Assumption (*a*) may seem more attractive; moreover, an early separation of the earth from the sun is also indicated by the approximate equality of the age of the earth (from radioactive measurements) and of the universe (from the red shift). Moreover, it seems that such a freak event as the formation of the planetary system could have occurred more easily at a stage when the density of stars in the universe was larger and the probability of collisions correspondingly greater than at the present time.

Department of Physics
Cornell University
April 1940

[9] E. Teller and G. Gamow, private communication.

SPECTROPHOTOMETRIC OBSERVATIONS OF THE MINIMUM OF ζ AURIGAE

C. A. WIRTANEN

ABSTRACT

The variation in brightness of ζ Aurigae during the recent eclipse has been observed photographically at eight different wave lengths, using the 10-inch Cooke camera equipped with a coarse grating and a low-dispersion prism. Plates were measured with the Schilt microphotometer. Seven early-type stars in the same field, ranging from 3.3 to 7.3 mag., served to establish the zero point and the scale at each wave length.

The light-variation of ζ Aurigae was observed spectrophotometrically by crossing the low-dispersion prism on the 10-inch Cooke triplet with a coarse objective grating. The aperture was reduced to $2\frac{1}{2}$ inches to improve the color-curve of the objective. With this aperture, measurable spectra of seventh-magnitude stars can be obtained with a 1-hour exposure. The spectra were widened by means of a fine screw which moves the plateholder carriage in right ascension, the carriage being shifted by 0.01 mm once every 6 minutes during the exposure. On the original plates the width of the spectra is 0.12 mm, while the interval from $H\beta$ to $H\epsilon$ is 2.7 mm. A part of the field is reproduced in Plate III, in which ζ Aurigae is shown in three phases with one of the comparison stars. Eastman Super Panchro-Press plates were used; they were developed 15 minutes in Rodinal 1:32 at 68° F., with potassium bromide added to reduce background fog.

The plates were measured with the Schilt microphotometer, using a 1-mm diaphragm, which produces an illuminated area 0.2 mm in diameter on the plate. Two regions in good focus were selected for measurement, the yellow part of the spectrum being measured at two points on either side of λ 5500, and the violet part at six points from $H\gamma$ to $H\eta$. Settings on these eight points were made with an accuracy of about 0.03 mm. Figure 1 shows the general appearance of the "tracings," the upper curve being that of a B9 star.

The magnitudes of ζ Aurigae were read from characteristic curves determined by the central images and the grating images of the

PLATE III

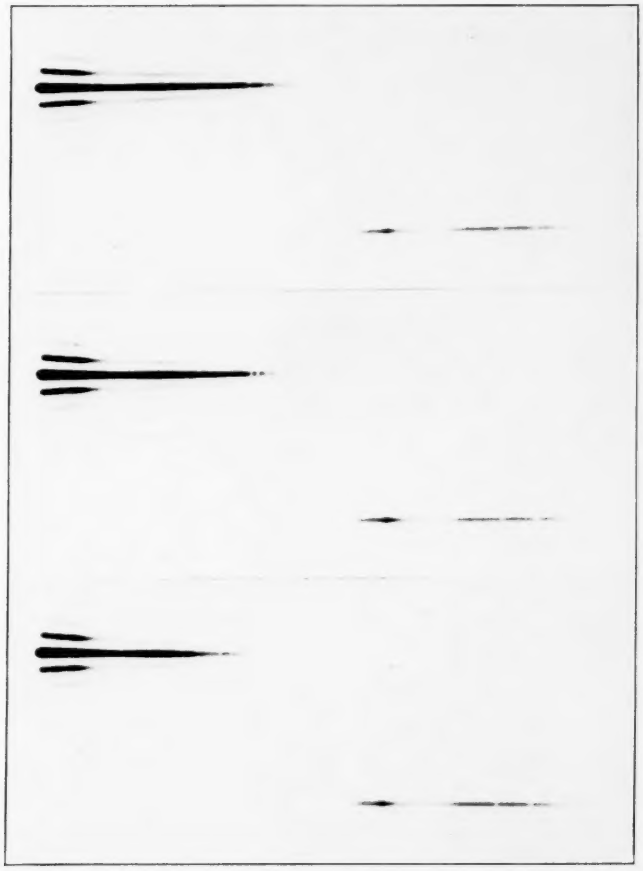

ζ AURIGAE AND THE REFERENCE STAR HD 32188 AT THE RIGHT

(*a*) November 13, 1939; maximum. (*b*) January 28, 1940; partial eclipse. (*c*) January 6, 1940; total eclipse.

seven comparison stars. Three plates in different regions of the sky yielded the following values for the grating constants:

	First Order	Second Order
λ 5500	2.17±0.04	3.31±0.05
4200	1.90±0.04	3.04±0.05

For the two points near λ 5500, Harvard visual magnitudes reduced to the I.A.U. photovisual system[1] were adopted for the seven comparison stars. Photographic magnitudes were obtained by applying

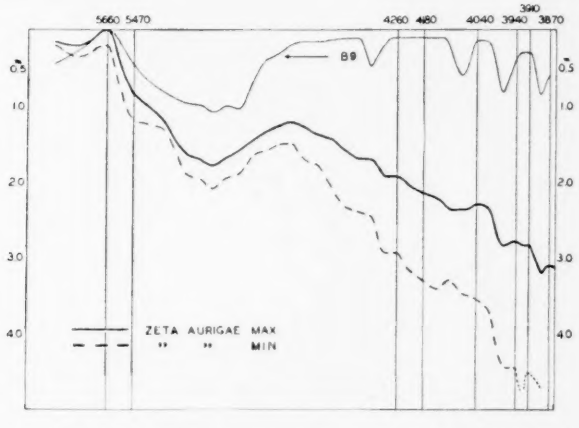

FIG. 1.—Tracings of ζ Aurigae at maximum and minimum referred to the same zero point. In the topmost tracing of HD 31069, B9, the zero point is abritrary. The vertical lines indicate the points measured.

King's color indices.[2] These were regarded as suitable for the points in the violet, since the average spectrum of the comparison stars is close to A0 and since there is practically no progression of spectral type with magnitude. The comparison stars are listed in Table 1. Eight reduction curves, one for each wave length, were used for each plate. In every case of normal exposure the magnitudes of ζ Aurigae in the yellow were determined from its grating images; magnitudes in the blue and violet were determined from its central image.

The magnitudes, as derived from each plate, are given in Table 2.

[1] *Harvard Obs. Mimeograms* (3d ser.), No. 1.

[2] Russell, Dugan, and Stewart, *Astronomy*, p. 734, 1927.

TABLE 1

Star	Sp.	m_{pv}	m_{pg}	Star	Sp.	m_{pv}	m_{pg}
HD 32630	B3	3.30	3.06	HD 32296	A2	6.55	6.63
30823	A0	5.71	5.71	33462	B8	6.94	6.87
31069	B9	6.02	5.98	31866	A2	7.31	7.39
32188	A0	6.19	6.19				

TABLE 2

G.M.T.	Wave Lengths							
	5660	5470	4260	4180	4040	3940	3910	3870
1939 Dec. 12.19	3.61	3.82	5.20	5.34	5.40	5.64	5.72	5.65
15.16	3.59	3.81	5.18	5.38	5.48	5.63	5.69	5.66
17.09	3.66	3.91	5.28	5.38	5.54	5.76	5.75	5.78
17.21	3.61	3.80	5.36	5.42	5.50	5.82	5.91	5.79
18.09	3.65	3.77	5.23	5.37	5.52	5.69	5.75	5.69
18.17	3.64	3.80	5.22	5.42	5.50	5.68	5.65	5.67
18.96	3.56	3.87	5.26	5.52	5.46	5.63	5.74	5.77
19.09	3.73	3.81	5.33	5.49	5.52	5.78	5.82	6.09
19.16	3.65	3.81	5.23	5.36	5.53	5.72	5.79	5.78
19.25	3.59	3.79	5.34	5.42	5.58	5.74	5.71	5.86
19.35	3.54	3.79	5.27	5.47	5.46	5.74	5.82	5.71
20.07*	3.71	3.93	5.46	5.52	5.66	6.02	6.23	6.29
21.04	3.78	3.95	6.10	6.35	6.52	7.53	7.50	7.35
21.08	3.91	3.95	6.22	6.40	6.52	7.71	7.78	7.84
21.27	3.66	3.85	6.05	6.38	6.55	7.53	7.38	7.42
1940 Jan. 6.10	3.73	4.13	6.06	6.34	6.54	7.42	7.48	.....
6.23	3.65	4.02	6.13	6.49	6.68	7.56	.....	.....
26.13†	3.81	4.19	6.17	6.58	6.65	.....	7.13	.....
26.19†	3.84	4.17	6.40	6.58	7.00	7.55	7.56	.....
27.05	3.81	4.16	6.16	6.42	6.69	7.51	7.51	7.75
27.10	3.86	4.16	6.21	6.52	6.77	7.80	7.57	.....
27.26	3.65	3.96	6.05	6.39	6.52	7.24	7.26	.....
28.04	3.87	4.03	5.44	5.68	5.82	6.14	6.13	6.16
28.08	3.77	3.83	5.37	5.58	5.67	6.15	6.33	6.05
Probable error of one entry	0.04	0.05	0.04	0.04	0.05	0.07	0.08	0.09

* Twelve-minute exposure. † Plates fogged, poor seeing.

The bottom line gives the average internal probable error at each point. This was derived from the interagreement of the plates obtained during one night, excepting the two plates taken on January 26. On these two plates the fogging due to the full moon and the poor definition due to bad seeing combined to make the settings with the microphotometer uncertain. A graphical representation of the observations is given in Figure 2. It will be seen that the points in the violet do not present a steady progression with wave length.

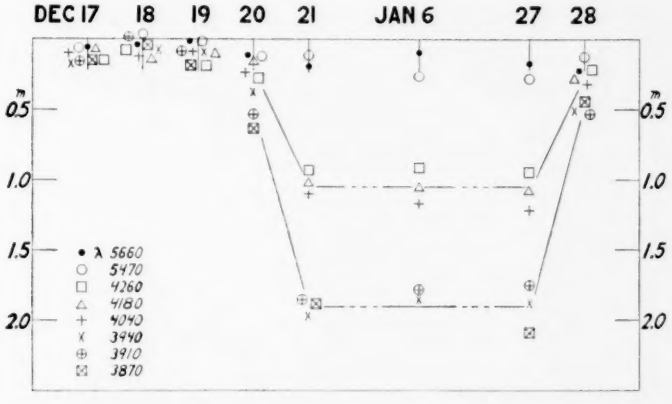

FIG. 2.—Graphical representation of Table 2. Mean values of each night are subtracted from the means of December 12 and 15.

This is due to the fact that the points at λ 3940 and at λ 3910 are within the heavy wings of the H and K lines in ζ Aurigae. The measures are in good agreement with those of other investigators at previous eclipses, as may be seen by a comparison with the summary published by Hall.[3]

I wish to acknowledge a number of suggestions made by Dr. E. T. R. Williams, and particularly to thank Professor Vyssotsky for his continued interest after having suggested the problem.

LEANDER MCCORMICK OBSERVATORY
UNIVERSITY OF VIRGINIA

[3] *Ap. J.*, **90**, 317, 1939.

NOTES

NOTES ON PROPER-MOTION STARS*

This note is a continuation of two earlier ones.[1] Table 1 consists of two parts, the first of which contains 38 subdwarfs found recently by the writer. This list brings the total number of known subdwarfs to 140. The second part of Table 1 gives eight of the ten stars listed by Luyten[2] as having a low luminosity. The remaining two stars could not be identified from the rough co-ordinates given by Luyten. It is seen that the white dwarf is confirmed, being of the 40 Eridani type; but some of the other stars are in no way exceptional, and only two (or possibly three) of them appear to be subdwarfs.

Six binaries were discovered. They are Wolf 531 (AB = 12.5 Mo; $1\frac{1}{2}''$, Δm = 1.2); Wolf 676 (13.0 M3+, 3″, $\Delta = 2\frac{1}{2}$); Wolf 1495 (11.3 M2, $\frac{1}{2}''$, $\Delta = \frac{1}{2}$); Ross 534 (A = 11.5 K6, B = 14.3 M3, 7″); Ross 486 (10″); and Wolf 1561 (8″). The last two pairs occur in Table 2.

The white dwarf Wolf 672 noted earlier[1] was found to be of the 40 Eridani type; and its parallax, from the companion, 0″.04.

Over 1500 proper motion stars have now been observed by the writer for spectral class, including most of the stars with large trigonometric parallax accessible from this latitude. Using these stars for purposes of calibration, spectral parallaxes were derived for all stars observed; stars with spectral parallax not less than 0″.09 for which no trigonometric parallax is as yet available are given in Table 2. It is estimated that the probable error of the spectral parallaxes is about 20 per cent, apart from possible errors in the apparent magnitudes; the latter are mostly estimates by the writer.

The planet Pluto was observed with the same spectrograph, on panchromatic film. No absorptions such as shown by the outer planets could be seen.

* *Contributions from the McDonald Observatory, University of Texas*, No. 23.

[1] *Ap. J.*, **89**, 548, 1939; **91**, 269 and 366, 1940.

[2] *Harv. Ann. Cards*, Nos. 521 and 525, 1940.

TABLE 1

Star	α	δ	m_{vis}	μ	Sp.	π (Sp.)
Karpov Anon.	0:04.1	+ 8:29	12.9	1".10	K4:	0".007
Ross 570	3 13.6	− 7 30	10.7	0.34	A6	.002
Ross 580	3 34.7	−11 18	12.0	0.36	Go:	.003
Ross 797	5 49.4	−14 24	10.7	0.53	F9	.005
Ross 612	6 56.3	+ 6 34	12.0	0.50	G6	.005
Hertzsp. 11	8 37.7	+36 37	11.5	0.43	Go	.004
Furuhj. 24	8 58.9	+39 13	11.8	0.47	F7	.003
Wolf 334	9 51.9	+33 06	12.2	0.49	G2	.004
Ross 892	10 22.3	+ 1 55	11.1	0.38	F8	.004
Ross 106	10 44.2	+56 59	12.6	0.51	K1	.005
Furuhj. 31	11 05.8	+45 58	12.5	0.74	K1	.005
+36°2165	11 07.3	+36 17	9.9	0.52	F4	.005
+14°2481	12 07.0	+13 50	10.2	0.46	F6	.005
Wolf 420*	12 27.4	+12 31	14.3	0.37	K3:	.003
Wolf 1447	12 29.4	+15 50	11.7	0.35	A6	.001
Wolf 449	12 50.7	+13 06	11.5	0.38	F6	.003
Ross 979	13 05.7	− 8 20	13.6	0.48	Ko:	.003
L 1338-3	13 27.9	+24 44	12.6	0.96	K3	.007
Wolf 508	13 43.8	+16 00	13.2	0.39	Ko	.004
Ross 1025	13 52.4	+25 58	12.5:	0.42	G5	.004
Ross 1027	13 56.4	+48 09	12.5	1.45	K4	.009
Ross 993	14 36.9	+41 59	13.1	0.68	K3	.006
Ross 1038	15 07.6	+ 6 25	12.0	0.96	G2:	.004
Ross 510	15 23.7	+17 04	13.2	0.97	K5	.009
Ross 805	15 26.6	−11 02	11.5	0.46	F8	.004
Wolf 624	15 56.4	+ 5 41	12.8	0.51	F8	.002
Ross 527	16 24.6	+48 23	13.0	0.44	G8	.003
Furuhj. 45	16 25.2	+44 55	11.5	0.75	G5	.006
+17°3154	16 59.3	+17 20	8.8	2.29	G1	.015
Wolf 754	17 26.5	+ 1 06	13.4	0.47	K3	.005
−8°4501	17 42.0	− 8 44	10.8	0.46	F5	.004
Ross 135	17 45.9	−24 37	11.8	0.50	G1	.004
Wolf 816	18 05.0	+20 01	12.5	0.53	K1	.005
Wolf 834	18 11.3	+20 29	13.2	1.00	K5	.009
Wolf 1465	18 30.4	− 8 20	14.1	1.28	K4:	.004
Ross 711	18 31.4	+28 38	11.4	0.36	A8	.002
Wolf 851	18 36.5	+ 0 52	12.3	1.90	K4	.010
Ross 767	20 53.1	+34 36	12.1	0.42	F4	.002
Kpv 1126–68	14 45.9	+ 7 59	15.0	0.94	Ao	.....
Wolf 536	14 33.1	− 0 24	12.8	0.56	K3	.006
−15°1776	7 16.6	−15 10	9.7	0.54	G5	.013
L 1787	12 51.5	+16 17	13.3	1.37	K4	.006
Ross 484	13 13.9	− 2 34	10.8	0.65	K4	.018
Kpv 1126–25	14 58.2	+ 9 05	11.6	0.50	Ko	.007
L 1064–75	18 11.3	+ 1 29	12.5	0.73	M5	.09
L 1064-2	18 12.0	+ 4 40	12.8	0.57	G5	0.003

* Subdwarf if motion is real; stellar, not nebulous.

TABLE 2

Star	α	δ	m_{vis}	μ	Sp.	π (Sp.)
Wolf 44	0:55.1	+60:50	10.8	0.″91	M3	0.″10
+61°195 (=A)	0 56.3	+61 48	9.5	0.74	M1+	.11
Wolf 47 (=B)	0 57.0	+61 50	13.7	0.82	M7	.14:
Wolf 66	1 20.4	+ 9 14	12.6	0.46	M5	.09
Ross 10	1 31.9	+56 45	12.2	0.51	M5	.09
Ross 555	1 46.8	−11 17	11.2	0.79	M4	.11
Ross 15	1 52.5	+58 14	12.3	0.39	M5+	.13
Ross 556	2 38.4	+25 06	10.7	0.90	M4	.14
Wolf 1322	3 53.8	+25 49	12.2	0.80	M5	.09
Ross 594	4 23.6	+39 39	13.3	0.53	M6+	.14:
Wolf 1539	4 46.7	+ 6 19	11.8	0.32	M5	.13
+52°911	4 55.0	+53 03	9.9	1.96	M1	.09
Ross 42	5 26.7	+ 9 45	11.4	0.30	M6	.24:
Wolf 237	5 39.5	+44 06	12.5	0.67	M5+	.11
AC82°1111	5 50	+82 06	10.0:	1.30	M2	.10:
Ross 79	6 05.4	+10 21	10.1	0.93	M4	.18
Ross 417	6 14.5	− 6 36	12.8	0.67	M5+	.10
−44°3045	6 54.9	−44 09	11.0:	1.14	M5	.18:
Ross 986	7 03.3	+38 43	12.0	1.12	M5	.13
+36°1638 (=A)	7 25.4	+36 26	10.8	0.41	M3+	.11
Ross 989 (=B)	7 25.4	+36 26	12.2	0.41	M5	.10
Ross 882	7 39.4	+ 3 48	11.6	0.64	M6	.22
L 829–19 AB	8 49.2	−12 45	11.9	0.62	M5+	.11
Ross 686 (=A)	8 55.6	+ 5 38	12.1	0.47	M5	.11
Ross 687 (=B)	8 55.6	+ 5 38	12.5	0.47	M4+:	.07:
Ross 439	9 24.0	− 6 55	11.6	0.71	M4+	.11
Wolf 330	9 49.8	+35 51	13.0	0.33	M5+	.09
L 1113–55	10 30.9	+ 5 38	12.2	0.68	M6	.17
Ross 104	10 54.8	+23 22	10.3	0.45	M3	.12
L 1405–28	11 36.9	+27 17	10.9	1.06	M3	.09
Ross 128	11 42.6	+ 1 23	11.0	1.40	M5+	.23
Ross 689	12 00.6	+70 06	13.1	0.59	M6	.11:
Ross 690	12 18.4	+64 35	11.3	0.73	M4	.11
Ross 695	12 19.6	−17 38	11.2:	2.53	M4+	.13:
Wolf 414	12 23.9	+ 8 59	11.5	0.70	M4+	.11
Wolf 427	12 30.0	+10 23	11.0	0.56	M4	.12
Wolf 461	12 55.6	+ 6 13	13.3	1.01	M6+	.14:
Ross 486A	13 23.2	− 1 50	11.5	0.51	M4+	.12
Ross 486B	13 23.2	− 1 50	14.3	0.51	M5+:	.05::
Ross 845	14 07.8	−11 33	13.5	0.79	M6:	.09:
Ross 848	14 14.8	− 9 09	12.7	1.13	M5	.09
−11°3759	14 28.9	−12 06	11.4	0.69	M4	.10
Ross 52	14 49.5	+23 58	11.5	0.74	M5	.13
Ross 802	15 31.5	−13 47	13.0	0.81	M5+:	.09:
Ross 868 (=A)	17 16.0	+26 42	11.3	0.47	M5	.16
Ross 867 (=B)	17 16.0	+26 42	13.5	0.47	M6	.09:
Furuhj. 48	17 16.7	+41 50	11.3	0.85	M3+	.09
L 1064–75	18 11.3	+ 1 29	12.5	0.73	M5	.09
Wolf 1084	20 40.5	+54 57	15.3	1.87	M7+:	.11:
Ross 265	21 57.0	+16 07	10.7	0.36	M3	.10
+0°4810	21 57.1	+ 0 56	9.2	0.55	M0+	.11
−5°5715	22 04.4	− 5 08	10.0	1.03	M5	.25
Wolf 1561A	22 12.1	− 9 18	13.5	0.68	M6:	.09:
Wolf 1561B	22 12.1	− 9 18	14.5	0.68	M7	0.11:

G. P. KUIPER

McDONALD AND YERKES OBSERVATORIES
June 1940